1-1-2013

Assessment of Damage in Concrete Structures Using Acoustic Emission

Marwa Abdelrahman
University of South Carolina

Follow this and additional works at: http://scholarcommons.sc.edu/etd

ASSESSMENT OF DAMAGE IN CONCRETE STRUCTURES USING ACOUSTIC EMISSION

by

Marwa Abdelrahman

Bachelor of Science
Helwan University, 2010

_____

Submitted in Partial Fulfillment of the Requirements

For the Degree of Master of Science in

Civil Engineering

College of Engineering and Computing

University of South Carolina

2013

Accepted by:

Dr. Paul Ziehl, Major Professor

Dr. Fabio Matta, Committee Member

Dr. Juan Caicedo, Committee Member

Dr. Lacy Ford, Vice Provost and Dean of Graduate Studies

DEDICATION

To my husband and daughter, To my parents.

ABSTRACT

Evaluating the integrity of concrete structures is an essential procedure to ensure structural safety and durability. Non-destructive testing (NDT) is needed for localizing and characterizing the growing damage in existing structures and also for quality control of new structures. Visual inspection is a commonly used method; however it is not suitable for early detection of damage and very dependent on the experience of the inspector. More research is needed to establish advanced methods for structural health diagnosis such as acoustic emission (AE). Acoustic emission is notably sensitive to active damage in concrete structures. This thesis includes three studies that mainly investigate the effectiveness of AE for condition assessment.

The first study aims to present a review of AE-based methods for evaluating the state of in-service structures during load testing. Discussion on the reliability of the proposed methods for different types of structures is provided. Acceptance criteria and quantification limits are summarized based on previous researches. AE has shown promising results in assessing the structural condition of concrete members and its ability to detect micro-cracking is well established. The extensive applications of AE accomplished in field are fairly discussed and some recommendations were given for effective diagnosis. This study attempts to pave the way for the standardization of AE as an inspection and evaluation method for in-service concrete structures.

v

The second study discusses the feasibility of utilizing AE for corrosion detection and quantification. The high sensitivity of AE enables it of detecting the weak stresses emerged due to corrosion initiation and propagation. The ability of AE to monitor the corrosion process was proven by several studies on small and medium scale specimens. Locating the corrosion damage by AE was successfully achieved in laboratory. Quantifying the corrosion damage is examined by means of intensity grading charts for cracked and un-cracked prestressed concrete specimens. However, further research is needed to establish the quantification limits and to extrapolate the results to in-service structures.

The third study investigated the ability of AE to detect damage in prestressed concrete specimens. The study included eight beams that were monitored during cyclic load tests. Five specimens were preconditioned to different levels to present possible practical circumstances. Index of damage based on AE-cumulative energy was investigated for damage assessment. The results were in well agreement with the observed damage. However, this method is not convenient for field application as it involves exceeding the maximum admissible damage during the test. Thus, a modification to the index is proposed to facilitate field implementations. The modified index of damage showed a clear trend with the growing damage and the detection of yielding point was enabled in both cracked and un-cracked specimens.

The studies presented in this thesis provide an overview of different AE-based methods that can serve as guidance for future researchers as well as a case of study for a newly developed method. The outcomes of these studies verify the viability of using AE for structural health diagnosis. AE showed promising ability for corrosion damage

assessment. However most of AE-methods require the aid of a benchmark for absolute conclusions. Further investigation is needed for the standardization of AE as an independent non-destructive evaluation method.

TABLE OF CONTENTS

LIST OF TABLES

CHAPTER 1

INTRODUCTION

1.1 BACKGROUND

Deterioration of concrete has significant effect on the performance and serviceability of structures. Many factors can contribute to the deterioration of concrete structures such as; poor construction, overloading, aging, corrosion of steel, chemical reactions, natural disasters, etc. Unfortunately, damage propagation is a time dependent process with serious effect on structural capacity and durability. Deterioration signs can be visible such as concrete cracking or excessive deflections which can be detected with visual inspection. In these cases, the concrete member has probably reached significant level of damage. Early detection of damage minimizes the repair costs and preserves the service-life of the structure.

Inspection and maintenance costs of infrastructures present significant share of the domestic income. The American Society of Civil Engineers (ASCE) report card in 2013 stated grade C+ for bridges; one of nine of the nation's bridges are rated as structurally deficient. Annual cost of $20.5 billion is needed to address these deficiencies by 2028. Corrosion related repairs are a significant contributor to this value. Condition assessment of existing structures is needed for maintenance scheduling and funding prioritization and by extension minimizing the required costs.

More advanced methods are needed for effective structural health diagnosis. Acoustic emission (AE) technique is used by the studies in this thesis for damage

1

assessment. The high sensitivity of AE enables it to detect the stress waves emerged by local deformations such as cracking. These waves are detected by sensors placed on the on the surface of the material. Analysis of the detected signals using AE parameters provides an insight to the behavior of concrete.

Many studies were conducted to investigate the applicability of AE for damage assessment during load testing (Ono 2010; Nair and Cai 2010). Several studies examined the feasibility of using AE for detecting corrosion damage (Song and Shayan 1998; Ohtsu and Tomoda 2008; Mangual et al. 2013). Most of the researchers focused on developing new AE-based damage quantifying methods instead of establishing the existing methods. This led to differences in the results of these methods when applied to different specimen type or size or using different sensor type. A review of the previously proposed methods is given in this study in an effort to eliminate the gaps in perceiving AE-based methods and provide guidance for future studies and applications.

1.2 OBJECTIVES AND SCOPE

The main objectives of this study can be summarized as follows:

1. Give a brief review of AE-based damage assessment methods which have been developed for load testing of concrete structures, evaluation of the reliability of these methods to detect different damage mechanisms associated with prestressed and passively reinforced concrete structures, state the established limits for classification of the accumulated damage, and point out the field applications that has been carried out using AE and also provide useful conclusions toward the standardization of AE for evaluation and inspection of in-service structures.

2. Examine the feasibility of using AE for early detection of corrosion damage by discussing the studies that has been conducted in this category and summarize the proposed methods and elaborate their efficiency for detection and quantification of corrosion damage. The study aims to provide guidance for future researchers so the results can be further extrapolated to field application.

3. Investigate the utility of a damage index based on cumulative AE energy (Benavent-Climent et al. 2011) gathered during cyclic load testing (CLT) of prestressed girders. Examine the ability of AE to assess damage on members with different structural conditions by pre-cracking and corroding some of the specimens before conducting the CLT test.

4. Propose a modification to the index of damage that may broaden the applicability of this parameter and facilitate field implementations.

1.3   LAYOUT OF THESIS

The thesis consists of six chapters. In Chapter 2, a brief description of the AE technique is presented along with definitions of basic AE parameters.

Chapters 3 through 5 were written in paper form and submitted for publication as journal articles. The description of some AE parameters may be repeated in these chapters.

Chapter 3 is titled "Review of Acoustic Emission as a Condition Assessment Method for Concrete Structures", where an extensive review of AE based condition assessment methods for concrete structures during load tests is presented.

The title of Chapter 4 is "A Review of Acoustic Emission Application for Corrosion Detection in Concrete Structures". In this chapter AE based corrosion

detection methods are discussed and the applicability of AE to detect corrosion is addressed.

Chapter 5 is titled "Acoustic Emission Based Damage Assessment Method for Prestressed Concrete Structures". This chapter investigates the applicability of an AE condition assessment method for prestressed concrete beams. A modification for the method is also proposed and validated.

A summary of the main findings of the research included in the thesis is presented in Chapter 6. Recommendations for future researchers are included in this chapter.

CHAPTER 2

LITERATURE REVIEW

2.1 INTRODUCTION

Acoustic emission is the waves that are generated as energy from elastic or plastic deformations occurring in the material. ASTM E1316 (2006) defines acoustic emission (AE) as "the class of phenomena whereby transient elastic waves are generated by the rapid release of energy from localized sources within a material, or the transient elastic waves so generated". AE waves can be generated as a result of various sources including dislocations, micro-cracking, and other changes due to the increase in the strain. The method is very sensitive (in the kHz range) which enables it to detect damage long before it is visible. AE sensors record the vibrations created by the waves when they reach the material's surface. An AE sensor consists of piezoelectric crystal encased in aluminum or steel casing to protect it from damage. The piezoelectric crystal convert the detected wave to electric signal, amplify it (internally or using external pre-amplifier), and send it to the data acquisition system. Figure 2.1 shows a schematic for AE monitoring process.

The passive ability of AE, external excitation or stimulus is not required for data collection once sensors are placed, makes it a suitable candidate for real-time monitoring and structural health monitoring of in-service structures. The method has also shown promise in assessment of damage during load tests of different structures and materials including fiber reinforced polymer (FRP), steel, reinforced concrete (RC), and prestressed concrete (PC).

Numerous investigations were conducted to AE as a non-destructive evaluation (NDE) method for RC and PC structures, which are the main components of infrastructure such as highway bridges. The main challenge in these studies was wave attenuation and reflections due to the heterogeneous nature of concrete. Chapter 3 discusses in detail all the efforts that were conducted to produce AE damage evaluation methods for concrete structures. Additionally, Chapter 4 presents the studies that were conducted in an effort to use AE as a non-destructive test (NDT) method for detection and quantification of corrosion damage. Different measured AE parameters are presented in this chapter.

2.2 ACOUSTIC EMISSION PARAMETERS

As indicated earlier, AE waves are generated from a sudden release of energy. The strength of AE signals depends on a number of factors such as distance and orientation of the source with respect to the sensor as well as nature of transferring material. Detected AE signals are usually referred to as 'hit'. A more detailed analysis can be conducted on the waveform of each signal to calculate a number of parameters such as amplitude, rise time, duration, signal strength, energy, counts, etc. (ASTM E1316). Figure 2.2 shows an AE waveform schematic with some of the parameters described. The definitions of some commonly used AE parameters are described here:

1. **Hit**

   Hit is the process of detection and measurement of an AE signal on an individual sensor cannel (ASTM E1316).

2. **Event**

Event is the rise of AE activity that will cause multiple hits on different sensors (ASTM E1316). A single event can be detected on multiple sensors.

3. **Amplitude**

   Amplitude (also known as signal amplitude) is the largest voltage peak in the AE signal waveform; customarily expressed in decibels (dB) relative to 1 μV at the preamplifier input (dB) assuming a 40 dB pre-amplification. Decibels is the unit of measurement for AE signal amplitude A, defined by A (dB) = 20 log V_p; where V_p is the peak signal voltage in μV referred to the preamplifier input (ASTM E1316).

4. **Duration**

   Duration is defined as the time from the first threshold crossing to the end of the last threshold crossing of the AE signal from the AE threshold (ASTM E1316).

5. **Rise time**

   Rise time is the time from an AE signal's first threshold crossing to its peak (ASTM E1316).

6. **Counts**

   Counts are the number of times the AE signal crosses the detection threshold (ASTM E1316).

7. **Signal Strength**

   Signal strength is defined as he measured area of the rectified AE signal with units proportional to volt seconds (the proportionality constant is specified by the AE instrument manufacturer) (ASTM E1316).

$$S_o = \frac{1}{2}\int_{t_1}^{t_2} f_+(t)dt + \frac{1}{2}\left|\int_{t_1}^{t_2} f_-(t)dt\right|$$

where: S_o is the signal strength, f_+ is the positive signal envelope function, f_- is the negative signal envelope function, t_1 is the time at first threshold crossing, and t_2 is the time at last threshold crossing (Fowler et al. 1989).

8. **Average Frequency**

   Average Frequency is the ratio between number of counts and the duration of the AE signal.

9. **Peak Frequency**

   Peak frequency is the point in the power spectrum at which the peak magnitude occurs. The peak frequency is a 2 byte value reported in kHz.

10. **RMS**

    The root mean square (*RMS*) is a measure of continuous varying AE voltage. It is defined as the rectified time averaged AE signal measured on a linear scale and reported in volts.

11. **RA value**

    RA value is the ratio between rise time and maximum amplitude in Volts from an AE signal.

2.3 ACOUSTIC EMISSION SOURCE LOCATION

AE has the ability to locate the source of emitted waves. This technique is very similar to that used in seismology to locate the epicenter of earthquakes (Ono 2010). If the speed of AE wave in the tested material is known, source location can be performed using the arrival times of AE signals at different sensor locations. Since it requires more than one sensor, only AE events are detectable using this technique. The algorithms that

perform source location are well established and usually embedded in the data acquisition software. AE source locations can be done in a linear or planar or three-dimensional space based on the number of sensors used. AE source location is challenging since the nature of the material, presence of existing cracks in the source-to-sensor path, and the dimensions of the tested member might lead to false events as a result of wave reflections. Previous research showed that AE source location is feasible in RC or PC structures if proper filters were used (Xu 2008; ElBatanouny et al. 2012)
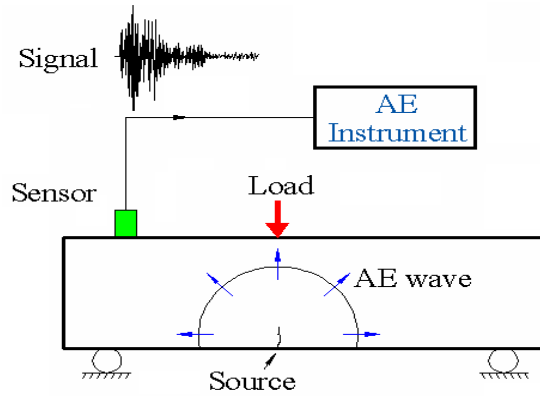
Figure 2.1: AE monitoring process (adopted from ElBatanouny 2012)
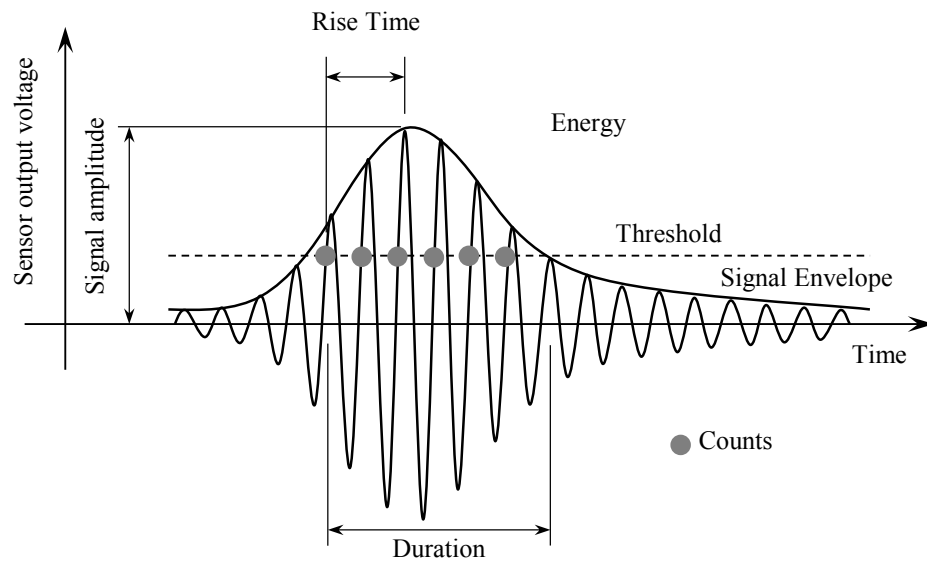
Figure 2.2: Schematic showing some parameters of an AE waveform

CHAPTER 3

REVIEW OF ACOUSTIC EMISSION AS A CONDITION ASSESSMENT METHOD FOR CONCRETE STRUCTURES[1]

---

[1] Marwa Abdelrahman, and Paul H. Ziehl. To be submitted to ACI Materials Journal.

3.1   ABSTRACT

The need for effective evaluation of structures integrity has arisen due to the severe degradation in the condition of in-service structures. This paper gives a brief overview of acoustic emission technique and its applicability for structure health diagnosis. Emphasis was given to the discussion of the established damage assessment criteria for concrete structures. An approach to set limits for damage classification is illustrated. These limits are dependent on the type of concrete, RC and PC, and the results of similar specimens loaded under similar condition should be comparable. Examination of some recent applications of AE was performed in attempt to conduct an improved structural health monitoring as well as to discuss the gaps in perceiving AE technique. This study appraises a movement toward the standardization of AE testing procedure.

Keywords: Structural health monitoring, nondestructive evaluation, acoustic emission, load tests

3.2   INTRODUCTION

Structural health monitoring (SHM) of in-service structures is of a great importance. A better understanding of the active state of an existing structure aids in maintenance scheduling and funding prioritization. Continuous monitoring techniques and real time damage detection systems enable early detection of structural deficiencies and provide data to improve existing visual inspection techniques. This may reduce both the number of inspections required and the length of each inspection.

Nondestructive testing techniques (NDT) include methods used to inspect components, materials, or systems without being adversely affected by the inspection (ASNT 1996). According to ASNT 1996, NDT can be classified as either active or

12

passive depending on the energy input to a system. Active techniques, such as ultrasonic or radiography, are based on pulsing energy into the inspected specimen and monitoring the recorded signals. Passive techniques includes methods in which an energy input is not required for response, rather the response is a result of structural response to external loading. Examples of passive NDT include acoustic emission (AE), dye penetrant testing, and leak detection (Bray and Stanley 1997). It is noted that many modern AE equipment is manufactured such that an active mode may be used. The signals detected with AE, is generated from the stressed material itself while defects occur, this differentiates AE from many NDT methods which may detect false defects such as a geometric discontinuity due to wave or signal dispersal. The high sensitivity of AE and its ability to detect damage occurring in real-time, make it a strong candidate for serving as an efficient SHM tool and give it an advantage over other nondestructive testing methods (Pollock 1986; Ziehl 2008; Ziehl and Pollock, 2012).

Acoustic emission (AE) is defined by the American Society of Testing and Materials (ASTM E 1316-06) as 'the class of phenomena whereby transient elastic waves are generated by the rapid release of energy from localized sources within a material or the transient elastic waves so generated'. So when cracking or any other irreversible changes take place ultrasound waves are generated. These mechanical waves propagate through the material to piezoelectric transducers placed on the surface of the loaded structure where these waves are converted to electrical signals. Signals from sensors are then amplified and data can be analyzed for structure health diagnosis. The sensitivity of AE enables it to detect cracks in the micro-level phase (invisible cracks in the micrometer range). Figure 3.1 shows a schematic of wave generation and detection.

AE activity has been shown to rise as a result of various forms of deformations and fractures such as crack propagation or fretting of crack faces against each other (Ono 2010). However, existing cracks, visible cracks in the millimeter range, will not produce AE signals if they are not active, i.e. growing. Given the passive nature of the technique, the use of AE does not require the location of a specific defect to be known in advance. As a result, global inspection of a structure can be carried out effectively and quickly using AE when appropriate sensor coverage is used. Many studies have investigated the feasibility of using acoustic emission technique for structural health monitoring and nondestructive evaluation (NDE) in the last two decades (Ono 2012; Nair and Cai 2010). These studies have resulted in numerous methodologies and parameters proposed for damage assessment. The evaluation is based on results from AE data gathered during load tests. Some of the methods can also be used in continuous monitoring of in-service structures. These methods utilize AE waveform parameters which differ based on degree of damage and material properties.

This is a review of AE methods available for SHM and focuses on the comparison between different methods and evaluation of the methods based on the ability to best assess various damage mechanisms specific to both prestressed and passively reinforced concrete structures. The study aims to provide guidance for future researchers in terms of limits for damage assessment criteria and their applicability to different concrete structures.

3.3   RESEARCH SIGNIFICANCE

Structural health monitoring using AE not only helps to detect accumulated damage but also can be used to identify the potential defects. This allows owners to repair damage

14

at early stages and by extension saves time and expenses. The study presented here investigates AE techniques that can be used to describe damage in concrete structures. The established limits for classification of the accumulated damage will be reported; thus a better approach of AE diagnoses for structural health can be achieved. It can also be considered a step towards the standardization of AE as a nondestructive evaluation (NDE) method for in-service structures.

3.4   HISTORICAL BACKGROUND

Investigation of the acoustic emission technique started in the 1930s. The first published studies were on prognostication of rock explosions in mines in the early 1940s (Ono 2010). Later, research on the uses of AE in aerospace and geotechnical fields was carried out. In early 1950s, Dr. Joseph Kaiser began to research the generation of stress waves as a result of material deformation. In this work Kaiser found that the amplitude and intensity of AE waves during deformation are dependent on material properties. The Kaiser effect was proposed in 1953 using tensile experiments on metals (Kaiser 1953). More details about the Kaiser effect are provided later. In 1954, Schofield began the first research program in the United States on AE applications in material engineering and defined continuous and AE burst emissions (Schofield et al. 1958). In 1958, an investigation was conducted where generation of AE waves during deformation of mild steel was detected. This study was significant as it proved that AE waves initiated close to the specimen yield and also prior to failure (Lean and Plateau 1959a,b). During the same period several studies were conducted in the former Soviet Union on the prediction of coal bursts and fracture of rocks (Shamina 1956; Vinogradov1964; Knill et al. 1968). Based on these investigations, implementation of AE technique for failure prediction

commenced in the early 1960s (Green et al. 1963; Green et al. 1964; Dunegan 1963). In the last 20 years the technique has developed significantly and AE evaluation of infrastructures such as bridges and dams has begun. Different damage detection and quantification methods have been proposed and examined. The applicability of AE damage quantification techniques investigated in a laboratory setting and the eventual transition to in-service structures has also occurred during this time frame (Ono 2010; Vidya and Raghu 2012). Recent studies used AE during load testing of in-service highway bridges (Xu 2008; Olaszek et al. 2010). The proliferation of the technology during this time period with particular emphasis on the use of the technique applied to concrete structures has motivated this study.

3.5   BASICS OF ACOUSTIC EMISSION

Acoustic emission is the term used to describe elastic stress waves generated from rapid release of energy. AE sensors consist of piezoelectric crystals which are placed in casing for protection and attached using a simple acoustic coupling. The sensors are highly sensitive, operating in the kHz range; this sensitivity enables the detection of cracks long before they are visible (Bray and Stanley 1997; Ziehl 2008). The sensitivity of AE sensors along with their wide ranges of operation makes AE an ideal candidate for assessment of in-service structures. Sensors are available with a wide variety of sizes and different operation ranges.

The emitted transient elastic waves are typically short pulses that depend on the dynamics of the source. From submicroscopic dislocations to gross cracking, the energy and amplitude of the emissions change over a wide range. The emissions can be classified into burst or continuous emission as shown in Figure 3.2. Burst emission is

16

defined by individual pulses during which higher amplitudes can be recognized. This type of emissions can emerge from cracking and fractures. Continuous emission waveforms are inseparable. Such emissions can be attributed to plastic deformations, friction, flow noise, etc. (Ono 2010).

3.5.1 AE key parameters:

A number of AE parameters are typically measured for signal analysis. To assess these parameters, a voltage threshold is set to selectively reject signals defined by maximum amplitudes lower than the threshold. These rejected signals are classified as noise and simply disregarded. This threshold can be user adjustable, fixed, or automatic floating (ASTM E 1316-06).

The local material change which gives rise to acoustic emission can be considered as "event". One event may cause various "hits" which is the detection and measurement of an AE signal on an individual sensor channel (ASTM E 1316-06). AE data analysis involves measurement of key parameters of each hit. Some of these parameters are illustrated in Figure 3.3 (Pollock 1986) and defined by ASTM E 1316-06 as shown in Appendix A.

3.5.2 Kaiser Effect:

The Kaiser effect is the absence of detectable acoustic emission, at a fixed sensitivity level, until previously applied stress levels are exceeded (ASTM E 1316-06). An example of the effect is shown graphically in Figure 3.4. In this figure; when a specimen is loaded (from A to B), unloaded (from B to C) and reloaded (from C to D); AE activity is generated on the first loading (AB) but there is no emissions on the unloading phase (BC) or in the reloading (CB) until the previous load is exceeded. This

17

irreversibility of AE activity indicates no or minor damage. The absence of Kaiser Effect is called the Felicity effect in which some emissions are detected during the reloading stage (Fowler 1986). The Felicity effect is clarified in Figure 3.4 as when the specimen is loaded to point D, unloaded to point E and then reloaded to point G; AE activity is detected at point F during the reloading stage which is at lower load than the previous reached load D. The occurrence of Felicity effect is an indication of structurally significant defects (Fowler and Gray 1979; Pollock 1995; Ziehl and Fowler 2003). On the basis of this phenomenon, the Felicity ratio was developed. This ratio is also called load ratio (Ohtsu et al. 2002) and is defined as the load at the onset of AE activity on the subsequent loading divided by the previous loading, therefore a Felicity ratio lower than unity is an indication of damage (Yuyoma et al. 1994; Hearn and Shield 1997; Yuyoma et al. 1998).

The Felicity effect was investigated in a study conducted in 2002 where three full scale box girders of span 21.3 m (69 ft. 11 in.) were tested in bending. The girders had various damage levels due to delayed ettringite formation (DEF) and alkali-silica reaction (ASR) (Tinkey et al. 2002). Beam BG1 had minor damage, beam BG2 had intermediate damage and beam BG4 was heavily damaged. The beams were equipped by six 60 kHz resonant sensors on the expected flexure zone with 1.8 m (6 ft.) spacing. The results showed that the Felicity ratio can be correlated to the level of damage as shown in Figure 3.5 (Tinkey et al. 2002).

3.6 AE DAMAGE ASSESSMENT PARAMETERS

This paper reviews the AE parameters that have been investigated by different studies. A review map was initially created to give an overview of the efforts that have

been conducted as shown in Figure 3.6. The reviewed studies were divided according to the type of specimen, specimen size, loading protocol, type of sensor used and the investigated parameters. As seen in Figure 3.6, the studies related to each group were written underneath it in brackets with the same numbering of the authors shown in the figure. The parameters are discussed in further details in the following sections.

3.6.1 Intensity Analysis

Intensity analysis is a method which was developed to characterize damage in structural elements. This method was primarily introduced to quantify damage in fiber reinforced polymer (FRP) vessels and tanks (Fowler et al. 1989). Intensity analysis is performed by calculating two parameters, historic index and severity, from the AE waveform parameter signal strength. Historic index, $H_{(t)}$, is a form of trend analysis that estimates the changes of slope in the AE signal against time by comparing the average signal strength of the most recent events to the average signal strength of all events (Fowler et al. 1989). The parameter attempts to provide a historical approach to the level of damage present in the element. Severity, S_r, is defined as the average signal strength of a number of events (J) having the largest numerical value of signal strength. Fowler proposed a value of J equal to 10 for FRP vessels(Fowler et al. 1989), but a value of 50 events is widely accepted by the later studies for RC and PC members (Nair and Cai 2010; Golaski et al. 2002; Lovejoy 2008). Historic index and severity are shown in Equations 3.1 and 3.2, respectively. In these equations, N is number of hits up to and including time (t), S_{oi} is the signal strength of the *i-th* event, and K is empirically derived factor that varies with number of hits. The value K has been derived based on material

type as shown in Table 3.1. By plotting the maximum severity and historic index values the intensity of AE data is obtained.

$$H(t)= \frac{N}{N-K} \frac{\sum_{i=K+1}^{N} S_{oi}}{\sum_{i=1}^{N} S_{oi}}$$ (Eqn. 3.1)

$$S_r= \frac{1}{J} \sum_{i=1}^{i=50} S_{oi}$$ (Eqn. 3.2)

Plotting the resulting intensities of an AE data set, the resultant plot has been divided into regions based on the level of damage occurring within the element or structure. For FRP vessels and steel pipes these damage zones have been clearly defined based on numerous uses of the method. An example of a plot developed for FRP vessels is shown in Figure 3.7. The chart is divided into five sections corresponding to different damage levels. It can be seen that a clear trend is noticed where increasing damage is plotted up and to the right of the graph (Fowler et al. 1989). Boundaries of the grading bands may be adjusted from a historical database, depending upon specific structural properties, or for environmental conditions.

Several studies have been conducted to examine the applicability of AE intensity analysis when applied to reinforced concrete (RC) structures (Proverbio 2011; Nair 2006; Shahidan et al. 2011; Basri et al. 2012; Shahidan et al. 2012; Lovejoy 2008). Lovejoy (2008) applied this analysis method in a study which included 31 RC full-scale beams having T and inverted T (IT) cross sections. The results of a typical full-scale RC test beam loaded with monotonically increasing magnitude loading/unloading cycles are shown in Figure 3.8. The specimens measured 8 m (26 ft. 3 in.) in span, 1.2 m (4 ft.) in depth and were instrumented with six AE resonant sensors; 60 kHz and 150 kHz. The results of this study (Lovejoy 2008) showed patterns similar to previous studies where data points of higher damage level plotted towards the top-right corner of the plot. The

20

data from the investigation was used to divide the developed plot into three regions based on the level of damage. As seen in Figure 3.8, the highest AE intensities occurred at load cycles corresponding to 47% and 100% of the ultimate capacity. The point plotted from 47% ultimate load occurred during the formation of diagonal tension cracks. At ultimate capacity a shear compression failure mode was observed.

Golaski et al. (2002) applied the intensity analysis to two full-scale prestressed concrete (PC) IT beams tested under repeated loading up to failure. The beams were 12 and 18 m (39 ft. 4 in. and 59 ft. 1 in.) long and instrumented with 10 sensors. The values of N and K used to calculate the historic index and severity are given in Table 3.1. AE intensity moved from zone A to D as the beam was loaded up to failure as shown in Figure 3.9.

3.6.2 Calm ratio versus Load ratio

The calm ratio versus load ratio is an alternative method of damage classification which is included in the Japanese code for NDT (NDIS-2421 2000) and was proposed by Ohtsu et al. (2002) based on a study including five RC beams tested under cyclic loading. AE data was gathered and evaluated in terms of the proposed ratios in an effort to classify the damage occurring in the test set. The Load ratio (also known as Felicity ratio or concrete beam integrity [CBI] ratio) is defined as the ratio of load level where AE events are newly observed in the subsequent loading cycle to the previous load level (Ohtsu et al. 2002). Calm ratio is defined as the number of cumulative AE activities during the unloading process divided by total AE activity during the last loading cycle up to the maximum (Ohtsu et al. 2002). The parameter used for the calculation of this ratio has varied between investigations. It has been seen that hits, cumulative energy, and

cumulative signal strength may be used for calculation (Lovejoy 2008; Ziehl et al. 2008; Liu and Ziehl 2009; Barrios and Ziehl 2012). The resultant plot from the calculation of these ratios is presented by plotting calm ratio versus load ratio and is usually divided into three levels of damage: minor, intermediate and heavy as shown in Figure 3.10 (NDIS-2421 2000). The differentiation of these areas is the subject of some debate within the literature and has yet to be clearly defined based on reinforcement type. It has been stated that the limits are dependent on specimen type, dimensions and also type and spacing of AE sensors used. Table 3.2 provides the limits used in previous studies along with the specimen type.

Figure 3.11 shows the results of three full scale prestressed girders of span 17.7 m (58 ft. 2 in.) and 1.1 m (45 in.) height that were tested by cyclic load test (CLT) loading protocol ACI 437.1R-07 (2007) and monitored by six 60 kHz resonant sensors (R6i) (Barrios and Ziehl 2012). One of the girders was subjected to fatigue loading before testing. Two possible sets (based on either minor or heavy damage) of intuitive limits, which are in agreement with the visual inspection, were proposed. The validity of different limits proposed by other authors were investigated in the same study and none of them could properly fit the data. Therefore, there are no consistent boundaries developed for using this method to quantify damage.

3.6.3   Peak Cumulative Signal Strength Ratio (PCSS ratio)

PCSS ratio compares the magnitude of emissions in terms of signal strength during the load hold of a reload cycle to that of the initial cycle. This evaluation criterion was developed by Ridge and Ziehl (2006) in a study where two strengthened RC beams with a span of 3.7 m (12 ft. 2 in.) were evaluated by acoustic emission. The beams were

monitored by four 60 kHz resonant sensors with particular emphasis on cumulative signal strength (CSS) during load holds. To use the methodology, cyclic loading conditions must be set such that the level of load during the reload cycle must be less than or equal to that of the initial load cycle. The method's hypothesis is that irrelevant emissions are reduced during holds (i.e. emissions occurring as a result of loading), thus AE activity occurring during load holds is more indicative of existing damage. PCSS ratios are calculated using the initial and reload cycles of each loadset, as given in Equation 3.3. This ratio increases with the increase of load. In this study, damage was observed at a value of PCSS between 30% and 50%. Therefore a value of 40% was chosen to indicate significant damage.

$$Peak\ CSS\ Ratio = \frac{Peak\ CSS\ at\ end\ of\ reload\ hold\ period}{Peak\ CSS\ at\ end\ of\ initial\ load\ hold\ period} \times 100\% \text{ (Eqn. 3.3)}$$

The parameter was further studied in an investigation which included four PC T-beams using twenty-four resonant sensors (PAC R6i-AST) (Xu et al. 2013). The beams were loaded with cyclic load test (CLT) methodology proposed by ACI committee 437 (2007) with addition of load cycles specially modified for the application of the PCSS calculation. The results of these tests did not show a clear trend and the criteria seemed to be less effective for detecting significant damage in PC. This may be attributed to the differences in behavior between passively reinforced concrete and prestressed concrete under sustained load which could be reflected in the amount of AE activity recorded during the load hold.

3.6.4 Relaxation Ratio

The relaxation ratio focuses on the AE activity during unloading as an indication of accumulated damage. It has been observed that AE activity during unloading increases

with the increase of damage (Colombo et al. 2005). The relaxation ratio evaluation method was proposed as a result of a study on 16 RC beams. A portion of these beams were tested at the University of Edinburgh, Scotland (data set 1 & 3) while the remaining beams were tested at Kumamoto University, Japan (data set 2). All beams were tested in cycles of increasing magnitude up to failure. AE energy was recorded during loading and unloading using resonant sensors (R6i) and broadband sensors (WD and UT-1000). Based on the recorded AE energy, the relaxation ratio was calculated for each load cycle according to Equation 3.4; where the average energy is calculated as the cumulative energy recorded for each phase divided by the number of recorded hits. If the relaxation ratio is lower than one, the cycle is called loading dominant. Loading dominate stages are an indication that no serious damage has accumulated. If the ratio is greater than one, the unloading or relaxation phase of the cycle is dominant and thus considered an indication of significant damage. Activity during the unloading portion of a cycle is often a resultant from the friction of existing cracks. Figure 3.12 shows the results of the beams of data set 1; the loading phase is dominant until the load reaches approximately 45% of the ultimate failure load then the relaxation phase becomes dominant. The beams of data set 2 did not reveal a clear trend. These differences between the results of the two data sets can be attributed to the variations of sensor type, dimensions of section, concrete properties and the mode of failure.

Liu and Ziehl (2009) investigated the applicability of the relaxation ratio on 14 small scale RC specimens with dimensions 152x152x762 mm (6x6x30 in.). Conventional and self-consolidating concrete (SCC) were used to create the specimens. Nine specimens were loaded to fail in flexure while the remaining five were shear specimens. All

specimens were loaded using the CLT protocol (ACI 437 2007). Four R6i sensors were attached to each specimen for AE monitoring. The results of flexural specimens showed that, in general, the relaxation ratio increases to a value of one until yield; then the value decreases in the post-yield cycles. No clear trend was seen in the shear specimens.

Xu et al. (2013) used this criterion in his study on four prestressed concrete beams described in the previous section. Relaxation ratio was computed for the first cycle of each loadset, a loadset includes two identical cycles. No clear pattern was recognized from the results of the beams as one showed high relaxation ratio before even being cracked and other two beams remained below the threshold of one until they were cracked and failed. Thus, relaxation ratio can be considered inaccurate for damage assessment in prestressed concrete members. Results of relaxation ratio behavior observed in different studies are summarized in Table 3.3.

$$Relaxation\ ratio\ = \frac{average\ energy\ during\ unloading}{average\ energy\ during\ loading\ phase} \qquad \text{(Eqn. 3.4)}$$

3.6.5 *b*-value and I*b*-value

This method was developed for seismology to quantify the magnitude-frequency relationship and has been recently adopted in AE. Similar to seismology, AE events with higher magnitudes occur less often than AE events with lower magnitudes. Gutenberg-Ritcher proposed a formula for calculating *b*-value as shown in Equation 3.5 where: M_L is Ritcher magnitude; N incremental frequency (i.e., the number of events with magnitudes in the range of $M_L \pm \Delta M/2$); a and b are empirical constants (Shearer 1999).

$$log_{10}N = a - bM_L \qquad \text{(Eqn. 3.5)}$$

$$log_{10}N = a - b'A_{dB} \qquad \text{(Eqn. 3.6)}$$

The method was adopted for AE by replacing the Richter magnitude with the amplitude of AE hits as shown in Equation 3.6 (Sammonds et al. 1994). It is hypothesized that micro-cracks (invisible) will have more AE hits with low amplitude while macro-cracks (visible) will have more AE hits with high amplitude. Therefore, a high *b*-value will indicate minor or no damage and a low *b*-value will indicate heavy damage (Sammonds et al. 1994). It was reported that to have comparable results to that from seismology a multiplier of 20 should be used with the *b*-value from AE (Shiotani et al. 2001).

Similar to *b*-value, an alternative method was proposed to evaluate slope failure and is called improved *b*-value, I*b*-value, as shown in Equation 3.7 (Shiotani et al. 1994). Test results showed that the method successfully followed the progression of slope failures. In Equation 3.7: σ is the standard deviation; μ is the mean value of the amplitude distribution; α_1 coefficient related to the smaller amplitude; and α_2 coefficient related to the fracture level. This method was applied in AE by modifying the I*b*-value as shown in Equation 3.8 where: $N(\mu - \sigma)$ is the number of hits with an amplitude higher than $\mu - \sigma$, and $N(\mu + \sigma)$ is the number of hits with an amplitude higher than $(\mu + \sigma)$ (Aggelis et al. 2009).

$$Ib = \frac{logN(\mu - \alpha_1\sigma) - logN(\mu - \alpha_2\sigma)}{(\alpha_1 + \alpha_2)\sigma} \qquad \text{(Eqn. 3.7)}$$

$$Ib = \frac{log_{10}N(\mu - \sigma) - log_{10}N(\mu + \sigma)}{2\sigma} \qquad \text{(Eqn. 3.8)}$$

The number of AE hits that should be included in either of the two methods varies in the literature between 50 and 130, yet a number of 100 hits was often selected (Shiotani et al. 2000; Ono 2010; Colombo et al. 2003; Aggelis et al. 2009). Figure 3.13

26

shows trials for choosing the number of events for calculating *b*-value (Colombo et al. 2003).

Colombo et al. (2003) used *b*-value parameter on a RC beam with a span of 2m (6 ft. 6 in.). The beam was subjected to cyclic loading and monitored with eight 60 kHz resonant sensors (R6i). The *b*-value behavior was related to the micro-cracking and macro-cracking observed during the test. Damage quantification was carried out and the results are shown in Table 3.4. As interpreted from the results, minimum *b*-value indicates the formation of macro-cracks and maximum *b*-value denotes micro-cracking stage.

Aggelis et al. (2009) applied the improved *b*-value (I*b*-value) in their study of two RC and two fiber reinforced concrete specimens tested in bending. The fiber reinforced specimens were half plain concrete and half vinyl fiber reinforced mortar. All the specimens were 150 x 150 x 530 mm (6 x 6 x 21 in.) in dimension and reinforced with two reinforcing bars of 13 mm (0.5 in.) diameter on the tension side. Twelve 60 kHz resonant sensors were used for data acquisition. It was observed that as the load was increased in steps the range of *Ib*-value decreased. A threshold of 0.05 was used such that *Ib*-values lower than 0.05 (which equals to 1 after applying the multiplier of 20) indicates significant damage (Figure 3.14).

3.7   FIELD APPLICATIONS

3.7.1   Intensity analysis

In Golaski et al. (2002) study mentioned before, intensity analysis was performed on several concrete bridges. A new prestressed bridge was tested with both dynamic and static conditions through using two heavy trucks equaling the nominal capacity of the

structure. All data points from this test plotted in zone A indicating no serious damage, as shown in Figure 3.15. A new concrete-steel bridge was also monitored and showed intensity A for all sensors (no damage).

An old viaduct with prestressed concrete beams was tested in the same study (Golaski et al. 2002) using 12 resonant sensors (55 kHz) with spacing of 1.45 m (4.1 ft). A "comparative criteria" was used based on comparing the values of conventional AE parameters (amplitude, duration and energy) gathered by each independent channel with the mean values of these parameters from all channels. The area of tested beam was divided to areas with different intensities using the comparative criteria as seen in Figure 3.16.

In 2010, Nair carried out an investigation in which a prestressed concrete slab-on-girder bridge with span of 16.8 m (55 ft. 1 in.) was investigated (Nair and Cai 2010). The bridge was tested for 3 days to inspect girder-diaphragm connection which was instrumented by four 55 kHz resonant sensors. The maximum historic index and severity values calculated for each load case were plotted as shown in Figure 3.17. The nomenclature used to describe each load case is presented in Table 3.5. For example load case SR_T1L1_P1 is static rolling using truck one in lane one and pass one. As seen in Figure 3.17, the charts for the three days showed consistent qualitative evaluations.

3.7.2 Peak Cumulative Signal Strength Ratio (PCSS ratio)

This criterion was applied to a two-way post-tensioned (PT) concrete slab monitored with eight 60 kHz resonant sensors and tested with CLT and 24 hour load tests (ACI 318-11). A two-way RC slab was also included in the study (Ziehl et al. 2008). The RC slab was tested with CLT loading protocol and six sensors of the same type as before

28

were used. A threshold of 30% was adopted. This threshold was chosen for the results to be consistent with damage levels determined by CR versus LR criterion. A summary of the criteria, behavior and threshold values proposed in literature are given in Table 3.6.

3.7.3   Global performance index

A combination of CLT damage criteria (permanency, repeatability, and deviation from linearity) and AE damage criteria [cumulative signal strength ratio (I_{CSSR})] was used to develop a new parameter for damage assessment in statically indeterminate structures. The investigation included two-way RC and post tensioned slabs. Permanency and deviation from linearity detected damage at the same time while the repeatability limits seemed to need some modifications. Thus Global performance index was proposed to assess damage and can be calculated using Equation 3.9 (Ziehl et al. 2008).

$$I_G = \frac{1}{5}\left\{\alpha_r i_r + \alpha_P \frac{I_P}{10} + \alpha_{DL} \frac{I_{DL}}{25} + \alpha_{CRvsLR} \frac{I_{CRvsLR}}{0.45} + \alpha_{CSSR} \frac{I_{CSSR}}{30}\right\} K_G \leq 1.0$$

(Eqn. 3.9)

where i_r=index of repeatability defined as

$$i_r = \begin{cases} 2 - \dfrac{I_R}{95} & if\ I_R \leq 95 \\ \dfrac{1}{5}|I_R - 100| & if\ 95 < I_R < 95 \\ \dfrac{I_R}{105} & if\ I_R \geq 105 \end{cases}$$

I_P and I_{DL} are permanency and deviation from linearity indexes. I_{CSSR} is calculated similar to the PCSS ratio illustrated in a previous section. α_r,α_P, α_{DL}, α_{CRvsLR} and α_{CSSR} are variables to take into consideration the importance of each index given the type of structure under inspection. The factor K_G accounts the degree of knowledge of the structure (load tests, load history, the number of load tested members with respect to the total number of similar members in the building structure, etc.); i.e. high value of K_G is

29

used if limited information is available of the structure and vice versa. The contribution of AE is the CSSR index (I_{CSSR}) and the normalized CR versus LR index(I_{CRvsLR}) which is the distance from the point of no damage (load ratio=1.0, calm ratio=0) on the CR versus LR plot. The calm ratio is first normalized to the load ratio to give the calm and load ratio equal weight then the distance from the point of no damage to the loadset under consideration is calculated as shown in Equation 3.10.

$$I_{CRvsLR} = \sqrt{(normalized\ CR)^2 + (1 - LR)^2} \qquad \text{(Eqn. 3.10)}$$

Values of global performance index exceeding unity are considered a sign of significant damage in the structure. During testing of the two-way slabs an increase of AE activity was associated with a rise in the global performance index value.

3.8   DISCUSSION

The presented AE damage quantification methods showed a promise for an effective NDT that can assess the global integrity of structures. However the applicability of some methods on different types of concrete, RC or PC, is questioned. Furthermore, in some cases the established damage classification limits, in similar material, changes for each study. Example of the number of sensors per surface area used for each damage classification method is shown in Figure 3.18. The least number of sensors were used in intensity analysis and CR versus LR (full scale specimens) while the highest number of sensors was used in Ib-value (small scale specimens). The results of each damage quantification method are discussed individually.

3.8.1   Intensity analysis

This method showed success in describing the degree of damage in test specimens regardless of the material used. However, the method is only standardized for FRP

vessels and tanks testing (ASTM E1067-11). For reinforced and prestressed concrete research had shown that the method is able to follow the general trend of damage detection, i.e. data points with higher damage are plotted towards the top-right of the plot. Recent studies proposed different damage quantification limits for reinforced concrete and prestressed concrete. Future research should use these limits and report whether the results agrees with the proposed limits in order to establish a database for means of standardization.

3.8.2 Calm ratio versus Load ratio

This method was widely investigated in reinforced concrete specimens. The damage quantification limits established by the Japanese code for NDT (NDIS) does not agree with results reported by a study on full scale specimens (Lovejoy 2008). This may be attributed to the fact that limits in this method could only be set on a single damage level; minor or heavy damage. Different limits were reported from prestressed concrete specimens with no agreement from different studies. In addition, the quadruple point, the point at the center of the chart, is a common point between the minor, intermediate and heavy damage which cannot physically occur.

3.8.3 Peak cumulative signal strength ratio (PCSS ratio)

This method showed promise only with reinforced concrete specimens. The method uses a limit of 40% to describe significant damage in the structure (Ridge and Ziehl 2006). It was reported that the method was unsuccessful in prestressed concrete specimens due to differences in mechanical behavior (Xu et al. 2013).

3.8.4 Relaxation ratio

This method was proposed to estimate the ultimate bending capacity RC beams on three test sets. The reported results for the first test set show that this ratio exceeded the value of one at approximately 45% of the ultimate load. However the method was unsuccessful for the other test sets (Colombo et al. 2005). The applicability of this method for prestressed concrete structures is also questioned (Xu et al. 2013). Yet a recent study showed that the method may be able to capture presence of visual observed cracks in prestressed concrete girders (ElBatanouny et al. 2012a).

3.8.5 *b*-value and I*b*-value

Research showed that *b*-value and I*b*-value analysis can be used as an indication of damage. Damage is reflected through a drop in the value of the parameters calculated in these methods. In general *b*-values and I*b*-values less than unity are considered as indication of significant damage (Ono 2010; Aggelis 2009; ElBatanouny et al. 2012b). *b*-values less than 1.2 were also correlated to macro-cracking in RC members (Colombo et al 2003).

3.8.6 Field applications

Only three methods were used in field applications; intensity analysis, PCSS ratio, and global performance index. The intensity analysis results were consistent with the general trend of damage detection observed in field studies. The results of PCSS ratio showed an increasing trend with the increase of the applied load and a value of 30% was determined as a damage threshold. The global performance index uses AE data in conjunction with CLT acceptance criteria. The method gives an indication of occurrence

of significant damage in RC structures if the index exceeded a value of one. However, limited research was conducted on this method.

3.9 CONCLUSIONS AND RECOMMENDATIONS

The conclusions of this study can be summarized as follows:

1. Intensity analysis enabled successful damage identification in both laboratory and field tests. The results shows that the method may be independent on scale

2. The calm ratio versus load ratio is not reliable as there are no consistent limits for damage classification.

3. PCSS ratio was successfully used to assess damage for RC members in laboratory and field. The method failed to detect damage in PC members.

4. No clear trend was seen when the relaxation ratio was used for RC and PC members.

5. A b-value and Ib-value lower the unity are related to significant damage.

6. Global performance index was developed from a field test; it uses data from AE and CLT protocol. A value exceeding unity is considered as an indication of significant damage.

A series of benchmark tests is needed to compare between different AE condition assessment methods. AE damage assessment criteria should set limits for damage classification based on standardized laboratory load tests. A clear definition of damage should be given with the proposed limits. These limits should be dependent on type of concrete, RC and PC, and the results of similar specimens loaded under similar condition should be comparable. After establishing damage classification limits for different criteria field tests should be commenced on structures with known conditions to verify

the applicability of these methods to full scale specimens in field environment. The repeatability of test results has to be ensured through standardizing loading protocol, sensors placement, sensor type, and limits for AE damage assessment criteria.

3.10 APPENDIX A: TERMINOLOGY

Signal amplitude: is the magnitude of the peak voltage of the largest excursion attained by the signal wave form from a single emission event, usually reported in dB.

Duration: the time between AE signal start and the signal (the time between the first threshold crossing and the last threshold crossing of the signal.)

Rise-time: the time between AE signal start and the peak amplitude of that AE signal (measured in microseconds).

Signal strength: the measured area of the rectified AE signal, with units proportional to volt-sec.

Signal energy: the energy contained in a detected acoustic emission burst signal with units usually reported in joules or values that can be expressed in logarithmic form (dB, decibels).

Count: the number of times the acoustic emission signal exceeds a preset threshold during any selected portion of a test, and the *count rate* is the number of counts during a fixed period of time.

Frequency: the number of cycles per second of the pressure variation in a wave.

3.11 REFERENCES

Aggelis, D.G., Shiotani, T., Momoki, S., and Hirama, A. (2009). "Acoustic emission and ultrasound for damage characterization of concrete elements", ACI Mater J, 106 (6), 509‑514.

American Concrete Institute (ACI). (2011). "Building code requirements for structural concrete." ACI 318–011, ACI Committee 318, Farmington Hills, MI, 503.

American Concrete Institute (ACI). (2007). "Test load magnitude, protocol and acceptance criteria." ACI 437.1R-07, ACI Committee 437, Farmington Hills, MI, 38.

ASNT. (1996). "Nondestructive testing handbook. 2nd ed." Columbus, OH: American Society for Nondestructive Testing (ASNT), 581.

ASTM E1067/E1067M-11. (2011). "Standard Practice for Acoustic Emission Examination of Fiberglass Reinforced Plastic Resin (FRP) Tanks/Vessels." American Standard for Testing and Materials, 1-15.

ASTM E 1316-06. (2006). "Standard terminology for nondestructive examinations." West Conshohocken, Pennsylvania: ASTM International, 30.

ASTM E 2478-06. (2006). "Standard practice for determining damage-based design stress for fiberglass reinforced plastic (FRP) materials using acoustic emission." West Conshohocken, Pennsylvania: ASTM International, 6.

Barrios, F., and Ziehl, P. (2012). "Cyclic Load Testing for Integrity Evaluation of Prestressed Concrete Girders." ACI Structural Journal (scheduled for publication).

Basri, S.R., Bunnori, N.M., Abdul kudus, S., Shahidan S., Md Jamil, M.N., and Nor, N.M. (2012). "Evaluation of Reinforced Concrete Damage Using Intensity Analysis in Acoustic Emission Technique" International Conference on System Engineering and Modeling, IPCSIT vol. 34, Singapore.

Bray, D. E. and Stanley R. K. (1997). "Nondestructive evaluation: a tool in design, manufacturing, and service." New York: CRC Press, 586.

Colombo, S., Main, I.G., and Forde, M.C. (2003). "Assessing damage of reinforced concrete beam using "b-value" analysis of acoustic emission signals", J Mater Civil Eng, 15 (3), 280‑286.

Colombo, S., Forde, M., Main, I., and Shigeishi, M. (2005). "Predicting the ultimate bending capacity of concrete beams from the 'relaxation ratio' analysis of AE signals", Construction and Building Materials, Volume 19, 746–754.

Dunegan, H.L. (1963). "Acoustic emission: a promising technique." UCID 4643. Lawrence Radiation Laboratory: Livermore, CA; 203–238.

ElBatanouny, M., Mangual, J., Barrios, F., Ziehl, P., and Matta, F.(2012a). "Acoustic Emission and Cyclic Load Test Criteria Development for Prestressed Girders", Structural Faults and Repair, Edinburgh, Scotland, UK July 3-5.

ElBatanouny, M.K., Larosche, A., Mazzoleni, P., Ziehl, P., Matta, F., and Zappa, M. (2012b). "Identification of Cracking Mechanisms in Scaled FRP Reinforced Concrete Beams using Acoustic Emission", Experimental Mechanics, DOI 10.1007/s11340-012-9692-3 (online).

Fowler, T. J., and Gray, E. (1979). "Development of an Acoustic Emission Test for FRP Equipment." American Society of Civil Engineers Convention and Exposition, Preprint 3538, Boston, 1-22.

Fowler, T.J. (1986). "Experience with acoustic emission monitoring of chemical process industry vessels", Progress in Acoustic Emission III, JSNDI, 150-162.

Fowler,T.J., Blessing, J., Conlisk, P., and Swanson, T.(1989). "The MONPAC Procedure." Journal of Acoustic Emission, 8(3), 1-8.

Golaski, L., Gebski, P., and Ono, K.(2002). "Diagnostics of Reinforced Concrete by Acoustic Emission," Journal of Acoustic Emission, Volume 20, pp. 83-98, 2002.

Green A.T., Lockman C.S., and Haines H.K. (1963). "Acoustical Analysis of Filament-Wound Polaris Chambers", Report 0672-01F. Aerojet-General Corporation: Sacramento, CA.

Green A.T., Lockman C.S., Brown S.J., and Steel R.K. (1964)., "Feasibility Study of Acoustic Depressurization System", Final Report, NASA CR-55472. Aerojet-General Corporation: Sacramento, CA.

Hearn, S.W., and shield, and C.K.(1997). "Acoustic Emission Monitoring as a Nondestructive Testing Technique in Reinforced Concrete", ACI Materials Journal, V. 94, No. 6, 510-519.

Kaiser, J. (1953). "Erkenntnisse und Folgerungen aus der Messung von Ger¨auschen bei Zugbeanspruchung von metallischen Werkstoffen." Archiv f˙ur das Eisenh¨uttenwesen 24(1–2),43–45.

Knill, I.L., Franklin, I.A., and Malone, A.W. (1968). "A study of acoustic emission from stressed rock." International Journal of Rock Mechanics and Mining Sciences 5,87–121.

Lean, J.B., and Plateau, J. (1959a). "Observation des ondes sonores prenant naissance au cours de la d´eformation plastique des m´etaux", en relation avec le probl`eme de la rupture fragile de l'acier doux. M´emoires Scientifiques de la Revue de M´etallurgie, 56(1),91–99.

Lean, J.B., Plateau, J., and Crussard, C. (1959b). "Contribution `a l'´etude du m´ecanisme de la rupture fragile de l'acier doux." M´emoires Scientifiques de la Revue de M´etallurgie, 56(4), 427–452.

Liu, Z. and Ziehl, P. (2009). "Evaluation of RC Beam Specimens with AE and CLT Criteria." ACI Structural Journal, Vol. 106, No. 3, pp. 1-12.

Lovejoy, S. (2008). "Acoustic Emission Testing of Beams to Simulate SHM of Vintage Reinforced Concrete Deck Girder Highway Bridges," Structural Health Monitoring, Vol. 7, 327-346.

Nair, A. (2006). "Acoustic emission monitoring and quantitative evaluation of damage in reinforced concrete members and bridges." Master's thesis, Department of Civil and Environmental Engineering, Louisiana State University and Agricultural and Mechanical College.

Nair, A. and Cai, C.S. (2010). "Acoustic emission monitoring of bridges: Review and case studies." Engineering structure, 32 (6), 1704-1714.

NDIS-2421. (2000). "Recommended Practice for In-Situ Monitoring of Concrete Structures by Acoustic Emission." Japanese Society for Non-Destructive Inspection, Tokyo.

Ohtsu, M., Uchida, M., Okamoto, T., and Yuyama, S. (2002). "Damage assessment of reinforced concrete beams qualified by acoustic emission." ACI Structural Journal 99 (4), 411–417.

Olaszek, P., Swit, G., and Casas, J.R. (2010). "Proof load testing supported by acoustic emission: an example of application." A: International IABMAS Conference on Bridge Maintenance, Safety and Management. "V International IABMAS Conference on Bridge Maintenance, Safety and Management". Philadelphia: CRC Press, 472-479.

Ono, K. (2010). "Application of Acoustic Emission for Structure Diagnosis." Konferencja Naukowa, 317-341.

Pollock, A.A. (1986). "Classical Wave Theory in Practical AE Testing." Progress in AE III, Proceedings of the 8th International AE Symposium, Japanese Society for Nondestructive Testing, 708-721.

Pollock, A. A. (1995). "Inspecting bridges with acoustic emission—inspection details about in-service steel bridges and monitoring weld operations": application guidelines.

Proverbio, E. (2011). "Evaluation of deterioration in reinforced concrete structures by AE technique." Materials and corrosion, 62,161-169.

Ridge, A., and Ziehl, P. (2006). "Evaluation of Strengthened Reinforced Concrete Beams: Cyclic Load Test and Acoustic Emission Methods." ACI Structural Journal, Technical paper 103-S84, 832-841.

Sammonds, P. R., Meredith, P. G., Murrel, S. A. F., and Main, I. G. (1994). ''Modelling The Damage Evolution in Rock Containing Pore Fluid by Acoustic Emission.'' Eurock '94, Balkerna, Rotterdam, The Netherlands.

Schofield, B.H, Barreiss, B., and Kyrala, A. (1958). "Acoustic Emission under Applied Stress WADS." Technical Report 58-194. Lessells and Associates: Boston, MA.

Schumacher, T. (2008). "AE techniques applied to conventionally reinforced concrete bridge girders." Oregon DOT Report SPR633, 199.

Shahidan, S., Bunnori, N.M., Nor, N.M.,and Basri, S.R. (2011). "Damage severity evaluation on reinforced concrete beam by means of acoustic emission signal and intensity analysis." Industrial Electronics and Applications (ISIEA), 2011 IEEE Symposium, 337-341.

Shahidan, S., Bunnori, N.M., Bhardwaj, N., Nor, N.M., Basri, S.R., and Abdul Kudus S.(2012). "Intensity Analysis Method for Measurement the Damage Severity of Concrete Structure by Utilizing the Acoustic Emission Technique", International Journal of Applied Physics and Mathematics, Vol. 2, No. 1.

Shamina, O.G. (1956). "Elastic pulses in the fracture of specimens of rocks". Izvestiia Akademii Nauk SSSR, Seriia Geofizicheskaya 5(5), 513–518.

Shearer, P. M. (1999)." Introduction to seismology", Cambridge University Press, Cambridge, England, 1–189.

Shiotani, T., Fujii, K., Aoki, T., and Amou, K. (1994). ''Evaluation of progressive failure using AE sources and improved b-value on slope model tests.'' Prog. Acoust. Emiss VII, 7, 529–534.

Shiotani, T., Yuyama, S., Li, Z. W., and Othsu, M. (2000). ''Quantitative evaluation of fracture process in concrete by the use of improved b-value.'' 5th Int. Symposium Non-Destructive Testing in Civil Engineering, T. Uohoto, ed., Elsevier Science, Amsterdam, 293–302.

Shiotani, T., Ohtsu, M., and Ikeda, K. (2001). ''Detection and evaluation of AE waves due to rock deformation.'' Constr. Build. Mat., 15(5–6), 235–246.

Tinkey ,B.V., Fowler, T.J. , and Klingner, R.E. (2002). "Nondestructive Testing of Prestressed Bridge Girders with Distributed Damage", Texas DOT Report, FHWA/TX-03/1857-2, 108.

Vidya Sagar, R., and Raghu Prasad, B. K. (2012). "A review of recent developments in parametric based acoustic emission techniques applied to concrete structures", Nondestructive Testing and Evaluation, Vol. 27, Iss. 1, 2012.

Vinogradov ,S.D. (1964). " Acoustic Observations of the Processes of Fracture of Rocks"[in Russian]. Nauka: Moscow.

Wevers, M. and Lambrighs, K. (2009). "Applications of Acoustic Emission for SHM: A Review." Encyclopedia of Structural Health Monitoring.

Xu, J. (2008). "Nondestructive evaluation of prestressed concrete structures by means of acoustic emission monitoring", Dissertation, Dept. of Civil Engineering, Univ. of Auburn, Auburn, Alabama.

Xu, J., Barnes, R. W., and Ziehl, P. H. (2013). "Evaluation of Prestressed Concrete Beams based on Acoustic Emission Parameters." Materials evaluation, 71(2), 176-185.

Yuyama, S., Okamoto, T., and Nagataki, S. (1994). "Acoustic Emission Evaluation of Structural Integrity in Repaired Reinforced Concrete Beams." Materials Evaluation, 86-90.

Yuyoma, S., Okamoto, T., Shigeishi, T.,Ohtsu, M., and Kishi, T. (1998). "A Proposed Standard for Evaluating Structural Integrity of Reinforced Concrete Beams by AE." Acoustic Emission: Standards and Technology update, ASTM, STP 1353, 25-40.

Ziehl, P., and Fowler, T. (2003). "Fiber Reinforced Polymer Vessel Design with a Damage Approach." Journal of Composite Structures, V. 61, No. 4, 395-411.

Ziehl, P. (2008). "Applications of Acoustic Emission Evaluation for Civil Infrastructure." SPIE Smart Structures and Materials and Nondestructive Evaluation and Health Monitoring," San Diego, CA, 9.

Ziehl, P., Galati, N., Nanni, A., and Tumialan, G. (2008). "In-Situ Evaluation of Two RC Slab Systems - Part II: Evaluation Criteria." ASCE Journal of Performance of Constructed Facilities.

Ziehl, P., and Pollock, A. (2012). "Acoustic Emission", Chapter 1: Acoustic Emission for Civil Infrastructure, Intech (ISBN 979-953-307-372-8).

Table 3.1: K factor for Historic Index

Reference	Specimen type	N	K	specimen size
Fowler et al., 1989	FRP	N<J*	N/A	Pressure vessel, 7ft long, 7ft dia., with thickness≅ 3 in
		J≤N≤1000	K=0.8J	
		N>1000	K=N-200	
Golaski et al., 2002	PC	N≤50	N/A	Two full scale IT beams (12 and 18m long)
		51≤N≤200	K=N-30	
		201≤N≤500	K=0.85N	
		501≤N≤2000	K=N-35	
ASTM E 2478 –06	FRP	N<20	N/A	N/A
		20≤N≤100	0	
		100<N≤500	0.8N	
		N>500	N-100	
Lovejoy, 2008	RC	N<200	N/A	31 full scale beams (T and IT) S*=8m ,h*=1.219 m
		200<N<1000	K=0.8N	
		N>1000	K=N-200	
Nair and Cai, 2010	PC	N≤50	N/A	Slab on girder bridge. S=16.77 m (at girder-diaphragm connection)
		51≤N≤200	K=N-30	
		201≤N≤500	K=0.85N	
		N≥501	K=N-75	

*J is a specific number of events and is a function of the material under test, S is the span and h is the height.

Table 3.2: CR and LR thresholds for damage classification

Reference	LR Threshold	CR Threshold	Specimen type	Specimen size	Notes
NDIS-2421 (2000)	0.9	0.05	RC	N/A	_____
Ohtsu et al. (2002)	0.9	0.05	RC	5 Rec. beams, S=2.1to 2.8m	_____
Colombo et al. (2005)	0.3	0.6	RC	A beam with S=3m, h=0.275m	_____
Schumacher (2008)	0.9	0.4	RC	4 full scale beams (T-sec), S =6.6m, h=1.220 m	_____
Lovejoy (2008)	0.9	0.4	RC	31 full scale beams (T and IT) S=8m ,h=1.219 m	_____
Ziehl et al. (2008)	0.9	0.05	PT &RC	PT two-way slab (t=165mm) & RC two-way slab (t=265mm)	The PT slab had some structural deficits
Liu and Ziehl (2009)	1.0	0.5	RC	14 small scale (152x152x762 mm)	Flexural
	1.0	0.4			Shear
Barrios & Ziehl (2012)	0.7	0.3	PC ,normal weight (two possible graphical limits) Figure 11	3 light weight and 3 normal weight girders, S=7.7m, h=1.143m	_____
	0.9	0.75			
	0.71	0.04	Light weight		
Xu (2013)	0.7	0.5	PC	4 T-beams, S=2.95 to 7.01m, h=0.38m	One of the beams was predamaged

Table 3.3: Relaxation ratio results

Reference	Specimen type		Specimen size	Sensors used	Results
Colombo et al. (2005)	RC beams	Data set 1, Scotland (6beams, one of them (BF2c) was predamaged)	S= 2&3m h=0.27 and 0.275m	Resonant (R6I) &broadband (WD)	Data set1: loading phase is dominant (relaxation ratio <1) until load reached 45% of the ultimate failure load.
		Data set2, japan	S=2.2m, h=0.25m	Broadband (UT-1000)	Data set 2: no clear pattern
Liu and Ziehl (2009)	RC Small scale	flexure	152x152x762 mm	Resonant (R6I)	Increased until yielding (to value of one) and then decreased after yielding
		shear			no clear pattern
Xu et al. (2013)	PC. beams		S=2.95 to 7.01m, h=0.38m	Resonant (R6I)	Unreliable for PC.

Table 3.4: b-value quantitative results (Colombo et al. 2003)

1.0< b-value <1.2	Implies that the channel is very near to a large crack; i.e., Macro-cracks forming
1.2< b-value <1.7	Uniformly distributed cracking; i.e., macro-crack are constant
b-value >1.7	Micro-cracks are dominant or macro-cracks are opening

Table 3.5: Load case terminology (Nair and Cai 2010)

Type of live load	Meaning
SR	Static rolling, truck speed< 5 mph
SS	Static stopping, truck mid axle located at mid-span
D30	Dynamic, number following designation represents the speed of the truck (mph)
Truck designation	
T1	Truck 1
T2	Truck 2
Roadway designation	
L1	Lane1
L2	Lane 2
Sh	Shoulder lane
Load case repetition	
P1	Pass 1
P2	Pass 2

Table 3.6: Summary of PCSS ratio results

Reference	Criteria	Specimen type	Specimen size	Results
Ridge and Ziehl (2006)	Pass if <40%	RC	2 strengthened RC. beams, S=3.4m, h=0.305m	Increases with the increase of loading
Ziehl et al. (2008)	Pass if <30%	PT, RC	PT slab (t=165mm) & RC slab (t=265mm)	
Xu et al. (2013)	____	PC	4 PC beams, S=2.95 to 7.01m, h=0.38m	Didn't reveal clear trend (less effective for PC)
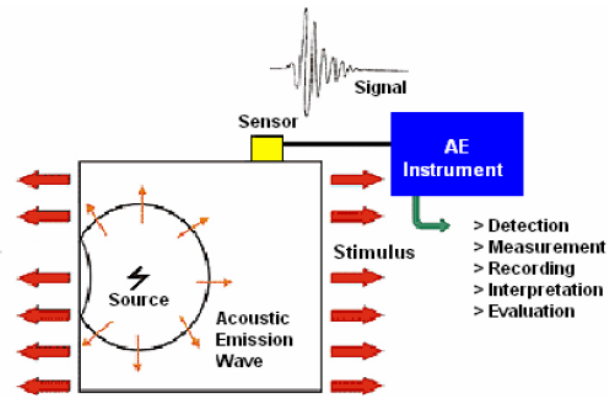
Figure 3.1: Principles of AE technology (Xu 2008)
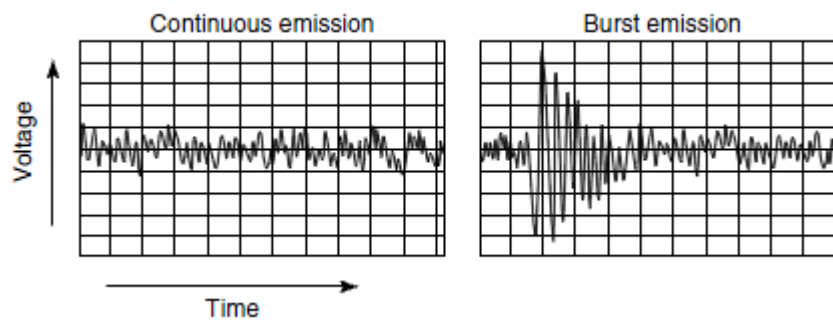
Figure 3.2: continuous emission and burst emission (Wevers and Lambrighs 2009)
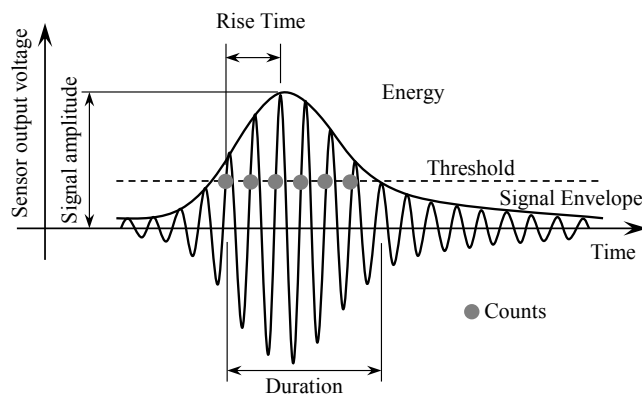
Figure 3.3: AE signal features (Xu 2008)
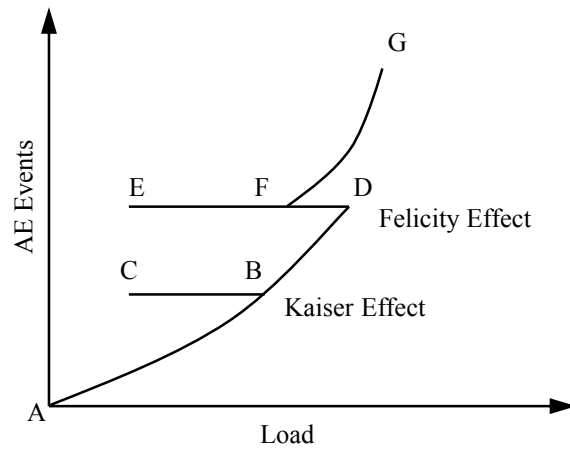
Figure 3.4: Emission on repeated loading (Pollock 1995)
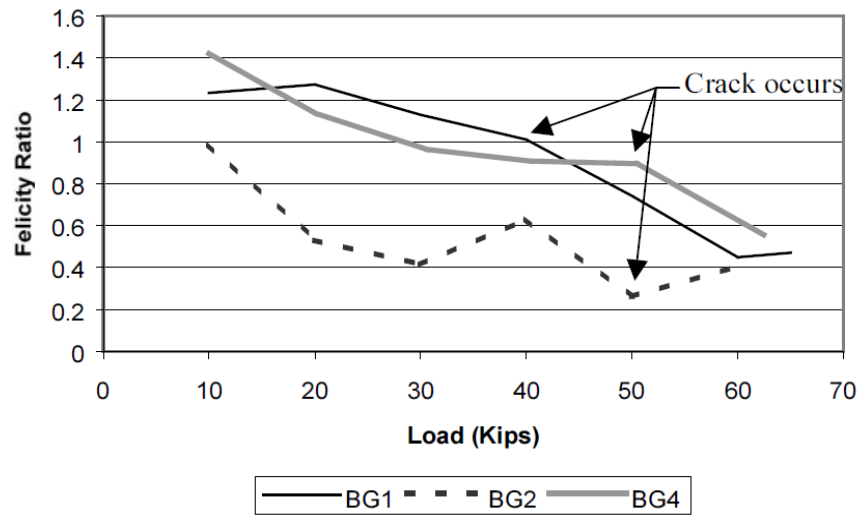
Figure 3.5: Felicity ratio for three full scale box girders tested in bending (Tinkey et al. 2002)
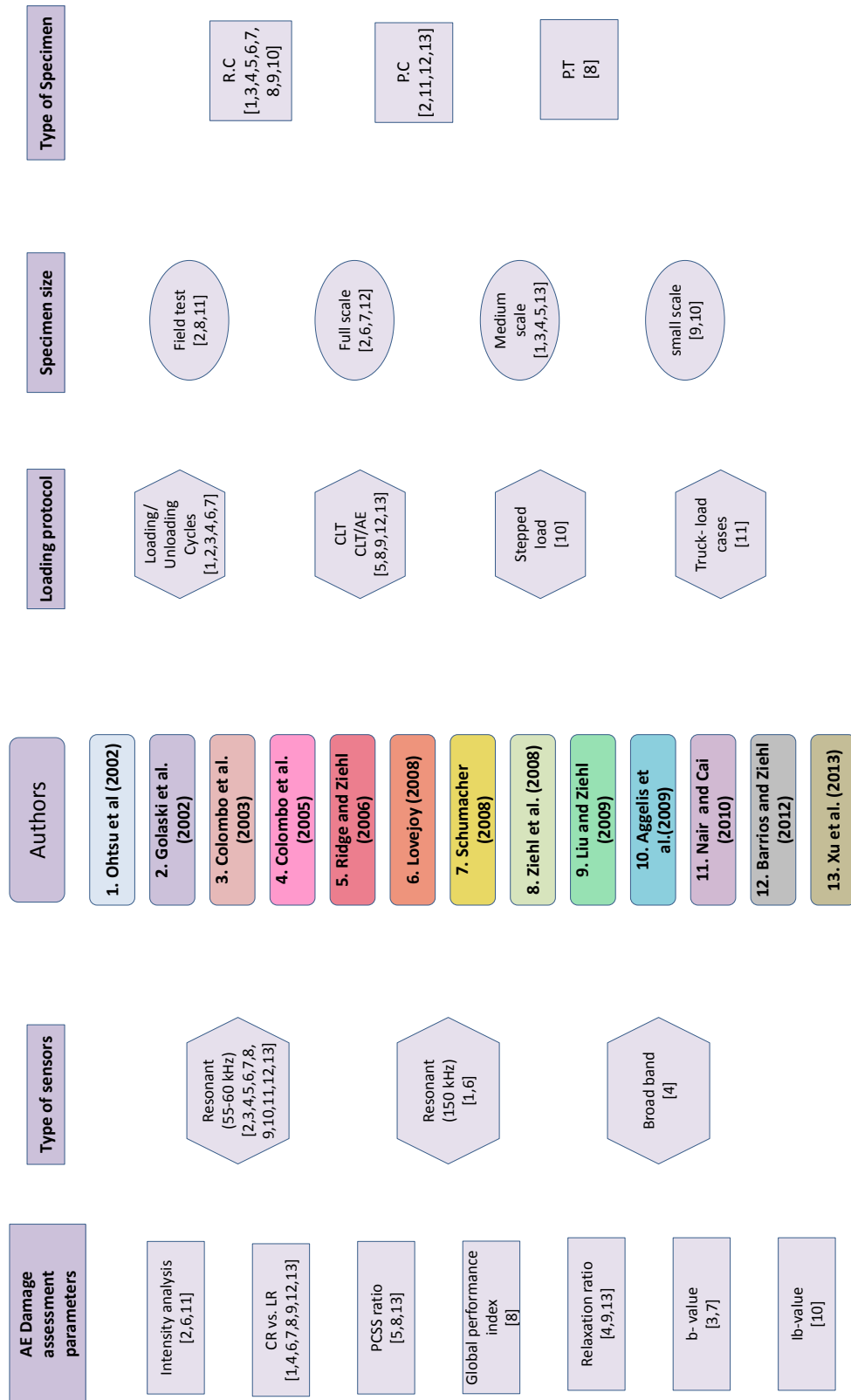
Figure 3.6: Review map
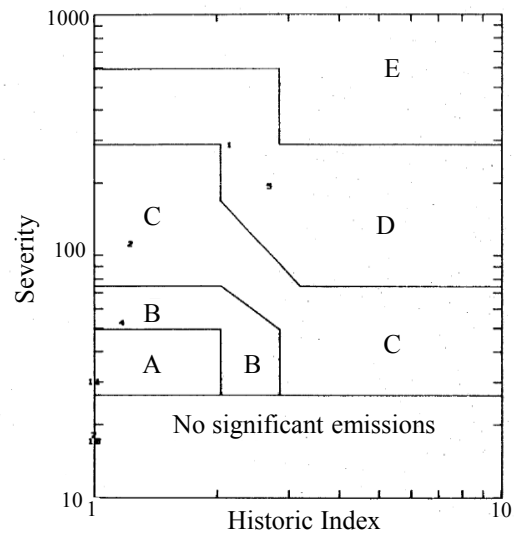
Figure 3.7: Intensity analysis chart for FRP vessel (Fowler et al 1989)
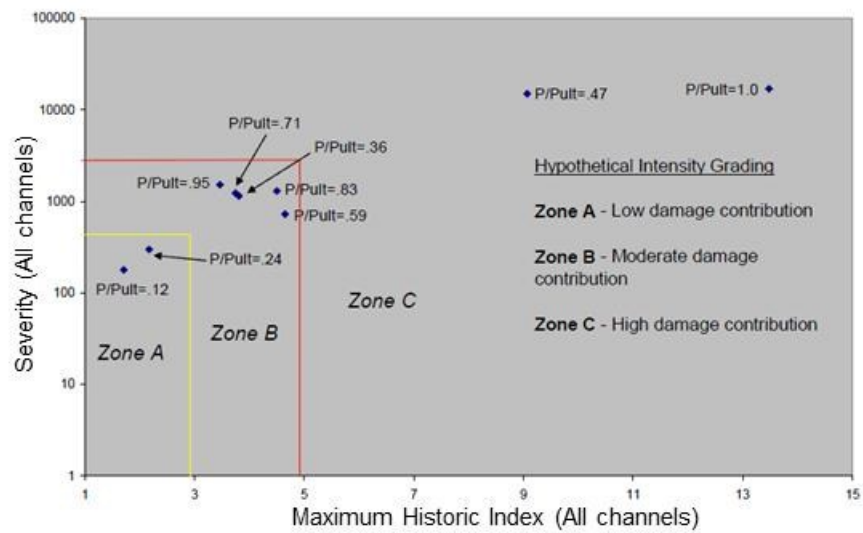
Figure 3.8: Intensity analysis for RC full scale test beam (Lovejoy 2008)
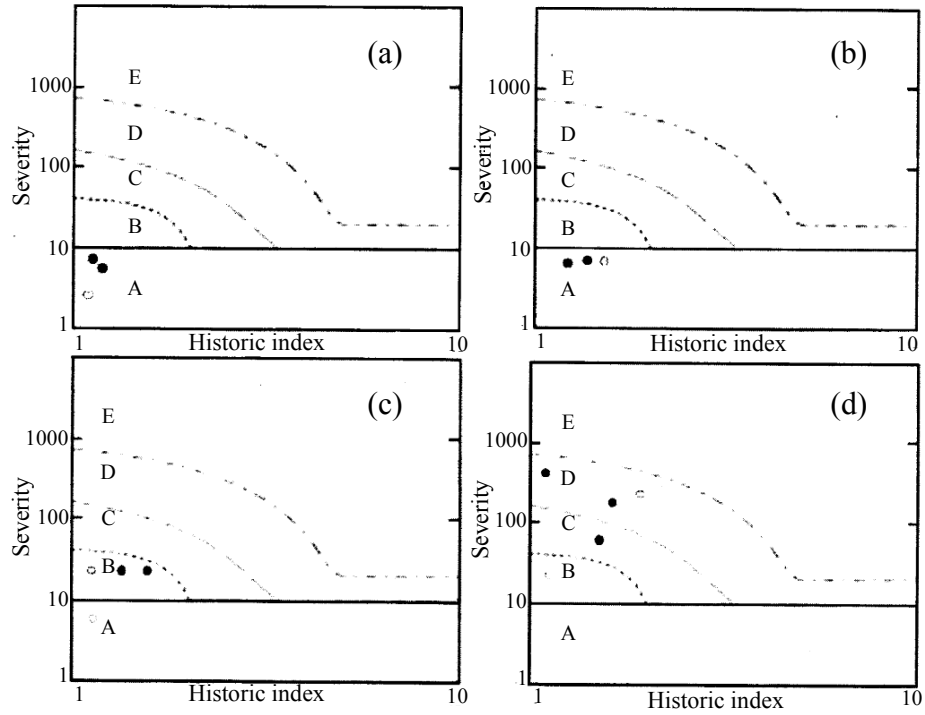
Figure 3.9: Intensity plots for different stages of loading: (a) 25% of failure load, (b) 40% of failure load, (c) 60% of failure load, and (d) failure load. Different colored dots indicate different measuring zones or sensor position (Golaski et al. 2002)
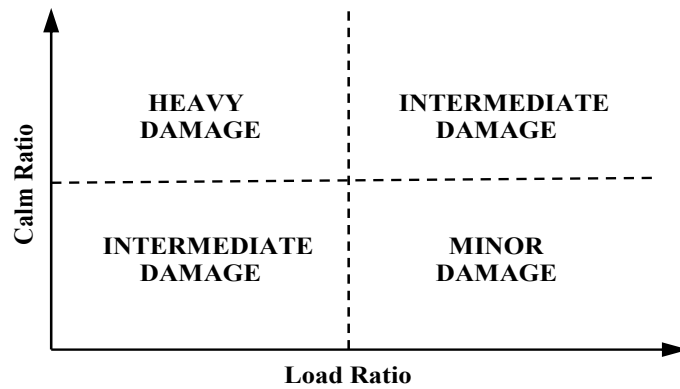
Figure 3.10: Damage classification based on calm ratio versus load ratio (NDIS-2421 2000)
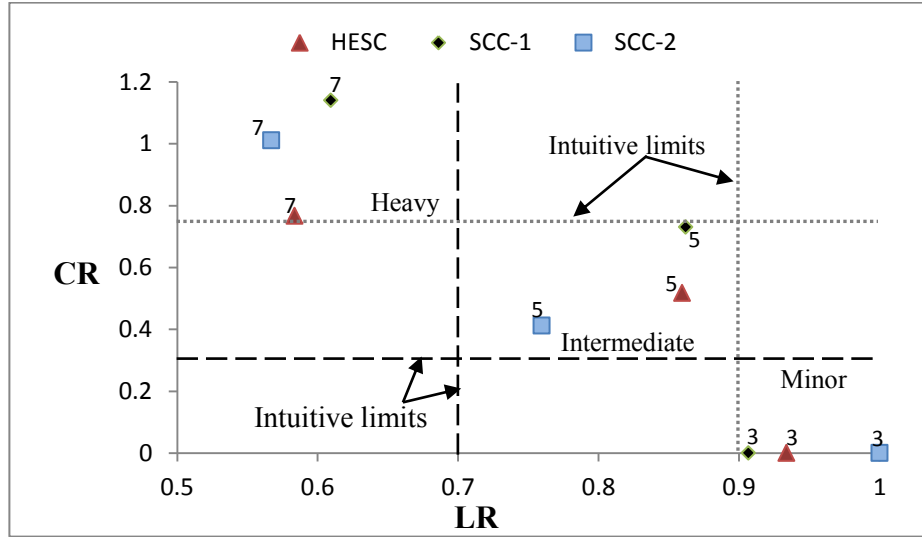
Figure 3.11: CR versus LR damage classification for three full scale prestressed girders (Barrios and Ziehl 2012)
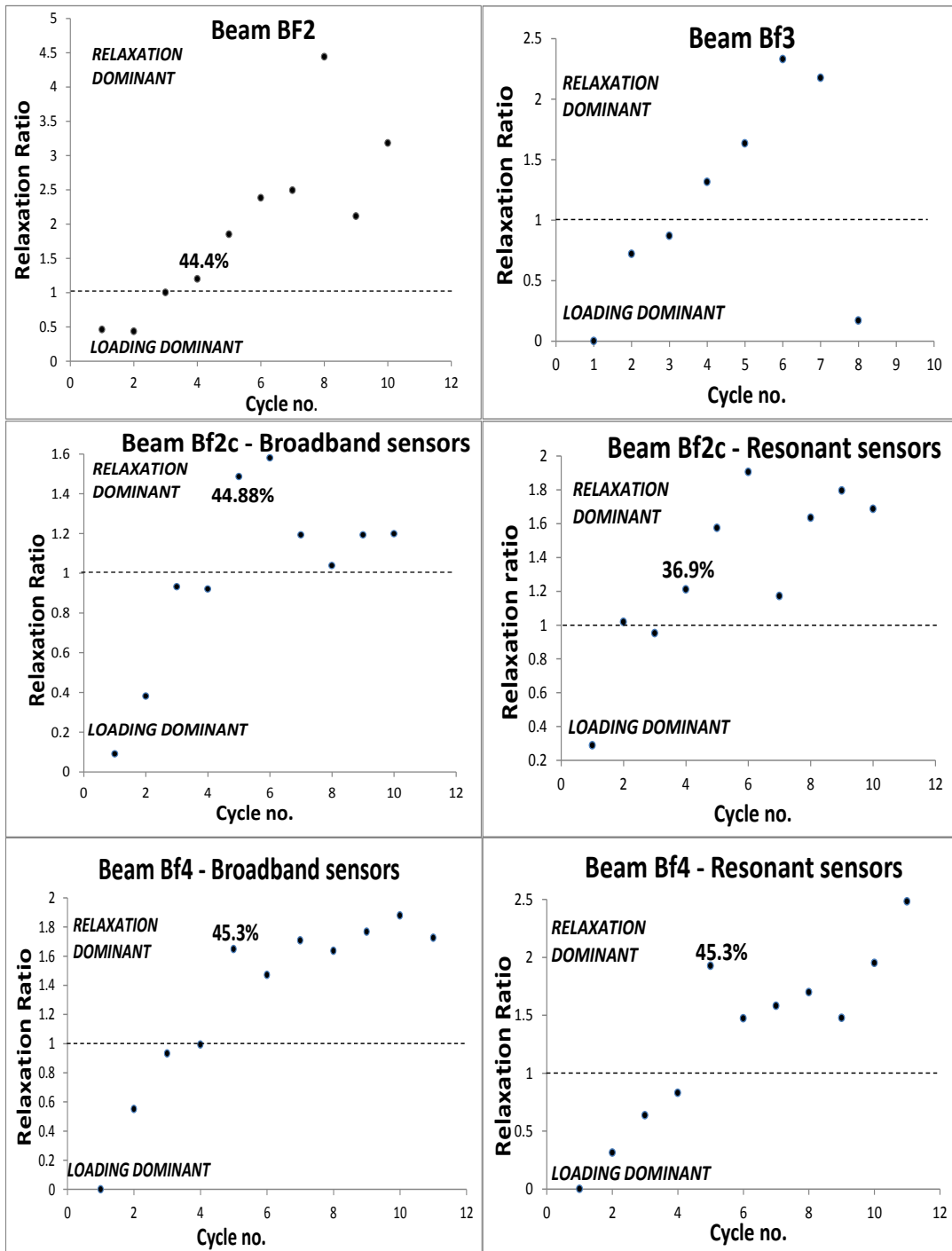
Figure 3.12: Relaxation ratio results of RC beams tested in cycles up to failure (Colombo et al. 2005)
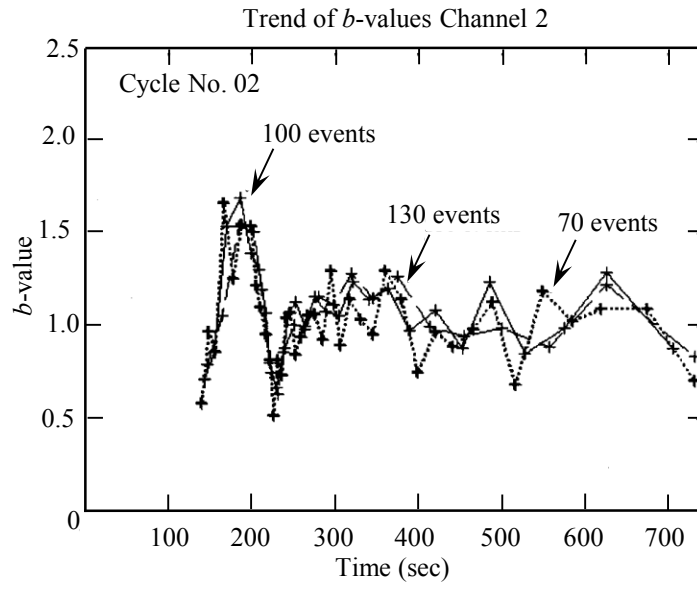
Figure 3.13: *b*-value over time calculated with using groups of, respectively, 70 (dotted line), 100 (continuous line), and 130 (dashed line) numbers of events to verify independence of final results from number of events chosen for calculation (Colombo et al. 2003)
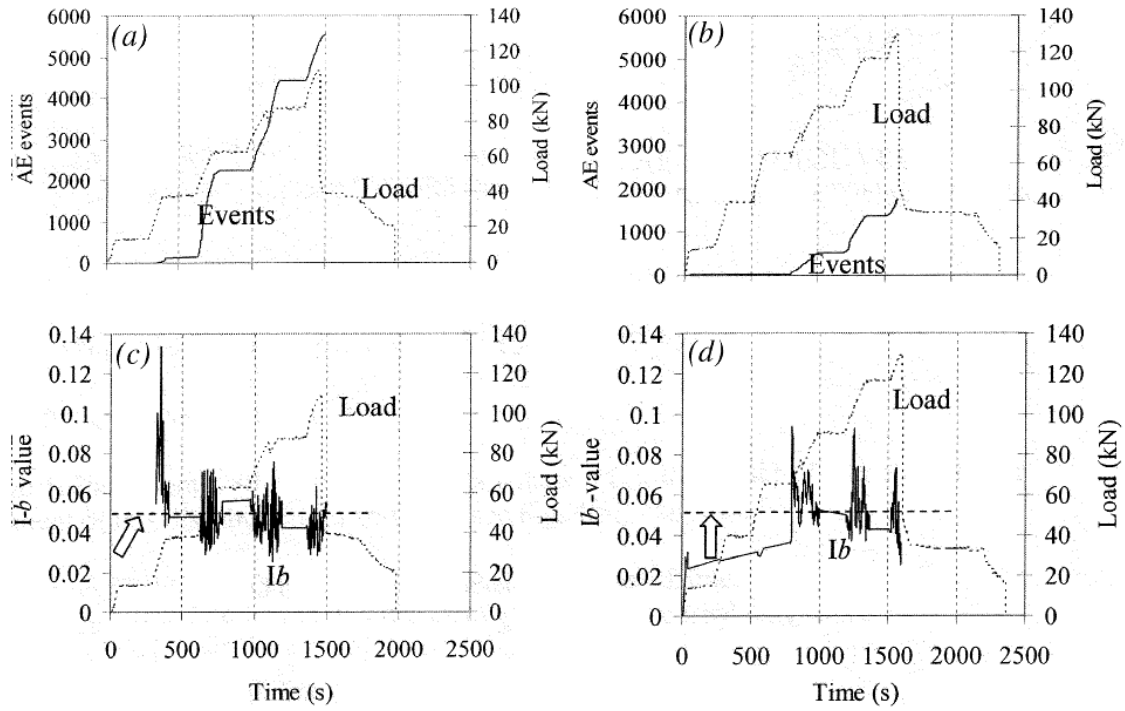
Figure 3.14: Step load and event time history for: (a) normal concrete; and (b) two-layer fiber concrete. Step load and Ib-value for: (c) normal concrete; and (d) two-layer fiber concrete. (Note: 1 kN = 225 lb; Ib-value should be multiplied by 20 according to Shiotani et al., 2001) (Aggelis et al. 2009)
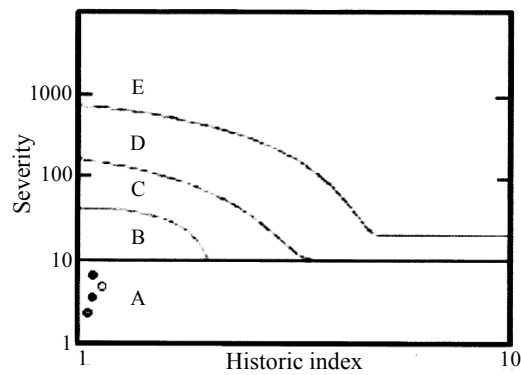
Figure 3.15: Intensity analysis for a new prestressed bridge (Golaski et al. 2002)

52
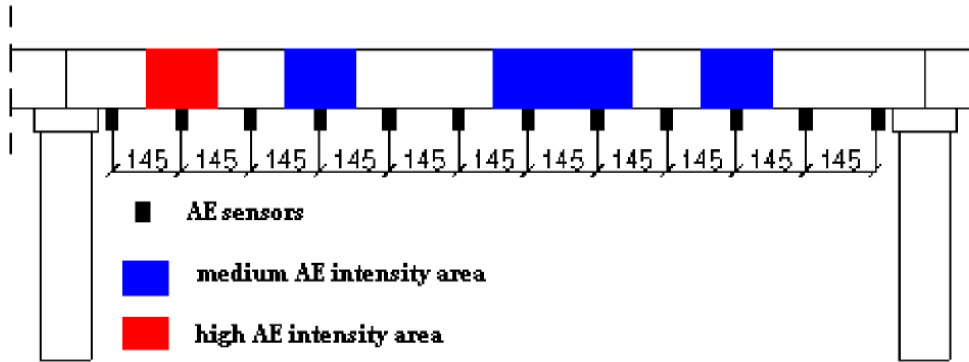
Figure 3.16: Measuring areas with different AE intensity (Golaski et al. 2002)
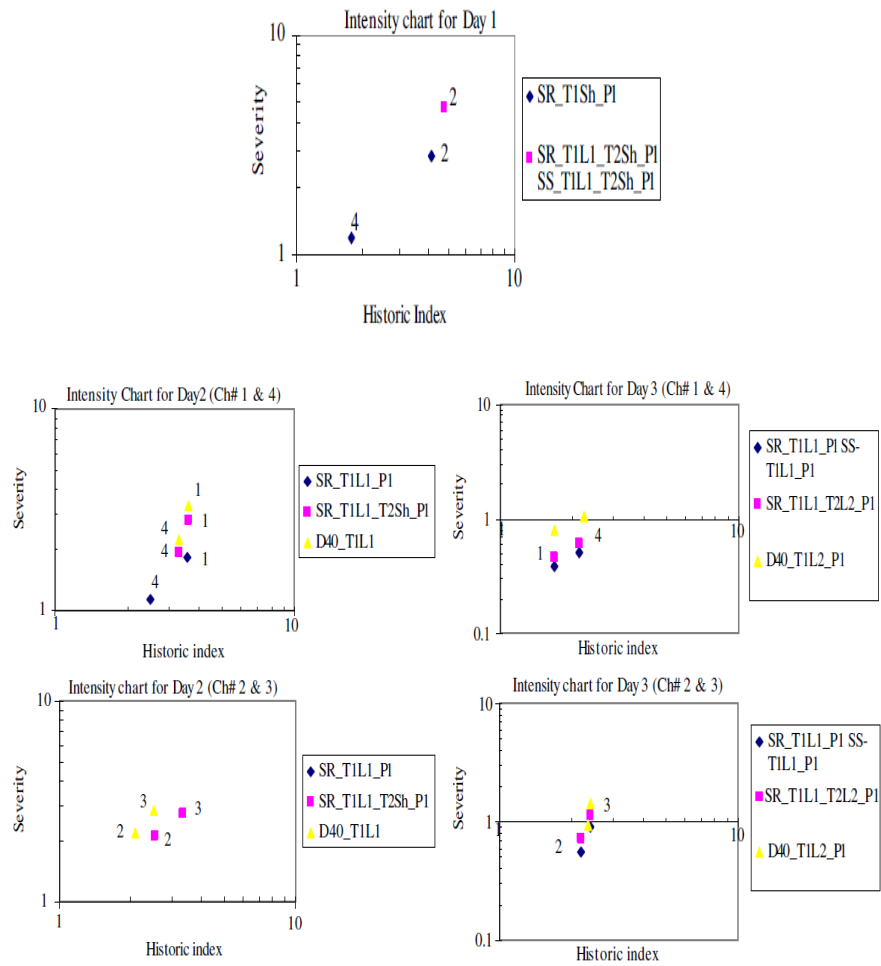
Figure 3.17: Intensity charts for load cases on 3 days (Numbers within the plot represent sensor #) (Nair and Cai 2010)
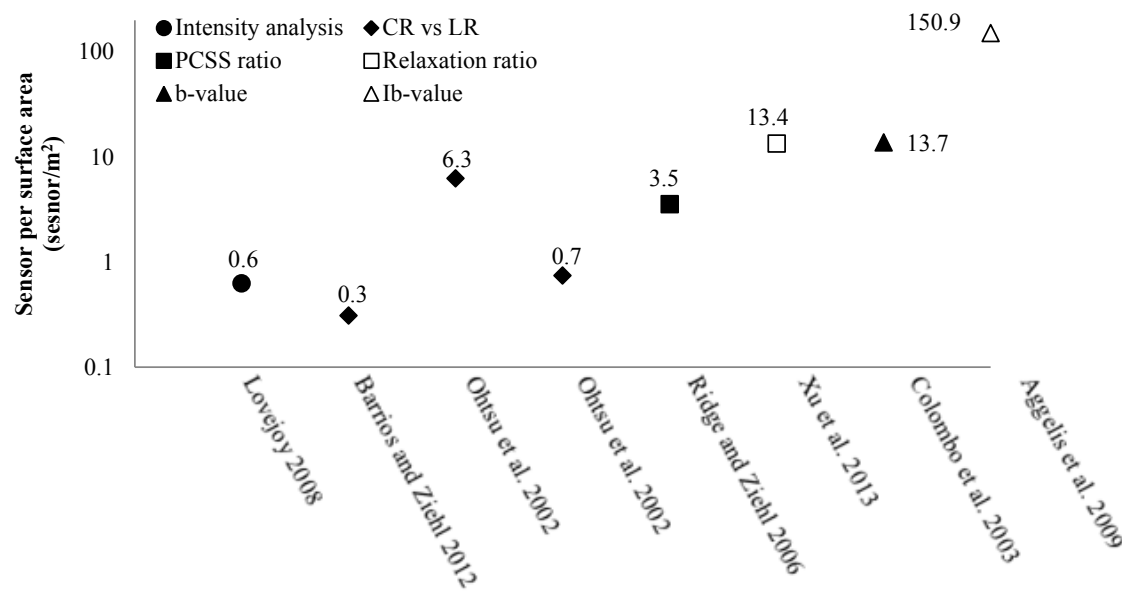
Figure 3.18: Number of AE sensors per surface area in some AE studies

CHAPTER 4

A REVIEW OF ACOUSTIC EMISSION APPLICATION FOR CORROSION DETECTION IN CONCRETE STRUCTURES[2]

---

[2] Marwa Abdelrahman, and Paul H. Ziehl. To be submitted to ACI Materials Journal.

4.1 ABSTRACT

Corrosion of steel in concrete is a primary cause for many prematurely damaged concrete structures. The effect of corrosion on safety and serviceability of concrete structures has extended the need for effective corrosion assessment. Detecting corrosion damage at early stages lowers the cost of required repairs and maintains the structural capacity of the building. Visual inspection and electrochemical techniques are the conventional methods used in field for corrosion inspection. Yet most of the corrosion damage is hidden in the concrete until it reaches significant levels. In addition, electrochemical techniques do not provide sufficient information about the rate and severity of corrosion. The acoustic emission (AE) technique is known with its high sensitivity which enables the detection of weak stresses and deformations. This technique can provide a better insight of the corrosion process in concrete. The feasibility of using acoustic emission for monitoring the corrosion process has been investigated in several studies. Different approaches to quantify the corrosion damage were used. AE activity was correlated with the corrosion rate during several laboratory tests. The paper in hand summarizes AE techniques that have been used to detect and quantify corrosion in both reinforced and prestressed concrete specimens as well as the attempts to use AE for corrosion damage allocation. The feasibility of using AE for detecting or monitoring corrosion in field is also discussed.

Keywords: nondestructive evaluation, acoustic emission, corrosion, reinforced concrete, prestressed concrete.

4.2   INTRODUCTION

Corrosion of reinforcing steel in concrete is a major concern for durability and safety of structures as well as the economic costs. In 2002, the U.S. Federal Highway Administration (FHWA) estimated the direct cost of corrosion in the U.S. to be $276 billion per year, which represents 3.1% of the U.S. gross domestic product (GDP). The share related to highway bridges (including steel bridges) was determined to be about $8.3 billion a year (Koch et al. 2001; Yunovich and Thompson 2003). Concrete structures in coastal areas and where de-icing salts are commonly used are more susceptible to this issue.

Corrosion of steel reinforcement in concrete has been responsible for severe damage up to the point of catastrophic failure. Exposure to moisture, high chloride content in concrete, insufficient cover, deicing salts, highly permeable mortar or poor grout quality; and other factors may contribute to steel corrosion and by extension regression of structural integrity. Provided below are some cases of damage related to steel corrosion in concrete:

- Collapse of Bickton Meadows footbridge, post-tensioned (PT) bridge, in Hampshire, UK in 1967 after only 15 years of service (NCHRP 1998).

- The unexpected collapse of Ynys-y-Gwas Bridge, UK, a segmental PT I-beam bridge in 1985 after 33 years of service (Woodward and Williams 1988; Trejo et al. 2009).

- Collapse of the Berlin congress hall prestressed roof, 1980 (Isecke 1982).

- Collapse of a multistory parking structure in Minnesota, 1984 (Heidersbach 1986).

- Cracking and spalling in 5 of 7 inspected beams of U.S. 131 Overpass, MI. Precast-pretensioned box beams with cast-in-place deck on top and transverse post-tensioning (Whiting et al. 1993).

- Complete failure of two strands and fracture of five wires of other strand in Precast-segmental PT single-box Bridge in England (Robson and Brooman 1997).

- Extensive concrete cracking and spalling over corroded tendons in PT girder flanges and prestressed piles in Gandy Bridges, Old Tampa Bay, FL. (Novokshchenov 1989).

The reported failures lead to increasing awareness of the significance of corrosion. The high alkalinity (pH above 12) of concrete, due to cement hydration, provides a protective environment for embedded steel against corrosion through the formation of a thin protective passive film which depresses the corrosion rate significantly (ACI 222 2001). However, the diminution of concrete alkalinity or the increase of chloride concentration in concrete breaks down this passive layer and results in corrosion initiation. The localized disintegration of the passive film, such as in the case of cracks, leads to pitting corrosion.

Effective non-destructive evaluation (NDE) and structural health monitoring (SHM) of in-service structures is needed to detect corrosion in the early stage. Visual inspection is the commonly used method, but it lacks accuracy as it cannot detect hidden damage and is also very dependent on the inspector experience. Electrochemical techniques such as half-cell potential and polarization resistance are also widely used in both laboratory and field applications for corrosion detection (Flis et al. 1992; Videm 1997; Novokshchenov 1997). However, half-cell potential (HCP) can sometimes be misleading

as it is highly affected by many factors such as temperature, concrete conductivity, membrane potential, and junction potential (Bennett and Mitchell 1992; Broomfield 1997). Additionally, HCP measurements require direct connection with the steel which makes it an intrusive method. Furthermore, it does not provide quantitative information about the corrosion rate as it only estimates the probability of corrosion at a local position.

Polarization Resistance (R_p) is commonly used to detect corrosion rate. Previous studies have proposed limits to determine the corrosion state of steel in concrete (Andrade et al. 1990; Clear 1989; Broomfield et al. 1993; Broomfield et al. 1994). There are different methods to compute Rp, but the most common one is the linear polarization resistance (LPR). This electrochemical method also has some drawbacks; a) it assumes uniform corrosion while pitting corrosion is a highly probable form of corrosion in concrete which may lead to misleading results, b) in some cases linear polarization readings are unstable, c) in case of dry concrete significant error due to concrete resistance is included in the readings, and d) the area of steel measured in the concrete is not precisely known which creates some errors in the R_p calculations.

Acoustic emission is a sensitive non-destructive method which has the ability to detect weak stress waves engendered in concrete. The ability of AE to detect concrete cracking during load testing has been previously demonstrated (Ziehl 2008; Ono 2010). AE has likewise shown promise for early corrosion detection and locating active corrosion damage.

This paper provides a review of efforts that have been made to examine using AE for the assessment of corrosion damage. The methods that have been proposed to detect and

quantify corrosion damage with AE are summarized in this study in an effort to provide useful recommendations for future research and field applications.

4.3   RESEARCH SIGNIFICANCE

Corrosion of steel in concrete is a major cause of damage for the civil infrastructure. The cost of repairs and replacement of corroded structures can be minimized through the early detection of corrosion. The commonly used inspection methods in the field depend on the apparent symptoms which are not visually observable, in the case of corrosion for internally reinforced concrete, until significant damage has accumulated. Several studies have been conducted to examine the feasibility of using acoustic emission (AE) for corrosion detection and quantification. AE has been reported to be correlated with corrosion rate. The ability of AE for early detection has also been proposed. A conclusion based on these investigations is needed to verify the reliability of AE for detecting and quantifying corrosion damage so that the method can be effectively utilized for field applications.

4.4   CORROSION DETECTION USING ELECTROCHEMICAL TECHNIQUES

Electrochemical techniques such as half-cell potential (HCP) measurements, galvanic current, and linear polarization resistance (LPR) are widely used for corrosion detection in both laboratory and field investigations. The half-cell potential method is an electrochemical technique that estimates the risk of corrosion of steel in concrete. A voltmeter and a reference electrode are used to measure the potential between the steel and the reference electrode. The copper/copper sulphate reference electrode (CSE) and silver/silver chloride in potassium chloride solution are commonly used reference electrodes. A criteria established by ASTM C867 (2009) for the possibility of corrosion

60

based on the HCP reading is given in Table 4.1. Potential mapping, using the results at different locations, can be plotted if the corrosion location is unidentified. This method requires the steel to be in direct contact with the negative terminal of the voltmeter which requires drilling through the cover to reach the steel reinforcement.

The localized breakdown of the passive film creates an active region which acts as an anode while the passive area acts as a cathode. This circumstance creates a galvanic cell. Some studies use the galvanic current passing in this cell as a measure of corrosion. Linear polarization resistance (LPR) is another electrochemical technique that can estimate the corrosion rate. The mechanism of this method is to apply a potential scan of ±20 mV around the corrosion potential (E_{corr}) and measure the corresponding current. The slope of the line formed by plotting the resulted potentials and correspondent currents is the polarization resistance (R_p) (ASTM G59-97). The corrosion current (i_{corr}) can be calculated from Equation 4.1 which can be applied to calculate the corrosion rate (*CR*) using Equation 4.2.

$$R_p = \frac{\Delta E}{\Delta i} = \frac{b_a \times b_c}{2.303 \times i_{corr}(b_a + b_c)}$$
(Eqn. 4.1)

$$CR = \frac{0.13 \times i_{corr} \times EW}{A \times d}$$
(Eqn. 4.2)

where R_p is the polarization resistance, Ω-cm^2; ΔE is the change in applied potential relative to corrosion potential E_{corr}, mV; Δi is the current response to applied potential spectrum, mA; i_{corr} is the corrosion current, μA; b_a, b_c are the anodic and cathodic Tafel slopes respectively, mV; *CR* is the corrosion rate in milli-inch per year

(mpy); *EW* is the equivalent weight of iron, 27.92 g; A is the surface area of the anode, cm^2; and *d* is the density of iron, 7.8 g/cm^3.

4.5   ACOUSTIC EMISSION CORROSION DETECTION MECHANISM

During the corrosion process, the metallic iron is transformed into rust which has a volume of 2 to 6 times the volume of the original metal consumed in the reaction (Broomfield 1997). This increase in volume creates stresses due to expansion which induce cracking when they exceed the tensile strength of concrete. Corrosion is usually accelerated after cracking and later spalling of the concrete cover occurs exposing the reinforcing steel (Song and Shayan 1998). The applicability of AE for corrosion detection emanates from its high sensitivity to crack formation. In other words, AE can detect micro-cracking resulting from corrosion initiation which by extension leads to early corrosion detection. Recent publications, which used AE sensors attached directly to steel prestressing strands and rebars immersed in solution to detect corrosion, indicated that AE was able to detect the accumulation of salts and rupture of passive oxide films (Perrin et al. 2010; Prateepasen and Jirarungsatian 2011). Regardless that such emissions may be weak in concrete due to attenuation, it demonstrates the ability of AE as a suitable candidate for early corrosion detection. In addition, AE is suitable for quick and effective global structural health diagnosis using a proper sensor layout, unlike most conventional electrochemical techniques which give only local assessments (ElBatanouny 2012). The location of damage can also be determined using source triangulation techniques (Mangual et al. 2012; Mangual et al. 2013).

4.6 CORROSION DETECTION USING AE: CASE STUDIES

A review map summarizing the studies that have been conducted to investigate the ability of AE to detect corrosion in concrete was created as shown in Figure 4.1. The map divides the studies according to the type of specimen, specimen size, type of AE sensors, corrosion benchmarks and AE parameters that have been used. Each study is given a number and is cited using this number under the relevant groups. These studies are discussed in details in the following sections.

4.6.1 Conventional parameters

For corrosion detection using AE, conventional parameters which can be directly measured from the detected signals, such as number of hits and number of events, were initially investigated. In 1982, a study was conducted on six reinforced concrete (RC) specimens with dimensions of 150x150x510 mm (6x6x20 in.) (Weng et al. 1982). Each specimen was monitored using two sensors placed on the specimen ends while being subjected to accelerated corrosion testing (impressed voltage). An increase in both the rate of current and AE counts were observed at day 10, as seen in Figure 4.2, which was four days before visual cracking. This early increase was interpreted as a result of micro-cracking or progressive formation of corrosion products. To examine the ability of AE in natural corrosion circumstances (not accelerated), another test was included in the study. Five RC cylinders of 100 mm (4 in.) diameter and 560 mm (22 in.) length were immersed in 100 mm (4 in.) natural sea water for approximately 2.3 years. Potential measurements indicated that four of the specimens experienced active corrosion while the fifth specimen remained passive. Each specimen was monitored with one AE sensor at its mid-height for two weeks to assess the ability of AE to identify their condition. AE was able to

differentiate between noble and active specimens as the noble one exhibited lower AE activity.

In 1995, Zdunek and Prine tested a 300x300x300 mm (one-cubic-foot) RC block which had three rebars of 25 mm (1 in.) diameter; a top rebar at a depth of 25 mm (1 in.) and two bottom rebars at a depth of 250 mm (10 in.) from the top surface. To investigate the corrosion of the top rebar, the specimen was subjected to a cycle of 3 days wet/ 4 days dry for two months using 15% NaCl solution. AE activity was recorded using sensors attached to the ends of the top rebar in addition to electrochemical measurements that were recorded weekly. As seen in Figure 4.3, an increase in AE events was detected after 20 days (480 hours) from exposure which was related to corrosion initiation. The electrochemical results showed that corrosion initiated after 20 days when electrochemical impedance spectroscopy (EIS) was used while galvanic current and HCP readings indicated corrosion after 32 days. These results indicate that AE can detect corrosion earlier than most electrochemical techniques (Figure 4.3).

Li et al. (1998) correlated the corrosion rate with the acoustic emission rate through the corrosion of mild steel rebar of 20mm (0.8 in.) diameter and 400 mm (16 in.) length in HCl solution. Corrosion of steel rebars was investigated using three different approaches; rebar alone, rebar coupled with copper, and rebar with anodic current polarization. Each test was conducted using different concentrations of HCl solution of 1%, 5%, 10% and 15%. Specimens were observed using 12 channel AMS3 system (one sensor per specimen) and accumulated AE events were computed. The AE rate was found to increase with the increase of HCl solution concentration (Figure 4.4). In addition, AE activity of the polarized rebars was higher than that of rebar coupled with copper and

both were higher than the AE activity for the rebar standing alone (at the same concentration of HCl solution for the three specimens). These observations verify that AE activity is proportional to the corrosion rate. Further investigations of the corrosion process of rebar in concrete were included in the same study (Li et al. 1998). The test included three concrete blocks with dimensions of 300x300x175 mm (12x12x7 in.). Each block had three deformed rebars of 25 mm (1 in.) diameter. The blocks were subjected to wet-dry cycles using 15% NaCl solution (3 days wet and 4 days dry) for three months. Three sensors were used to monitor the corrosion progression of the top rebar which was at 25 mm (1 in.) from the top of the concrete block. Two sensors spaced by 25 mm (1 in.) were placed on one end of the top rebar and the third one was attached to the other end. The galvanic current and half-cell potential were also measured. The accumulated number of AE events showed a high rise at 20 days into the test, which was related to the initiation of micro-cracking. The galvanic current did not increase significantly until 32 days of exposure, at this time the HCP readings were more negative than -420 mV. This shows that AE was able to detect corrosion earlier than galvanic current and HCP measurements. Figure 4.5 shows AE versus galvanic current readings.

Idrissi and Limam (2003) studied the possibility of using AE to determine the concrete quality in terms of porosity through an accelerated corrosion test. Polarization tests were performed on reinforced mortar cylinders (water, cement and sand) of 30 mm (1.2 in.) diameter and 90 mm (3.6 in.) length, reinforced with carbon steel (XC48) with a diameter of 5 mm (0.2 in.). Some of the specimens were made using a standard mix (water cement ratio of 0.5) while the remaining specimens were made using a porous mix (water cement ratio of 0.75). The working electrode (the specimen), as well as counter

65

and reference electrodes were placed in 6% NaCl solution. AE activity was monitored through a resonant R15 sensor (resonant frequency of 150 kHz) placed at the end of the reinforcing bar. AE for the porous mortar showed high activity shortly after it was immersed in the solution unlike the standard mortar which exhibited a delay of 10 hours. These results verify the higher corrosion activity in the porous mortar. The measured current showed the same behavior as AE activity for the two specimen types (Figure 4.6 and 4.7).

Similar tests using the same experimental device and mortar mixes were performed by Assouli et al. (2005) except that simulated concrete pore solution (SCP), containing chloride ions for some specimens, was used instead of NaCl solution and a broad band sensor (WD) was used instead of the resonant sensor used in the previous study (Idrissi and Limam 2003). Specimen behavior was monitored during heating-cooling cycles which reproduce carbonation in the presence of chloride ions. For the test that included a solution with chloride ions AE activity (cumulated events number) increased with the heat treatment cycles while for the case of solution without chloride AE activity remained comparatively weak as seen in Figure 4.8. In the presence of chloride ions, half-cell potential and pH measurements showed that corrosion probability increases with the increase of the number of heat treatment cycles. These results indicated that higher levels of corrosion are associated with higher number of cumulated events.

The previous studies investigated corrosion of steel in reinforced concrete. Ramadan et al. (2008) examined the stress corrosion cracking (SCC) of 12.5 mm (0.5 in.) diameter high strength steel (eutectoid cold drawn steel) in a simulated concrete pore (SCP) solution. The SCP solution had high alkalinity (pH≈12) and was contaminated by

sulphate, chloride and thiocyanate. The specimen was monitored by 4 wide band (WD) sensors and tested under a constant tensile load until the wires broke (Figure 4.9). The cumulated AE hits by the different sensors are shown in Figure 4.10. No significant AE activity was detected until cracks initiated. AE activity was divided into three zones as shown in Figure 4.10. Zone A was related to nucleation of cracks due to localized corrosion; pits and crevices. Zone B was related to propagation of cracks and zone C to steel failure. SEM photographs showed that pitting and crevice corrosion exists near the fracture section of the tested sample.

4.6.2 Condition assessment methods

The mechanism of crack propagation during the corrosion of steel in concrete was investigated by applying Simplified Green's functions for moment tensor analysis (SiGMA) on the AE events (Farrid Uddin et al. 2003). An expansive agent was implanted into a 30mm (1.2 in.) diameter hole in a concrete specimen to simulate the cracking process due to corrosion. The specimen had the dimensions of 250x250x100 mm (10x10x4 in.) with 40 mm (1.6 in.) cover. Six AE broadband sensors (PAC, UT 1000) were used to monitor the specimen. AE-SiGMA analysis was carried out at four stages chosen during the experiment based on AE behavior. Using virtual reality modeling language (VRML), 3D-visualization of AE-SiGMA analysis results was performed. Crack locations and types at each stage were modeled and mapped as shown in Figure 4.11. The results supported the crack orientations developed by a two-domain boundary element method (BEM). Visual observation of the crack traces also agreed with AE-SiGMA; as crack trace 1 in Figure 4.12 was first detected and then cracks traces 2 and then 3. The difficulty with SiGMA analysis is the large number of sensors required

(sensor density) and the high resolution of the waveforms which limits its applicability to actual field structures.

The applicability of using AE for corrosion detection in RC specimens was also investigated by Ohtsu and Tomoda (2008). The specimen size was 400x250x100 mm (16x10x4 in.) with steel bars of 13 mm (0.5in.) diameter placed at 15 mm (0.6 in.) from the concrete surface. The initial measured chloride content was 0.125 kg/m^3(0.0078 lb/ft^3) in volume, 0.039% mass of cement, which is lower than the threshold of 0.3 kg/m^3 (0.019 lb/ft^3) described in the Japanese code (JSCE 2001) for initiation of corrosion. All surfaces of the specimens were covered with epoxy resin except the bottom surface. Both accelerated corrosion testing and cyclic wet-dry testing (week wet/ week dry) were performed using 3% NaCl solution. For AE monitoring, two broadband AE sensors were placed at the upper surface of each specimen. During the accelerated corrosion test (impressed current), two periods of high AE activity were detected (at 3 days and 7 days into the test) and were correlated to the onset of corrosion and nucleation of cracking. The HCP measurements started decreasing at the first high period but did not reach a value more negative than -350 mV, which corresponds to 90% probability of corrosion (ASTM C867), until 2 days after the second high period (Figure 4.13). The chloride concentration was estimated experimentally after each of the two high AE activity periods and at the end of the test and was calculated analytically for the whole test. The high AE activity periods coincided with the passing of the two thresholds proposed by the Japanese code (JSCE 2001) for onset of corrosion and for the performance based design; 0.3 kg/m^3 (0.019 lb/ft^3) and 1.2 kg/m^3 (0.075 lb/ft^3) respectively (Figure 4.14). As seen

in Figure 4.14, AE behavior matched the typical phenomenological model of corrosion loss stated for steel in sea water (Figure 4.15).

For the cyclic wet-dry test that was included in that study on similar specimens (Ohtsu and Tomoda 2008), one high AE activity period was observed at 40 days; at the same time chloride concentration exceeded the threshold of 0.3 kg/m^3 (0.019 lb/ft^3) and long before HCP readings indicated a high probability of corrosion. Other AE parameters were also investigated during this test; RA value, average frequency and b-value. These parameters can be calculated using Equations 4.3, 4.4 and 4.5, respectively; where N is the number of events, A is the amplitude, α is an empirical constant and b the value used here for corrosion characterization (large b-value indicates more AE events with small amplitude and vice versa). At 40 days where AE showed high activity, the RA value was high and the average frequency was low which corresponds to other than tensile cracks (Figure 4.16). At approximately 100 days where HCP measurements started decreasing, lower RA values and relatively high average frequency were observed which correlated to nucleation of tensile cracks. Lower b-value was also observed at the same time which indicates significant damage. High b-value was also related with corrosion initiation at 40 days as seen in Figure 4.17. The results were confirmed by visual and scanning electron microscopy (SEM) observations.

RA= rise time/ maximum amplitude $\hspace{6cm}$ (Eqn. 4.3)

Average frequency = counts/duration $\hspace{5.5cm}$ (Eqn. 4.4)

$log_{10}N = \alpha - blog_{10}A$ $\hspace{6.5cm}$ (Eqn. 4.5)

Corrosion stages were also identified by AE in another study on RC specimens with the size of 100x75x400 mm (4x3x16 in.), reinforced with one deformed rebar of 13

mm (0.5 in.) diameter and 20 mm (0.8 in.) cover (Kawasaki et al. 2010). Cyclic wet-dry testing was performed; one week in wet condition using 3% NaCl solution and one week in dry condition. AE activity was monitored through six R15, PAC sensors of 150 kHz resonance. Half-cell potential readings dropped to -350 mV after 126 days. This point was chosen to separate the test duration into two stages. Stage 1 was correlated to phase one and two on the phenomenological model of corrosion loss (Figure 4.15) and stage 2 was correlated to phase three and four. Improved *b*-value (*Ib*-value) was estimated for 100 AE hits using Equation 4.6; where σ is the standard deviation; μ is the mean value of the amplitude distribution; $N(\mu - \alpha_1\sigma)$ and $N(\mu - \alpha_2\sigma)$ are the number of hits with an amplitude higher than $\mu - \alpha_1\sigma$ and $\mu - \alpha_2\sigma$, respectively. *Ib*-value results showed two drops at 28 and 70 days in stage 1, also large events were observed at the same days. Stage 2 showed comparatively lower *Ib*-values which was related to high AE activity after 168 days (Figure 4.18). The drops of *Ib*-value in stage 1 were correlated with corrosion initiation and the lower *Ib*-values in stage 2 were correlated to nucleation of cracks. Crack locations and orientations were mapped using SiGMA analysis as seen in Figure 4.19. The events mapped in stage 2 are the ones that were related to corrosion as they were developed around the uncoated part of the rebar. The results were also correlated to SEM observations.

$$Ib = \frac{logN(\mu - \alpha_1\sigma) - logN(\mu - \alpha_2\sigma)}{(\alpha_1 + \alpha_2)\sigma} \qquad \text{(Eqn. 4.6)}$$

4.6.3 Quantification of corrosion using AE

The use of AE intensity analysis for quantification of corrosion damage has been recently proposed (ElBatanouny et al. 2011; Mangual et al. 2013). An AE intensity analysis chart for corrosion quantification was developed using results of accelerated

70

corrosion tests on eleven pre-cracked concrete specimens (Mangual et al. 2013). The specimens had dimensions of 115x115x510 mm (4.5x4.5x20 in.), reinforced with a central low-relaxation prestressing strand with a diameter of 13 mm (0.5 in.) and 50mm (2 in.) cover. The specimens were pre-cracked at the centerline to a crack width of 0.016 in. (0.4 mm) to allow the penetration of 3% NaCl solution and were subjected to constant potential during the test. The strands were not stressed to simulate the case of corrosion after cracking of concrete; in which the prestressing force would be diminished. Three 55 kHz resonant sensors (R6i) were attached to eight specimens to allow source allocation while the other three specimens were monitored with two sensors placed beside the central crack. Onset of corrosion and nucleation of cracking was detected using cumulative signal strength (CSS) corroborated with HCP measurements. AE source location showed that most of the damage occurred at the mid-section, where the crack exists. Corrosion quantification based on intensity analysis was proposed. Two indices were calculated to determine the intensity of AE; historic index, $H(t)$, and severity, S_r (Fowler et al. 1989). Historic index compares the signal strength of the most recent hits to the value of cumulative hits and can be calculated using Equation 4.7. Severity is defined as the average signal strength for the 50 events having the largest numerical value of signal strength and is calculated using Equation 4.8. An intensity analysis chart is developed as severity versus historic index and is divided into different regions that correspond to different levels of damage. Points of significant damage are plotted to the top right corner of the chart. In this study (Mangual et al. 2013), the chart was divided into four regions; region A corresponds to the passive condition, region B to de-passivated steel with measured experimental sectional losses less than 15%, region C for

corroded specimens with thin cracks and sectional loss extending to 21% and region D for specimens exhibiting severe longitudinal cracking and sectional loss between 23 and 28%. Figure 4.20 shows the resulted grading for the specimens, using data gathered by the sensor at the mid-section, along with their sectional loss.

$$H(t) = \frac{N}{N-K} \frac{\sum_{i=K+1}^{N} S_{oi}}{\sum_{i=1}^{N} S_{oi}}$$
(Eqn. 4.7)

$$S_r = \frac{1}{50} \sum_{i=1}^{i=50} S_{oi}$$
(Eqn. 4.8)

The same test setup and specimen size were used in another study except that the specimens were un-cracked (Mangual et al. 2012). The study included nine specimens that had different test durations varying from 43 to 350 hours. Intensity analysis was performed and the chart was divided into two regions according to HCP readings; region A for passive condition and region B for specimens that experienced onset of corrosion (although the corrosion was at an early stage) as shown in Figure 4.21. The trend of the data points agreed with the amount of damage concluded visually and using the experimental mass loss. The attenuation of AE signals in un-cracked specimens is smaller than that for cracked specimens, thus the chart boundaries are different in these two cases.

Intensity analysis was applied to long term corrosion testing on prestressed T-girders by ElBatanouny (2012). The specimens measured 4.98 m (16 ft. 4 in.) in length and were reinforced with two low-relaxation strands of 13 mm (0.5 in.) diameter. Three specimens were subjected to wet/dry cycles (3 days wet/ 4 days dry) using a 3% NaCl solution at the central part of the specimens. Two of the tested specimens (CC-0.8 and CC-0.4) were pre-cracked to crack widths of 0.4 mm and 0.8 mm, respectively. Four R6i resonant sensors (55 kHz) were attached to the surface of each specimen. Intensity

72

analysis was carried out for the two pre-cracked specimens using the chart boundaries developed by Mangual et al. (2013). The data point for specimen CC-0.8 was further towards the top-right of the chart (region D) as compared to specimen CC-0.4 (region C), as shown in Figure 4.22, which demonstrates more corrosion damage in CC-0.8. The LPR method indicated the same results as the intensity analysis. It is worth noting that the same chart boundaries (developed by Mangual et al. (2013) for cracked prestressed specimens) showed successful damage classification on different specimen sizes (small and medium scale specimens) and on different event rates (accelerated corrosion test and long term corrosion test).

4.7   EXTRAPOLATING RESULTS TO THE FIELD

All the reviewed studies were laboratory tests conducted on small scale specimens with the exception of ElBatanouny (2012) which included medium scale prestressed T-girders. AE intensity analysis enables quantification of corrosion damage in small and medium scale specimens using the same damage classification boundaries. This demonstrates that the method may be independent of specimen size which is an important advantage for field implementations. However, filtering is a crucial step to clean data from noise and wave reflections, especially for small scale specimens. It is recommended to set data collection threshold and parameters, for example hit lockout time (HLT) and hit definition time (HDT), to be similar to the reported values in the AE intensity analysis studies (ElBatanouny 2012, Mangual et al. 2013).

The sensor density (number of sensors per volume) used in all the studies that have investigated the use of AE to detect corrosion in concrete specimens is shown in Figure 4.23. As seen in the figure, intensity analysis used the least number of sensors per unit

volume. On the other hand, SiGMA analysis used the highest sensor density among the proposed methods. The number of sensors required to assess corrosion in real structures is an important factor for deciding which methods can be realistically employed. For example, using SiGMA analysis in field is questionable as this method requires a large number of sensors in a small area; each event has to be detected by six sensors placed in different planes to be plotted using SiGMA analysis.

In the field, AE activity will arise from different sources such as cracking due to loading, corrosion, friction between bearing pads and the structure, etc. Therefore, successful identification of AE activity from corrosion is essential. This may be accomplished by comparing the AE waveforms from different sources and using filters to identify corrosion related signals. Up to now, such methods do not exist, which compromises the applicability of AE to some structural members (superstructures). Piles and bent caps are less susceptible to AE activity from loads; therefore employing AE to detect corrosion in such members is more feasible at the present time.

4.8   CONCLUSIONS

1. Acoustic emission can detect the onset of corrosion and nucleation of cracking before most electrochemical methods such as half-cell potential and galvanic current. Corrosion initiation and cracking can be identified by two periods of high AE activity. Conventional parameter such as counts, number of hits, cumulative event number and cumulative signal strength were successfully used for this purpose. Condition assessment methods such as b-vale and Ib-value were also correlated to the corrosion activity.

2. Nucleation of tensile cracking due to corrosion was detected using the relationship between RA values and average frequencies. However, further research should investigate the feasibility of using this method to classify AE sources.

3. AE can effectively locate the corrosion damage by using source location techniques which enables owners to perform repairs.

4. SiGMA analysis can be used for mapping the location, type and orientation of cracks developed in the process of corrosion in RC specimens. However, the applicability of this method in field is questioned due to the large number of sensors required.

5. Quantification of corrosion damage can be performed using intensity analysis chart. The scale and event rate effects may not exert a significant influence on intensity chart criteria. However, more investigation is needed to establish the proposed damage classification boundaries in field.

The reported studies prove that AE is a suitable candidate for early corrosion detection. Unlike standard electrochemical techniques, AE is non-intrusive and enables global monitoring of a structural member with the ability to locate damage for further assessment. The method is passive, does not need external stimuli once the sensors are in place, which makes it suitable for long term deployment. The results of this study can be used by future researchers to determine the most effective AE techniques for corrosion detection and quantification.

4.9 RECOMMENDATIONS

Further studies should be conducted for verifying the behavior of AE parameters due to corrosion process in different types of concrete specimens and setting limits for corrosion quantification. Future researchers should put emphasis on classifying AE source by differentiating between AE signals due to corrosion and signals due to load related deteriorations. This classification would broaden the application of AE for monitoring in-service structures and provide sufficient justification for maintenance decisions. Studying the characteristics of AE signals (waveforms) produced in the two cases is a possible approach to achieve reliable source classification.

4.10 REFERENCES

ACI Committee 222. (2001). "Protection of Metals in Concrete Against Corrosion", ACI 222R-01, American Concrete Institute, Farmington Hills, Michigan, 41 pp.

Andrade, C., Alonso, M.C., Gonzalez, J.A. (1990). "An initial effort to use corrosion rate measurements for estimating rebar durability corrosion rates of steel in concrete." ASTM STP 1065, N.S. Berke et al. editors, ASTM, Philadelphia, 29-37.

Assouli, B., Simescu, F., Debicki, G., and Idrissi, H. (2005). "Detection and identification of concrete cracking during corrosion of reinforced concrete by acoustic emission coupled to the electrochemical techniques." NDT & E International, 38(8), 682-689.

ASTM C876. (2009). "Standard Test Method for Half-Cell Potentials of Uncoated Reinforcing Steel in Concrete." American Standard for Testing and Materials, 1-7.

ASTM G59. (1997-Reapproved 2009). "Standard Test Method for Conducting Potentiodynamic Polarization Resistance Measurements," American Standard for Testing and Materials, 1-4.

Bennett, J.E., and Mitchell, T.A. (1992). "Reference Electrodes For Use With Reinforced Concrete Structures, Corrosion 92-Nace, Paper191.

Broomfield, J.P., Rodriguez, J., Ortega, L.M., and Garcia, A.M. (1993). "Corrosion rate measurement and life prediction for reinforced concrete structures, In: Proceedings Of Structural Faults and Repairs-93, vol.2: pp.155 (Engineering Technical Press, University of Eidenbugh).

Broomfield, J.P., Rodriguez, J., Ortega, L.M. and Garcia, A.M. (1994). "Corrosion rate measurements in reinforced concrete structures by a linear polarization device, In: R.E. Weyers (ed.) Symposium on Corrosion of Steel in Concrete, Special Publication: SP 151-9, pp.163.

Broomfield, J.P. (1997). "Corrosion of Steel in Concrete, Understanding, Investigation and Repair", (Chapman and Hall).

Clear, K.C. (1989). "Measuring the rate of corrosion of steel in field concrete structures", Transportation Research Record 1211, (Transportation Research Board, National Research Council, Washington, DC.

ElBatanouny, M., Mangual, J., Ziehl, P., and Matta, F. (2011). "Corrosion Intensity Classification in Prestressed Concrete using Acoustic Emission Technique." Proc. American Society for Nondestructive Testing (ASNT) Fall Conference and Quality Testing Show 2011, Palm Springs, CA.

ElBatanouny, M.K. (2012). "Implementation of Acoustic Emission as a Non-Destructive Evaluation Method for Concrete Structures." Dissertation, Department of Civil and Environmental Engineering, University of South Carolina, Columbia, SC, 184.

Farid Uddin, A. K. M., Numata, K., Shimasaki, J., Shigeishi, M., and Ohtsu, M. (2004). "Mechanisms of crack propagation due to corrosion of reinforcement in concrete by AE-SiGMA and BEM". Construction and Building Materials, 18(3), 181-188.

Flis, J., Sehgal, A., Li, D., KHO, Y.T., Sabotl, S., Pickering, H., Osseo-Assare, K., and Cady, P.D. (1992). "Condition Evaluation of Concrete Bridges Relative to Reinforcement Corrosion", vol.2, method for measuring the corrosion rate of reinforcing steel, Natural Research Council, Washington, DC, SHRP-S/FR-92-104.

Fowler, T.J., Blessing, J., Conlisk, P., and Swanson, T.(1989). "The MONPAC Procedure." Journal of Acoustic Emission, 8(3), 1-8.

Heidersbach, R. (1986). "Corrosion Performance of Weathering Steel Structures", California Polytechnic State University, San Luis Obispo. Metallurgical Engineering Dept.

Idrissi, H., and Limam, A. (2003). "Study and characterization by acoustic emission and electrochemical measurements of concrete deterioration caused by reinforcement steel corrosion". NDT & E International, 36(8), 563-569.

Isecke, B. (1982). "Collapse of the Berlin Congress Hall Prestressed Concrete Roof", Materials Performance, PP. 36-39.

JSCE Concrete Committee. (2001). "Standard Specifications for Concrete Structures—Maintenance," Guidelines for Concrete, No. 4, Japan Society of Civil Engineers, 170 pp.

Kawasaki, Y., Tomoda, Y., and Ohtsu, M. (2010). "AE monitoring of corrosion process in cyclic wet–dry test". Construction and Building Materials, 24(12), 2353-2357.

Koch, G. H., Brongers, M. P. H., Thompson, N. G.,Virmani, Y. P., and Payer, J. H. (2001). "Corrosion costs and preventive strategies in the United States". FHWA-RD-01-156. Federal Highway Administration, Washington, D.C., 2001.

Li, Z., Li, F., Zdunek, A., Landis, E., and Shah, S. P. (1998). "Application of Acoustic Emission Technique to Detection of Reinforcing Steel Corrosion in Concrete," ACI Materials Journal, V. 95, No. 1, pp. 68-76.

Mangual, J., ElBatanouny, M.K., Ziehl, P., and Matta, F. (2012). "Corrosion Damage Quantification of Prestressing Strands Using Acoustic Emission." ASCE Journal of Materials in Civil Engineering, in press.

Mangual, J., ElBatanouny, M. K., Ziehl, P., and Matta, F. (2013). "Acoustic-Emission-Based Characterization of Corrosion Damage in Cracked Concrete with Prestressing Strand". ACI Materials Journal, 110(1), 89.

Melchers, R. E., and Li, C. Q. (2006). "Phenomenological Modeling of Reinforcement Corrosion in Marine Environments," ACI Materials Journal, V. 103, No. 1, Jan.-Feb., pp. 25-32.

NCHRP. (1998). "Durability of precast segmental bridges," NCHRP Web Document No. 15, Project 20-7/Task 92 (Editors: Poston, R.W. & Wouters, J.P.), National Cooperative Highway Research Program, Transportation Research Board, National Research Council, Washington, D.C., USA.

Novokshchenov, V. (1989). "Salt-Penetration and corrosion in Prestressed concrete Members", FHWA-RD-88-269.

Novokshchenov, V. (1997), Corrosion, 53(6): pp.489.

Ohtsu, M., and Tomoda, Y. (2008). "Phenomenological model of corrosion process in reinforced concrete identified by acoustic emission." ACI Materials Journal, 105(2).

Ono, K. (2010). "Application of Acoustic Emission for Structure Diagnosis." KonferencjaNaukowa, pp. 317-341.

Perrin, M., Gaillet, L., Tessier, C., and Idrissi, H. (2010). "Hydrogen embrittlement of prestressing cables." Corrosion Science, 52, 1915–1926.

Prateepasen, A., and Jirarungsatian, C. (2011). "Implementation of Acoustic Emission Source Recognition for Corrosion Severity Prediction." Corrosion, Vol. 67, No. 5, pp. 11.

Ramadan, S., Gaillet, L., Tessier, C., and Idrissi, H. (2008). "Detection of stress corrosion cracking of high-strength steel used in prestressed concrete structures by acoustic emission technique." Applied surface science, 254(8), 2255-2261.

Robson, A., and Brooman, H. (1997). "A3/A31 Flyover - Case History of an Externally Posttensioned Bridge," Proceeding of the Seventh International Conference on Structural Faults and Repair, Vol. 1, July 1997, pp. 307-315.

Song, G., and Shayan, A. (1998). "Corrosion of steel in concrete : causes, detection and prediction : a state-of-the-art review.", Vermont South, Vic. : ARRB Transport Research.

Trejo, D., Pillai, R.G., Hueste, M.B., and Reinschmidt, K.F. (2009). "Parameters Influencing Corrosion and Tension Capacity of Post-Tensioning Strands". ACI Materials Journal, 106(2), 144-153.

Videm, K. (1997). "Instrumentation and Condition Assessment Performed on Gimsoystraumen Bridge" In: Aage Blankvoll (ed.), Proceedings of International Conference-Repair Of Concrete Structures, From Theory To Practice In A MarineEnviroment, pp.375 (Norway).

Weng, M.S., Dunn, S.E., Hartt, W.H. Brown, R.P. (1982). " Application of acoustic emission to detection of reinforcing steel corrosion in concrete", Corrosion, 38 (1), pp. 9‑14.

Whiting, D., Stejskal, B., and Nagi, M. (1993). "Condition of Prestressed Concrete Bridge Components – Technology Review and Field Surveys," Publication No. FHWA-RD-93-037, Federal Highway Administration, McLean, VA.

Woodward, R.J. , and Williams F.W. (1988). "Collapse of Ynes-y-Gwas bridge, west Glamorgan", In: Proceedings Of The Institution Of Civil Engineers Part I, 84, PP.635-69.

Yunovich, M., and Thompson, N. (2003). "Corrosion of Highway Bridges: Economic Impact and Control Methodologies", ACI International, American Concrete Institute, Vol. 25, No.1, Detroit, USA, pp. 52-57.

Zdunek, A., and Prine, D. (1995). "Early Detection of Steel rebar Corrosion by Acoustic Emission Monitoring", Corrosion, Paper no. 547, ITI technical report no. 16, 1-9.

Ziehl, P. (2008). "Applications of Acoustic Emission Evaluation for Civil Infrastructure." SPIE Proc. SPIE Smart Structures NDE, San Diego, CA, 9.

Table 4.1: ASTM criterion for corrosion of steel in concrete (ASTM C867-09)

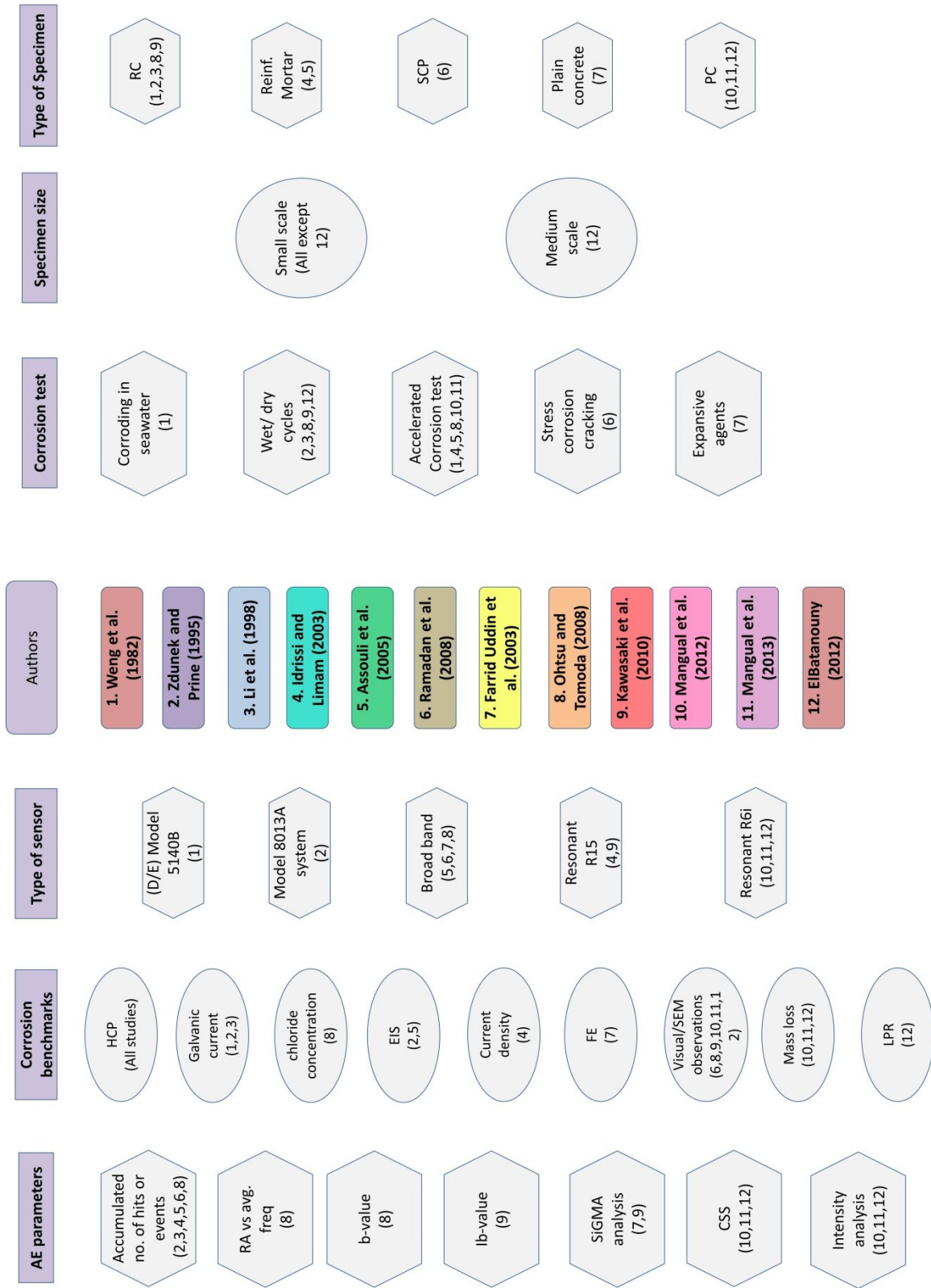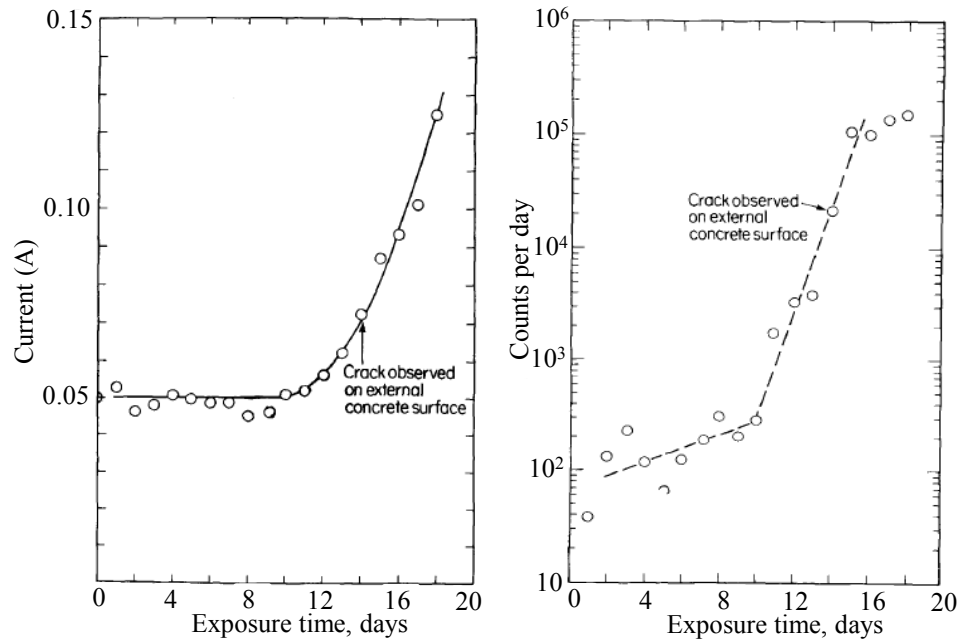| Measured Potential (mV/CSE)	Corrosion condition
> - 200	Low (10% risk of corrosion)
-200 to -350	Intermediate corrosion risk (uncertain)
< -350	High (90% risk of corrosion)

Figure 4.1:Review map

Figure 4.2: Impressed voltage test results on a RC specimen (Weng et al. 1982)
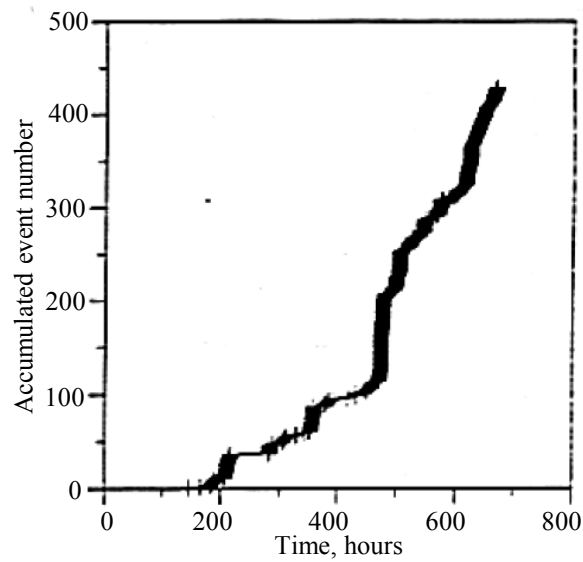
Figure 4.3: AE activity results versus time of exposure (Zdunek and Prine 1995)
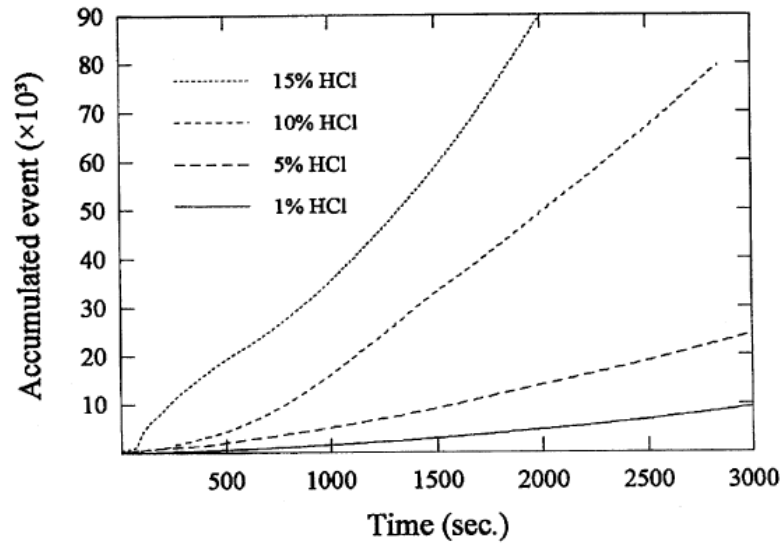
Figure 4.4: The influence of increasing the solution concentration on AE activity (Zongjin et al. 1998)
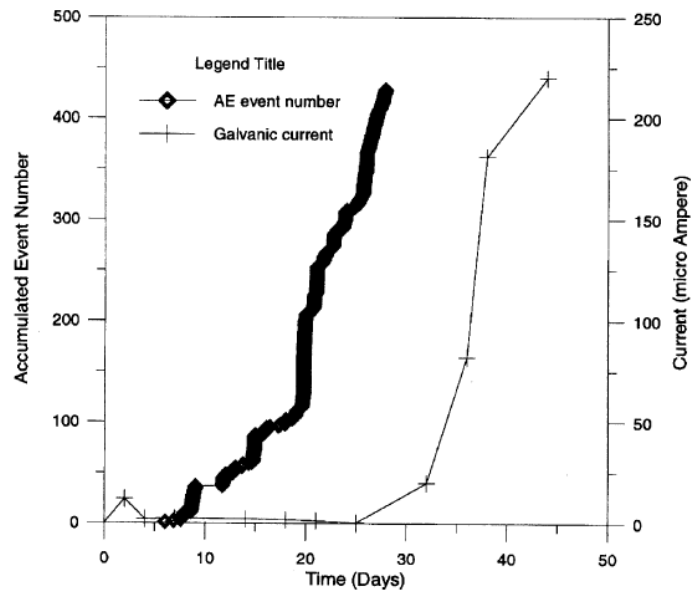
Figure 4.5: AE versus galvanic current readings (Zongjin et al. 1998)
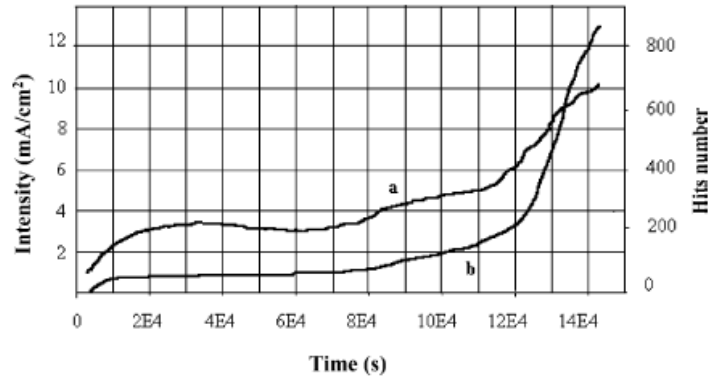
Figure 4.6: Current density (a) and AE activity (b) for standard mortar (Idrissi and Limam 2003)
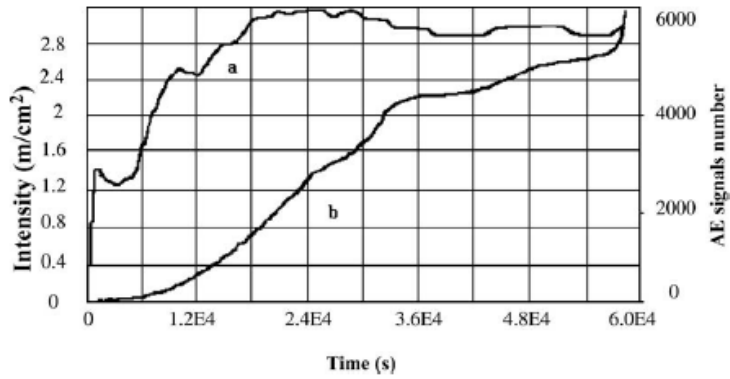
Figure 4.7: Current density (a) and AE activity (b) for porous mortar (Idrissi and Limam 2003)
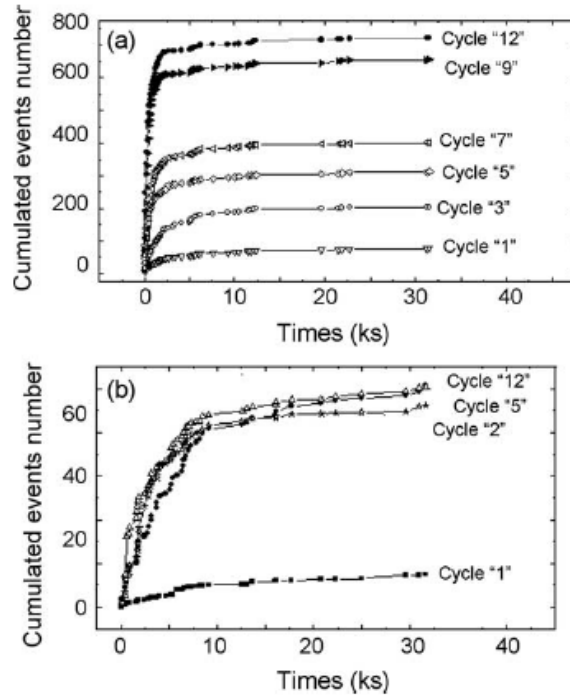
Figure 4.8: AE cumulated events curves for heat treatment cycles: a) with chloride, b) without chloride (Assouli et al. 2005)
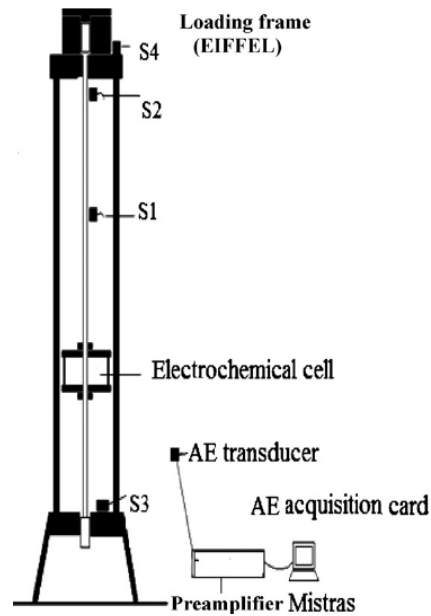
Figure 4.9: Test setup and sensors locations (Ramadan et al. 2008)
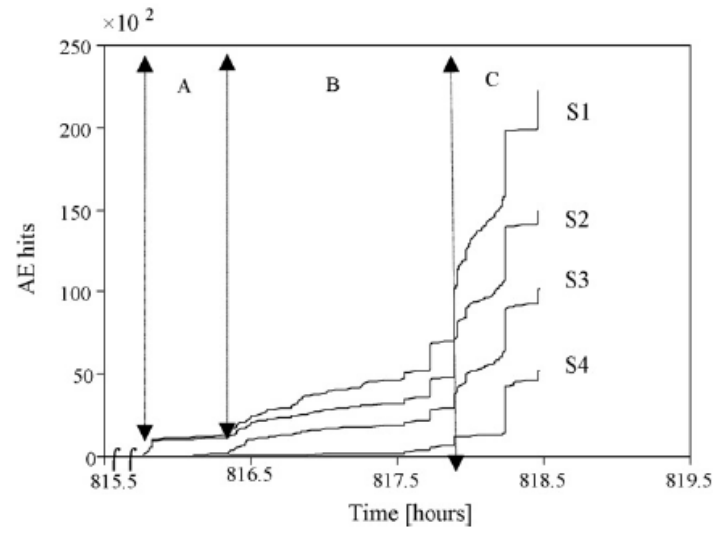
Figure 4.10: cumulative AE hits recorded during the test (Ramadan et al. 2008).

Shear crack   Tensile crack   Mixed-mode crack
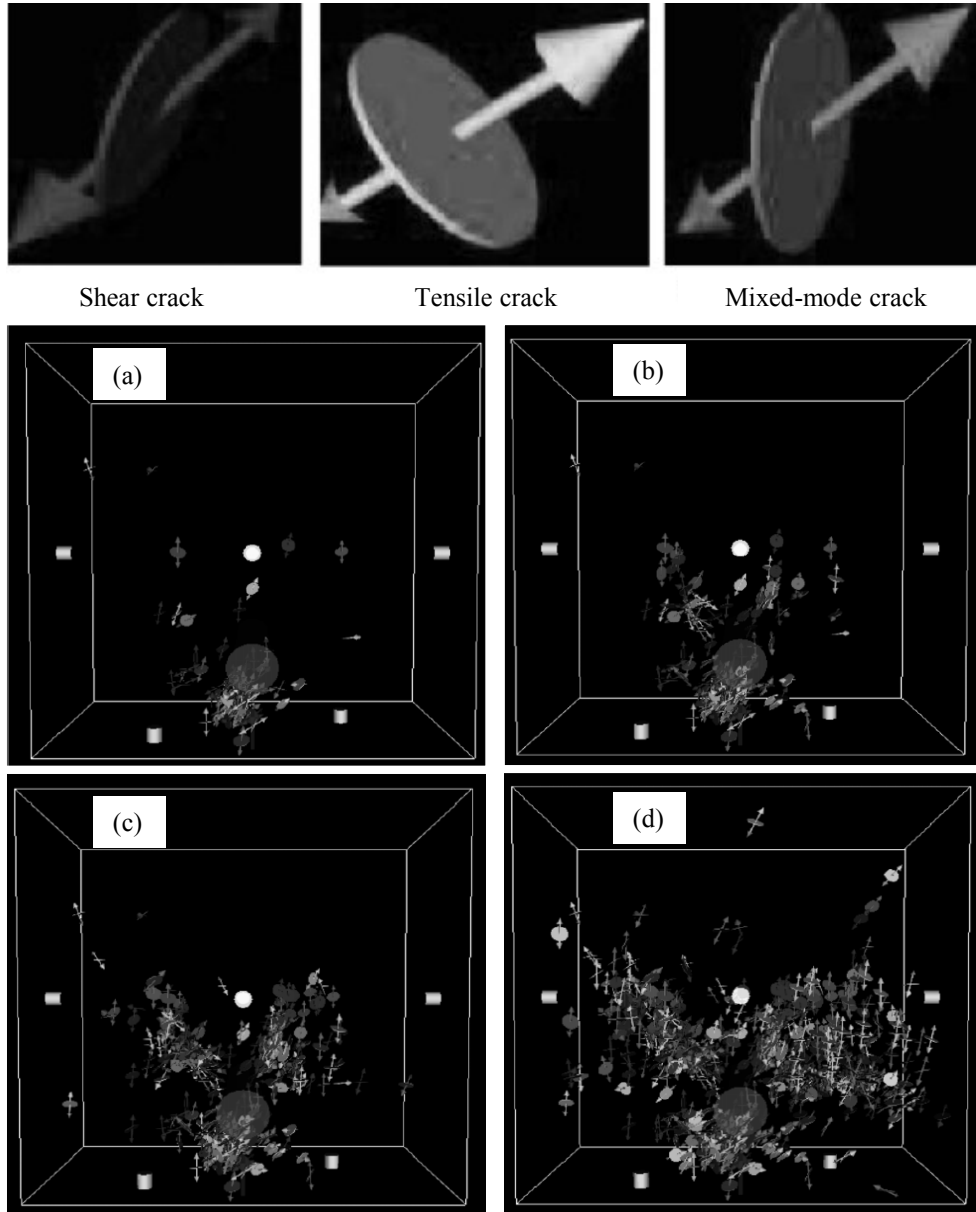
Figure 4.11: VRML visualization of AE-SiGMA; a) at stage 1, b) at stage 2, c) at stage 3, d) at stage 4 (Farrid Uddin et al. 2003).
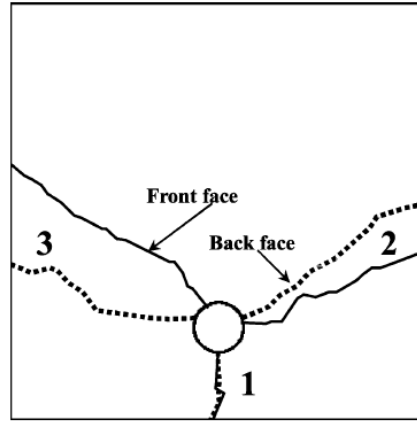
Figure 4.12: observed crack traces in the experiment (Farrid Uddin et al. 2003).
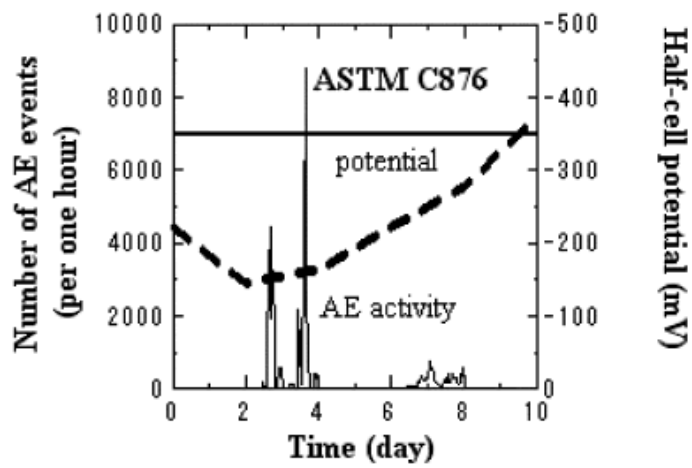
Figure 4.13: AE activity and half-cell potential in accelerated corrosion test (Ohtsu and Tomoda 2008).
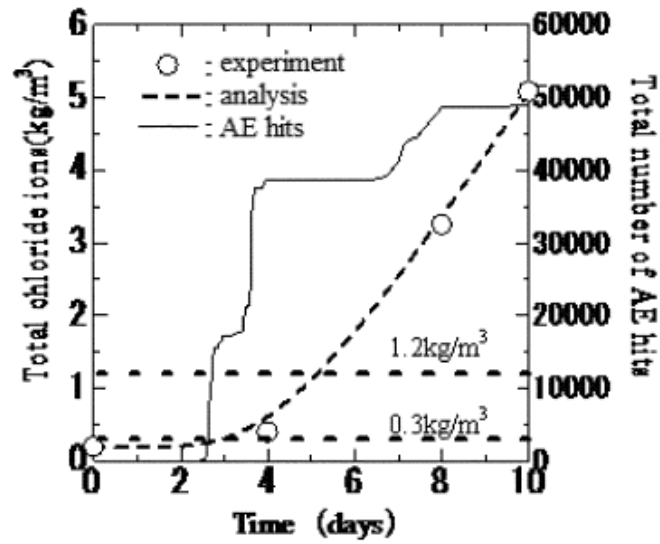
Figure 4.14: Total number of AE hits and chloride concentration (Ohtsu and Tomoda 2008)
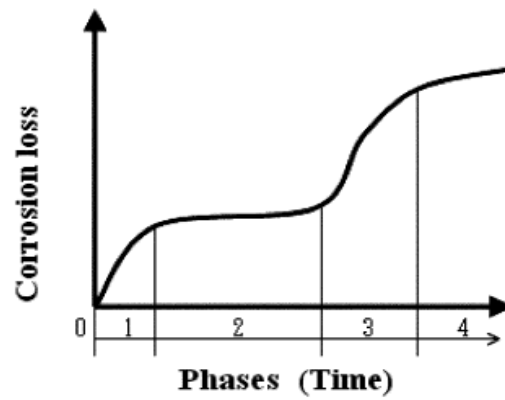
Figure 4.15: Typical corrosion loss of steel in seawater immersion (Melchers and Li 2006)
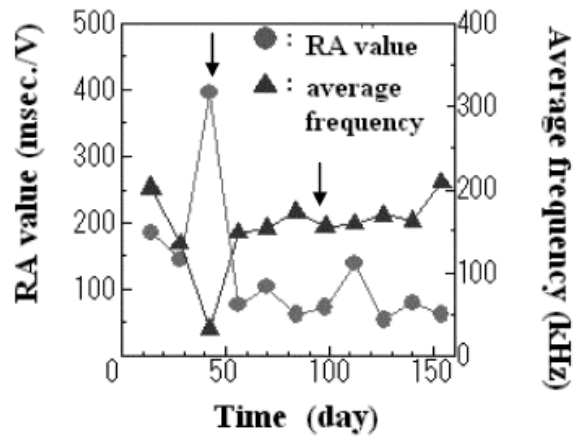
Figure 4.16: RA values and average frequencies in cyclic wet-dry test (Ohtsu and Tomoda 2008).
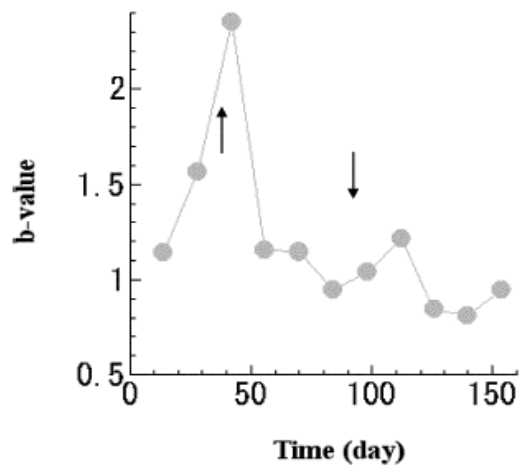
Figure 4.17: Variation of b-values in cyclic wet-dry test (Ohtsu and Tomoda 2008).
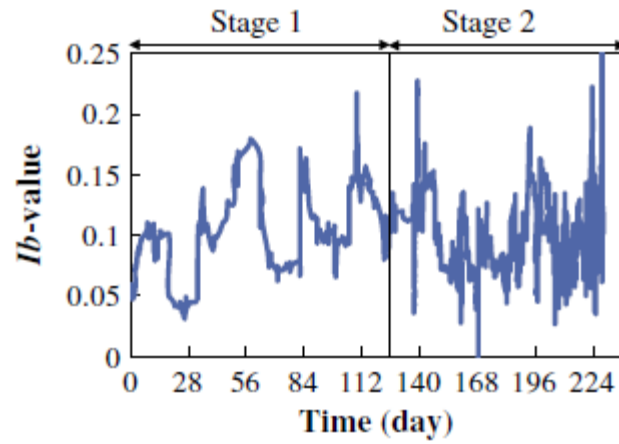
Figure 4.18: Results of Ib-value (Kawasaki et al. 2010).

(a) Stage 1

(b) Stage 2

(c) Total
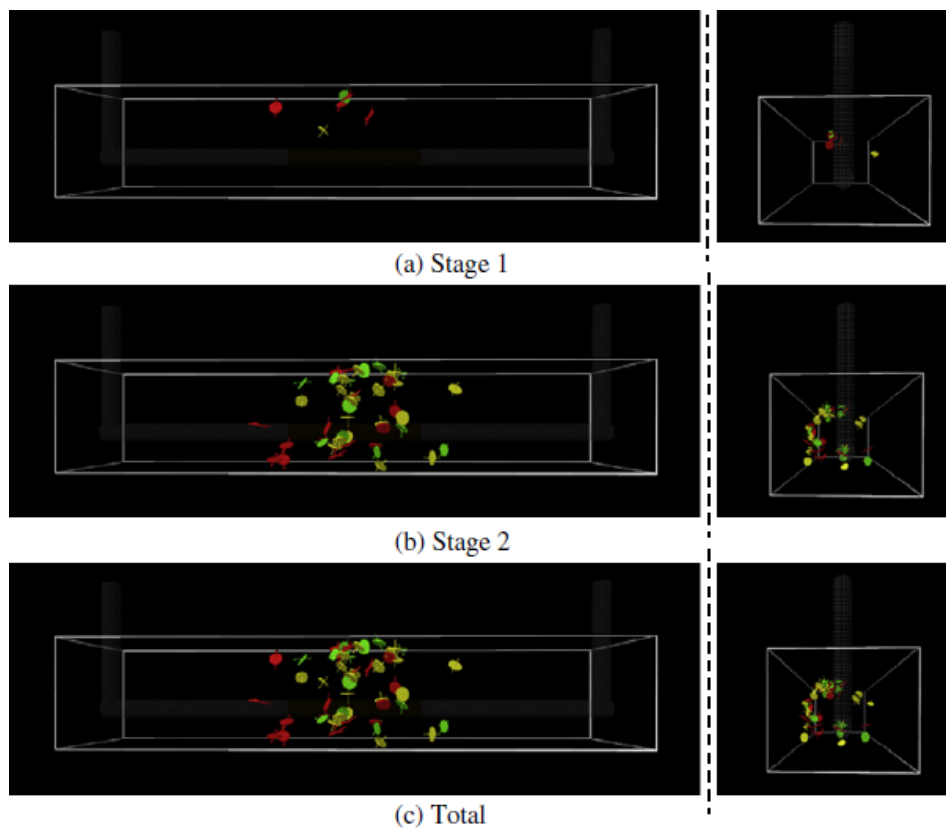
Figure 4.19: Results of SiGMA analysis (Kawasaki et al. 2010).
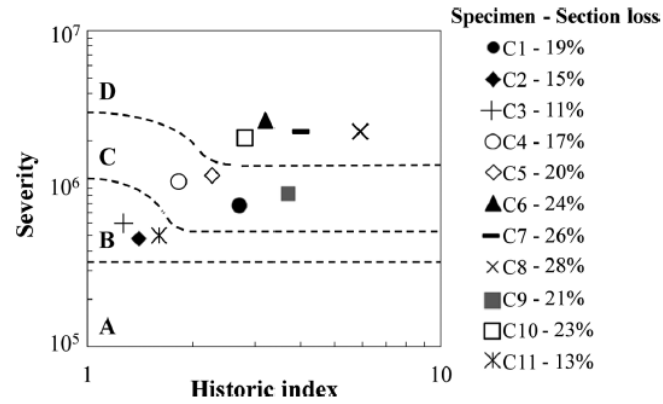
Figure 4.20: Results of damage classification using Intensity analysis for pre-cracked specimens (Mangual et al. 2013).
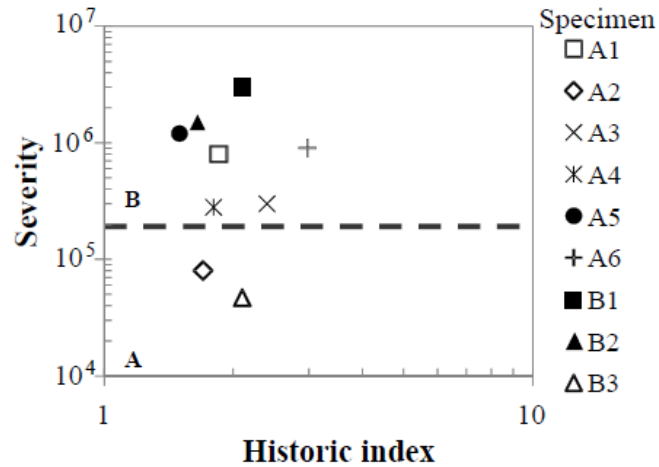
Figure 4.21: Intensity analysis results for un-cracked specimens (Mangual et al. 2012).
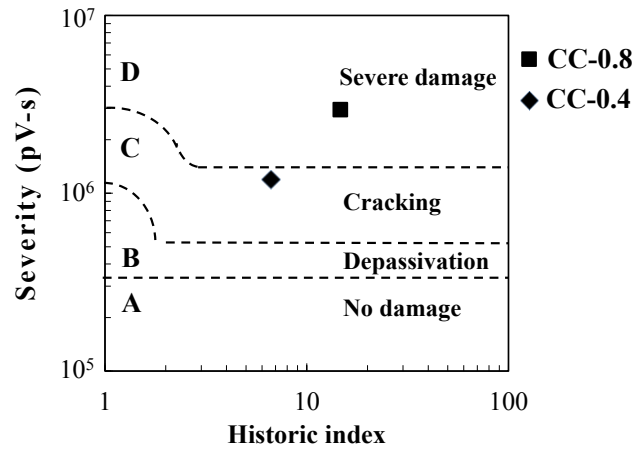
Figure 4.22: Intensity analysis results for cracked medium scale specimens (ElBatanouny 2012)
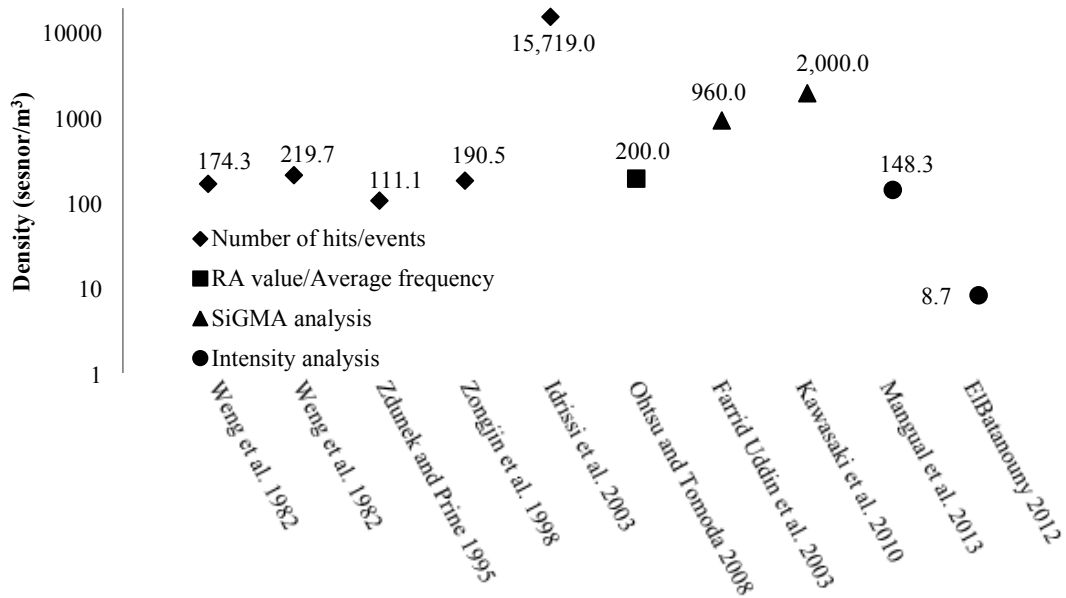
Figure 4.23: Density of AE sensors per concrete volume

CHAPTER 5

ACOUSTIC EMISSION BASED DAMAGE ASSESSMENT METHOD FOR PRESTRESSED CONCRETE STRUCTURES[3]

5.1 ABSTRACT

Eight prestressed specimens were subjected to cyclic load test while being monitored with acoustic emission (AE). Five of the specimens were pre-cracked and corroded to different levels, before conducting the test, to examine the ability of acoustic emission (AE) to detect damage for different structural conditions. Index of Damage introduced in a previous study based on the cumulative AE energy was investigated for damage assessment. The index values showed a clear correlation with the observed amount of damage. However, the method is constrained to laboratory applications as it requires the continuation of the test until the specimen surpass the level of maximum admissible damage. A modified index of damage (MID) is proposed in this study to ensure field applicability. The modified index showed promising results and enabled the detection of yielding point for both cracked and un-cracked specimens. Further work is needed to validate the acceptance thresholds and extrapolate the results to in-service structures.

Keywords: Cyclic load test, prestressed concrete, acoustic emission (AE), AE energy

5.2 INTRODUCTION

Deterioration of existing concrete structures has raised the need for advanced nondestructive testing (NDT) techniques to determine the current structural state of the members and to assist in the evaluation of repairs. NDT is also required for testing new structures to ascertain safety and serviceability of the members prior to service. Most of the classic NDT methods are only capable of detecting and, in some cases, imaging the apparent damage. Monitoring in-service structures with structural health monitoring

95

techniques such as acoustic emission (AE) can provide more insight to the behavior of concrete members and develop better diagnosis for the integrity of structures.

Many studies have investigated the feasibility of AE as a damage characterization technique for concrete structures (for example, Golaski et al. 2006; Aggelis et al. 2007; Shiotani et al. 2007; Ziehl et al. 2009; Ono 2010). The ability of AE to monitor crack formation and propagation has been proven by several studies for both reinforced and prestressed concrete (Xu 2008; ElBatanouny et al. 2012).

AE signals are gathered through sensors placed on the surface of concrete. Proper filtration of AE data should be carried out to discard non-genuine data before analysis. Different AE parameters and criteria have been proposed and evaluated in the literature for damage assessment. Several parameters have been developed based on the Kaiser Effect; the absence of detectable acoustic emission until previously applied load stress levels are exceeded, as the lack of this phenomenon can be considered an indication of damage (Kaiser 1953). Other criteria have been developed based on the different parameters measured from the waveforms such as signal amplitude, signal strength, frequency, etc. However, only a few studies have investigated the implementation of AE energy to develop a damage qualification method (Colombo et al. 2005; Benavent-Climent et al. 2011).

This paper examines the effectiveness of a damage index based on cumulative AE energy (Benavent-Climent et al. 2011) gathered during cyclic load testing (CLT) of prestressed girders. This load testing method has been proposed by ACI Committee 437 (ACI 2007) and includes a series of loading and unloading cycles with increasing magnitude up to a predefined maximum load level. The CLT method involves three

acceptance criteria based on load-deflection response for structural evaluation. The results of the CLT acceptance criteria for this study have been investigated by ElBatanouny (2012).

Most in-service structures have experienced different levels of damage. Some members could have encountered corrosion of reinforcing steel or may have developed cracks with various widths. The ability of acoustic emission to assess damage on members with different conditions should be examined. Therefore, five of the eight specimens in this study were preconditioned. These specimens were pre-cracked and corroded to different levels before the CLT test was conducted. AE was used to monitor the specimens during the CLT to investigate AE based damage evaluation methods for both pre-existing and newly developing damage. An existing damage assessment AE parameter based on AE cumulative energy, referred to as a damage index (Benavent-Climent et al. 2011), was examined. The results were used to propose a modification for this method to make it applicable for field conditions.

5.3 RESEARCH SIGNIFICANCE

Nondestructive evaluation (NDE) of in-service concrete structures is needed to monitor the ongoing deterioration and to assess the performance of repairs. Acoustic emission (AE) has proven to be a promising candidate as a damage assessment technique. However, its reliability is not well-established. Previous studies have been conducted on reinforced concrete (RC) members, but few investigations deal with prestressed concrete (PC). This paper examines the feasibility of a previously proposed AE parameter to quantify damage in PC flexural members. A critical modification to broaden the applicability of this parameter is also proposed. The results show the ability of AE to

97

detect damage and to provide a better understanding of the behavior of PC members with existing damage.

5.4   ACOUSTIC EMISSION

Acoustic Emission (AE) is the technique that detects and measures elastic waves initiated by a rapid release of energy from localized source within a material such as cracking or deformation (ASTM E 1316). The waveforms of AE signals (hits) include a number of parameters such as amplitude, duration, signal strength, and signal energy along with frequency information in the event that the waveform is digitized. AE is a highly sensitive technique (in the kHz range) which enables it to detect damage in the micro-cracking stage, long before it is visible. AE is a passive sensing technique by definition; therefore, it can be used for inspection by gathering data during load tests or for continuous monitoring of in-service facilities.   The proper sensor type and array should be used to cover the monitored area efficiently. For damage quantification, AE signals are analyzed and different parameters are utilized.

5.5   INDEX OF DAMAGE

This damage evaluation method was proposed by Benavent-Climent et al. (2011) based on the relation between the cumulative AE energy and plastic strain energy dissipated by concrete. This index was developed during the seismic loading of a reinforced concrete slab, with the dimensions of 2.7 x 2.7 x 0.125 m (106 x 106 x 5 in.), supported on four steel columns. The slab was subjected to fifteen seismic simulations using a uniaxial shake table that replicated the ground acceleration recorded during the Campano-Lucano earthquake (Italy, 1980). The peak acceleration was increased over the fifteen seismic simulations until it reached the limit of damage permitted for a level I

earthquake; which is defined by yielding of reinforcing bars or slippage of steel in concrete. The slab was monitored during the test by eight low frequency sensors of type VS30-V using a threshold of 45 dB. The plastic strain energy dissipated due to the cracking of concrete, friction between adjacent surfaces, and the rise of steel temperature inside the concrete was estimated based on the basic principles of dynamics and using the measured displacement and strain values.

Damage indices based on the ratio of strain energy dissipation divided by ultimate strain energy were developed and could effectively characterize damage for RC members tested in a previous study under seismic loading (Park and Ang 1985). Benavent-Climent et al. correlated the accumulated AE energy with plastic strain energy and subsequently an index of damage in terms of accumulated AE energy was developed. This index of damage was defined as *"the cumulative energy at any instant during the test divided by the cumulative energy at the end of the seismic simulation at which the RC member experiences the maximum allowable damage"* (Equation 5.1). Thus to be able to estimate the index value, the value of E_D^{AE} is needed. This realization can limit the applicability of this method in the field where the value of E_D^{AE} is not available. A previous study showed that AE energy is related to the volume of damaged concrete (Carpinteri et al. 2007). Further investigations on this approach may lead to a derivation of an equation to estimate E_D^{AE} for RC members.

$$ID = \frac{E^{AE}}{E_D^{AE}}$$ (Eqn. 5.1)

An investigation on the damage index was conducted by Larosche (2012) where five full-scale single prestressed pile to bent cap specimens were subjected to cyclic displacements. Each specimen was monitored with eight 55 kHz resonant (R6i) AE

sensors. Cumulative energy was estimated at each cycle using two AE sensors at the most damaged areas of the piles. These values were divided by the average cumulative energy attained at the end of the test for the different specimens. The results showed a clear trend when plotted versus the displacement of the corresponding cycle normalized by the average ultimate displacement. An exploration of this method for prestressed concrete girders subjected to cyclic load testing is conducted in this study.

5.6   EXPERIMENTAL PROCEDURE

5.6.1   Description of test specimens:

Eight prestressed T- beams with a length of 4.98 m (16 ft. 4 in.) were included in this study. Each beam was reinforced with two 13 mm (0.5 in.) low relaxation prestressing strands prestressed to 68% of ultimate strand stress [f_{pu} = 1,860 MPa (270 ksi)]. The cross section and reinforcement of the specimens is shown in Figure 5.1. All specimens were designed to fail in flexure. The test matrix included three pristine (un-cracked and not corroded) specimens and five pre-cracked corroded specimens. For pre-cracked specimens, a four-point bending test was used to load the specimens until the desired crack width was achieved. Four specimens were loaded to 60% of their nominal capacity to reach a crack width of 0.4 mm (0.016 in.) and the fifth specimen was loaded to 80% of its nominal capacity to achieve a crack width of 0.8 mm (0.032 in.). After the removal of load, the cracks close due to the prestressing force with the exception of specimen C5-0.8 where cracks were still visually observed. The pre-cracked beams were corroded and theoretical mass loss was calculated using the Auyeung et al. (2000) equation (Equation 5.2) which was developed for reinforcing bars embedded in concrete. This equation is a modified version of Faraday's equation as the latter can only be used

for stand-alone metals immersed in solution (Auyeung et al. 2000). In Equation 5.2, i is the current in Amperes and t is the time in seconds. The compressive strength of the concrete and condition of specimens are summarized in Table 5.1 (ElBatanouny 2012). The un-cracked specimens were identified by the letter "U" followed by the specimen number (for example U1) while the cracked specimens were identified by the letter "C" followed by the specimen number and crack width in millimeters (for example C1-0.4).

$$Mass\ loss=0.4651 \times \frac{i \times t \times 55.827}{2 \times 96,487} - 0.5624 \qquad \text{(Eqn. 5.2)}$$

5.6.2 Test setup and instrumentation

Specimens were simply supported and tested in flexure under four-point loading as shown in Figure 5.2. Each specimen was instrumented with two string potentiometers to measure the mid-span deflection. Two LVDT's were mounted at the ends of each pre-stressing strand to measure strand slippage. Widths of selected cracks were observed during the test by two crack mouth opening gages. For AE data acquisition, 16 AE sensors of 55 kHz resonant frequency (R6i) were attached to each specimen with the layout shown in Figure 5.2. Only the six sensors near mid-span (filled sensors in the figure) were used for AE data analysis in this study.

5.6.3 Loading Protocol

Specimens were loaded in increasing magnitude loadsets as stated in ACI 437.1R-07. All specimens were subjected to seven loadsets with the exception of specimens C5-0.8 (eight loadsets) and C3-0.4 (six loadsets). A loading rate of 0.90 kN/s (200 lbf/s) was used. Each loadset consisted of two twin cycles of approximately the same load. Figure 5.3 shows the load cycles versus time for specimen U2. As presented in the figure, the load during cycles 1, 2, 5 and 6 was ramped with constant rate without any load holds

until it reached the desired level, then it was held for four minutes and ramped down with the same rate. These cycles were performed to enable acoustic emission monitoring and are not a typical portion of the CLT test. The other cycles were implemented according to the CLT protocol as proposed by ACI Committee 437 (2007). Each of these cycles had five load steps with 2 minute holds in between except after the fifth load step in the odd cycles and after the fourth load step in the even cycles, as the load remained constant at these stages for four minutes instead of two. The changes in load hold period were also utilized for AE evaluation purposes.

The maximum load level in cycle 1 is equal to 75% of service load (P_s). The service load was calculated as the load that results in zero net flexural stress in the bottom fiber of the beam at the load points, consistent with Class U PC members (ACI 2011). The load during cycle two is 90% of the load achieved in cycle 1. The maximum load level in cycle 3 and 4 corresponded to the service load (P_s). For the third loadset; the specimens were loaded up to the theoretical cracking load (P_{cr}) during cycle 5 and to 90% of this load level during cycle 6. The cracking load was calculated as the load which develops tensile stress equal to f_t; maximum allowable tensile stress for Class U PC members (ACI 2011). For the following loadsets the maximum load was increased gradually until it reached 90% of the nominal capacity ($0.9P_n$) on the last loadset. To keep the actuator engaged a minimum load of 2.2 kN (500 lbf) was maintained throughout the test and was sustained for a period of five minutes after each cycle. For the ultimate failure load assessment, each specimen was loaded up to failure after test completion. More details on the test procedure can be found in ElBatanouny (2012).

5.6.4 Data Filters

In order to disregard the non-genuine data, AE data must be filtered. Background noise, friction between test instruments and the specimen, and mechanical and electrical noise are all examples of possible sources of false data that are not related to the structure response. Neoprene pads were used between the roller supports and the specimens to reduce friction. A special power supply was also used to minimize electrical noise.

After gathering the data, three data filters were applied. The first filter is an amplitude filter of 60 dB to delete all signals with lower amplitude. The second filter is based on duration and amplitude limits and designated as a D-A filter or Swansong II filter (Fowler et al. 1989; Tinkey et al. 2002). The third filter is dependent on the correspondence between rise time and amplitude and is referred to as an R-A filter. The limits set for the second and third filters are listed in Table 5.2.

5.7 RESULTS AND DISCUSSION

The load at which each specimen failed as well as the failure mode are presented in Table 5.1. A specimen is considered failed due to excessive residual deflection if it exceeded the maximum allowable residual deflection described by ACI 318-11 (2011) which is estimated to be 25.9 mm (1.02 in.) for these particular specimens. This excessive deflection was attributed to slipping of strands which was observed in all specimens except U1 and C5-0.8. Specimen C3-0.4 experienced convergence of two cracks at the edge of the constant moment zone at the bottom fiber which led to spalling of concrete; thus the beam was considered failed.

In order to investigate the effect of corrosion on the slipping of strands, an insufficient development length was deployed in all specimens and the strands that have

been used in some of the specimens were pre-corroded (specimens U1 and C5-0.8). The required development length for the prestressing strands was calculated according to the ACI equation (ACI 2011). It was found that a development length of 3.74 m (95 in.) is needed for the strands to reach their ultimate strength. The provided development length was 2.91 m (74 in.). This shortage of development length resulted in slipping of strands before reaching its ultimate capacity and thus strand rapture was not attained. The slipping of strands enhanced the ductility behavior of the specimens when compared to the brittle failure represented by strand rapture. The different behavior of specimens U1 and C5-0.8 can be attributed to the fact that they were the only specimens cast with pre-corroded strands. The bond between strand and adjoining concrete may have been improved by the corrosive layer of the strand (Janney 1954); consequently slipping was prevented in these specimens.

5.7.1 Damage index

Benavent-Climent et al. (2011) defined the index of damage (ID) as the cumulative AE energy at any point of the test divided by the cumulative AE energy when the max allowable damage is attained. In this study, cumulative energy was computed using the data gathered by the six sensors placed on the most damaged region (filled sensors in Figure 5.2).

For un-cracked specimens, the limit of admissible damage was defined by the onset of specimen yielding; which can be related to cracking initiation. The yield point was estimated from the envelope of the load-defection response as illustrated in Figure 5.4(a). The three un-cracked specimens were on the brink of yielding at cycle 8. Subsequently, the index of damage was calculated by dividing the cumulative energy at

104

the end of each cycle by the cumulative energy at the end of cycle 8. The index was computed only for the even cycles in order to have a clear pattern for the index with increasing load (as the twin cycles had approximately the same load). The results are plotted in Figure 5.5 versus the corresponding load of the cycle normalized by the ultimate failure load. Before yielding, all specimens had the same behavior then it deviated after yielding with different slopes (Figure 5.5). These specimens yielded at cycle 9 which had a maximum load of $0.70P_u$. ID values greater than one indicate that the accumulated damage exceeded the allowable limit and the specimen had yielded (which is true for cycles after cycle 8).

The permissible damage limit in pre-cracked specimens was defined by global yielding of the specimen estimated from the load- deflection relation as shown in Figure 5.4(b). All specimens that were pre-cracked to a crack width of 0.4 mm (0.016 in.) were on the verge of yielding at cycle 6, with the exception of specimen C3-0.4 which yielded after cycle 4. At the maximum load of these cycles, the crack width exceeded 0.33 mm (0.013 in.) which corresponds to level 2 cracks according to the ODOT crack comparator tool; where level 1 corresponds to hairline cracks with a maximum crack width less than 0.33 mm (0.013 in.); level 2 for cracks of max width between 0.33 mm (0.013 in.) and 0.63 mm (0.025 in.); and level 3 for cracks that exceeds 0.63 mm (0.025 in.) in width (Lovejoy 2008). The index of damage was calculated using cumulative energy at the end of the even cycles divided by the cumulative energy at the end of the cycle which had maximum admissible damage (at the brink of yielding). The results were plotted versus normalized load as shown in Figure 5.6. The results showed a clear trend for all the specimens that can be used to assess the amount of accumulated damage. However, the

value of cumulative AE energy at the onset of yielding is not readily determined in field which restricts the applicability of this method for damage assessment of real structures. Therefore, a critical modification to this index is proposed in the following section to present a method that could be used in field based on AE energy.

5.7.2   Modified Index of Damage (MID)

A modification to the Benavent-Climent et al. (2011) index is proposed to assess damage using cumulative AE energy. The suggested index is computed by normalizing the cumulative AE energy at any point of the test by the cumulative AE energy at the end of the initial load cycle. The modified index (MID) results for the three un-cracked specimens versus the normalized load are plotted in Figure 5.7. The modified index was also calculated at the end of the even cycles for consistency. An explicit pattern of the data points is observed where the point of yielding can be easily identified. As seen in Figure 5.7, the slope of the data line changed after cycle 8 where the yielding had started. A criterion for pristine girders can be developed based on the results such that MID value greater than 15 indicates yielding of the specimen.

The MID results for the preconditioned specimens are shown in Figure 5.8. The four pre-cracked specimens with a crack width of 0.4 mm (0.016 in.) yielded after MID values exceed a value of 8.0.

The heavily cracked specimen (C5-0.8) was preloaded to 80% of its nominal capacity before the test to reach the desired crack width. Thus, it did not show a yielding point during the cyclic load test (Figure 5.9) as it yielded in the pre-cracking stage. The ID value for this specimen could not be calculated as the value of cumulative energy at yielding is not available (the beam was not monitored in the pre-cracking stage). The

106

results of MID did not effectively describe the amount of existing damage in the beam (Figure 5.10). The cracks in this specimen were visual (open) and the camber was already lost after the pre-cracking stage. This means that the prestressing force was diminished before the cyclic load test and most of the damage had already occurred. Existing damage does not generate AE signals if it is not active, which explains the lower amount of AE data gathered at the end of the test for this beam. Thus, the use of MID method can be limited to specimens which are not exhibiting major damage. In cases of heavily damaged specimens the use of another damage assessment parameter is recommended.

5.8   CONCLUSIONS

A damage assessment parameter, based on AE cumulative energy, was investigated through monitoring eight PC specimens subjected to the cyclic load test (CLT) protocol as described in ACI 437 (2007). Five of the specimens were preconditioned to different levels. The conclusions drawn from this study can be summarized as follows:

1. The bond between the strand and the surrounded concrete was improved by the use of pre-corroded strands and consequently the slipping was prevented.

2. An AE damage assessment parameter, index of damage (ID), based on cumulative energy can be computed such that ID value less than one indicates that the max allowable damage, which is defined here as global yielding, has not been reached by the specimen.

3. The index of damage showed promising results for un-cracked and pre-cracked specimens, with initial crack width of 0.4 mm (0.016 in.). The results can be used to assess the amount of damage present in similar specimens. However, the method cannot be used in the field or for specimens that have already exceeded

the level of allowable damage; as the value of cumulative AE energy at maximum admissible damage would be unknown in these cases.

4. The proposed modified index of damage (MID) enhances the feasibility of this method for field applications. MID results showed a clear correlation with increasing damage and can readily identify the yielding point.

5. Evaluation criteria based on MID results are proposed where: MID greater than 15 for un-cracked specimens and MID greater than 8.0 for pre-cracked specimens indicate the specimen has yielded. Further investigation is needed to verify these limits and its applicability for actual field implementation.

6. Neither ID nor MID could quantify the amount of damage for the heavily cracked specimen (C5-0.8). However, in this case it was visually clear that the specimen had exceeded the level of permissible damage.

5.9 REFERENCES

Aggelis, D.G., Shiotani, T., Momoki, S., Terazawa, M. (2007). "Acoustic emission of full scale concrete beams for evaluation of joint effect." In: Ono K, editor. Advances in acoustic emission. Proceedings of the 6th international conference on acoustic emission, Lake Tahoe, Nevada, USA, October 29th–November 2nd,p. 390–5.

American Concrete Institute (ACI). (2007). "Test Load Magnitude, Protocol and Acceptance Criteria." ACI 437.1R-07, ACI Committee 437, Farmington Hills, MI, 38.

American Concrete Institute (ACI). (2011). "Building Code Requirements for Structural Concrete." ACI 318–011, ACI Committee 318, Farmington Hills, MI, 503.

ASTM E1316. (2006). "Standard Terminology for Nondestructive Examinations." American Standard for Testing and Materials, 1-33.

Auyeung, Y., Balaguru, B., Chung, L. (2000). "Bond Behavior of Corroded Reinforcement Bars." ACI Materials Journal, 97(2), 214-220.

Benavent-Climent, A., Gallego, A., Vico, J.M. (2011). "An Acoustic Emission Energy Index for Damage Evaluation of Reinforced Concrete Slabs Under Seismic Loads", Structural Health Monitoring, V.11, No. 1, pp. 69-81.

Carpinteri A, Lacidogna G and Pugno N. (2007). "Structural damage diagnosis and lifetime assessment by acoustic emission monitoring". Eng Fract Mech; 74(1–2): 273–289.

Colombo, S., Forde, M., Main, I., and Shigeishi, M. (2005). "Predicting the ultimate bending capacity of concrete beams from the 'relaxation ratio' analysis of AE signals." Construction and Building Materials, Vol. 19, 746–754.

ElBatanouny, M.K. (2012). "Implementation of Acoustic Emission as a Non-Destructive Evaluation Method for Concrete Structures." Dissertation, Department of Civil and Environmental Engineering, University of South Carolina, Columbia, SC, 184.

ElBatanouny, M.K, Larosche, A., Mazzoleni, P., Ziehl, P.H, Matta, F., and Zappa, E. (2012). "Identification of Cracking Mechanisms in Scaled FRP Reinforced Concrete Beams using Acoustic Emission." Experimental Mechanics, DOI 10.1007/s11340-012-9692-3, November (online).

Fowler, T., Blessing, J., and Conlisk, P. (1989). "New Directions in Testing." Proc. 3rd International Symposium on AE from Composite Materials, Paris, France.

Golaski, L., Swit, G., Kalicka, M., Ono, K. (2006). "Acoustic emission behavior of prestressed concrete girder during proof loading." J Acoust Emission 2006;24:187–96.

Janney, J. R. (1954) "Nature of Bond in Pretensioned Prestressed Concrete." ACI Journal, 50(9), 717–736.

Kaiser, J. (1953), "Erkenntnisse und Folgerungen aus der Messung von Ger¨auschen bei Zugbeanspruchung von metallischen Werkstoffen." Archiv f˙ur das Eisenh¨uttenwesen 24(1–2):43–45.

Larosche, A.K. (2012). "Behavior of Prestressed Pile to Bent Cap Connections and Damage Evaluation with Acoustic Emission." Dissertation, Department of Civil and Environmental Engineering, University of South Carolina, Columbia, SC, 207.

Lovejoy, S. (2008). "Acoustic Emission Testing of Beams to Simulate SHM of Vintage Reinforced Concrete Deck Girder Highway Bridges." Structural Health Monitoring, Vol. 7, 327-346.

Ono, K. (2010). "Application of Acoustic Emission for Structure Diagnosis." Konferencja Naukowa, 317-341.

Park, Y. and Ang, A. (1985). "Mechanistic Seismic Damage Model for Reinforced Concrete." J. Struct. Eng., 111(4), 722–739.

Shiotani T, Aggelis DG, Makishima O. Global monitoring of concrete bridge using acoustic emission. J Acoust Emission 2007;25:308–15.

Tinkey, B.V., Fowler, T.J., and Klingner, R.E. (2002). "Nondestructive Testing of Prestressed Bridge Girders with Distributed Damage." Research Report 1857-2, pp. 106.

Xu, J. (2008). "Nondestructive Evaluation of Prestressed Concrete Structures by Means of Acoustic Emission Monitoring." Dissertation, Dept. of Civil Engineering, Univ. of Auburn, Auburn, Alabama, 308.

Ziehl, P. (2008). "Applications of Acoustic Emission Evaluation for Civil Infrastructure." SPIE Proc., SPIE Smart Structures NDE, San Diego, CA, 9.

Ziehl, P., Engelhardt, M., Fowler, T., Ulloa, F., Medlock, R., and Schell, E. (2009). "Design and Live Load Evaluation of a Hybrid FRP/RC Bridge Superstructure System", ASCE Journal of Bridge Engineering, Vol. 14, No. 5, pp. 309-318.

Table 5.1: Description of Failure and condition of the specimens

Specimen	Compressive strength, MPa (psi)	Crack Width, mm (in.)	Theoretical sectional mass loss, %	Failure load, kN (kip)	Failure mode
U1	29.0 (4,200)	----	0%	103.7 (23.3)	strand rupture
U2	40.7 (5,900)	----	0%	113.9 (25.6)	excessive residual deflection
U3		----	0%	113.9 (25.6)	
C1-0.4		0.4 (0.016)	15%	101.0 (22.7)	
C2-0.4		0.4 (0.016)	15%	100.1 (22.5)	
C3-0.4		0.4 (0.016)	30%	76.5 (17.2)	concrete spalling at the bottom fibers
C4-0.4		0.4 (0.016)	30%	89.9 (20.2)	excessive residual deflection
C5-0.8	29.0 (4,200)	0.8 (0.032)	16%	89.9 (20.2)	strand rupture

Table 5.2: Data rejection limits for AE filters (ElBatanouny 2012)

D-A filter		R-A filter	
Amplitude (dB)	Duration (μs)	Amplitude (dB)	Rise time (μs)
60-67	>2,000	60-67	>300
68-75	>4,000	68-75	>450
76-83	>6,000	76-83	>600
84-91	> 8,000	84-91	> 750
92-100	>10,000	92-100	>900
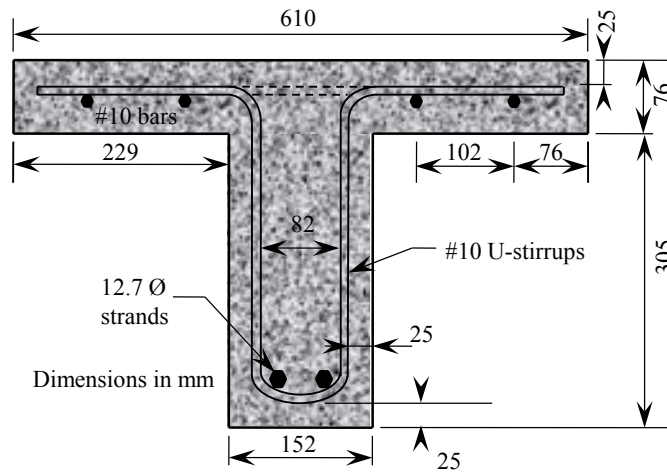
Figure 5.1: A schematic of the geometric properties and reinforcement
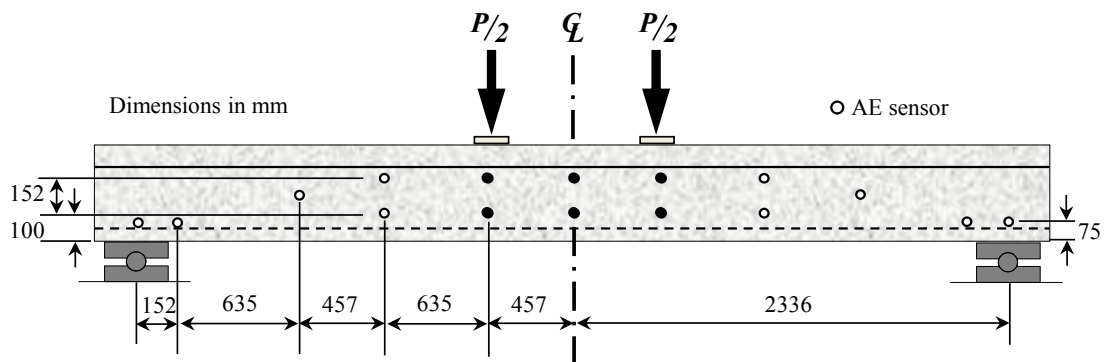
Figure 5.2: Test setup and AE sensors layout
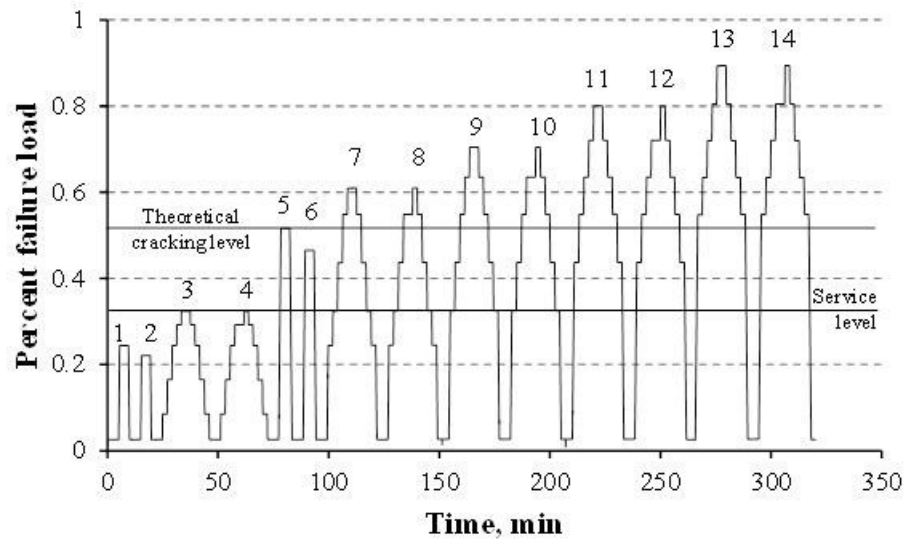
Figure 5.3: Specimen U2 loading protocol
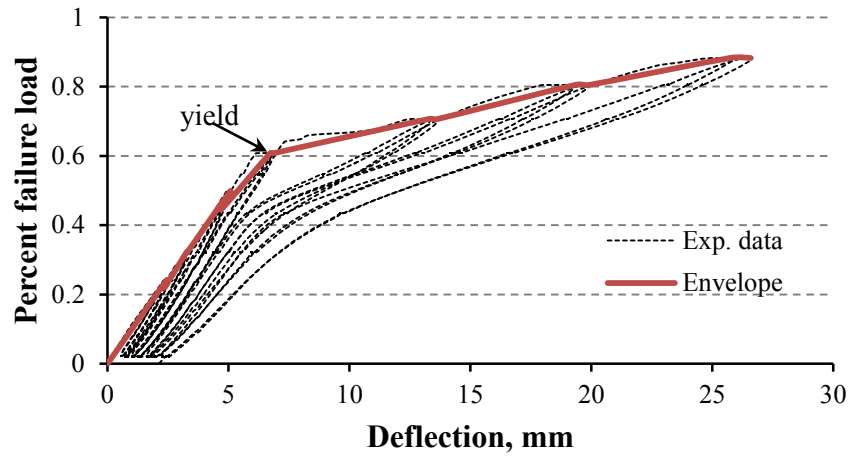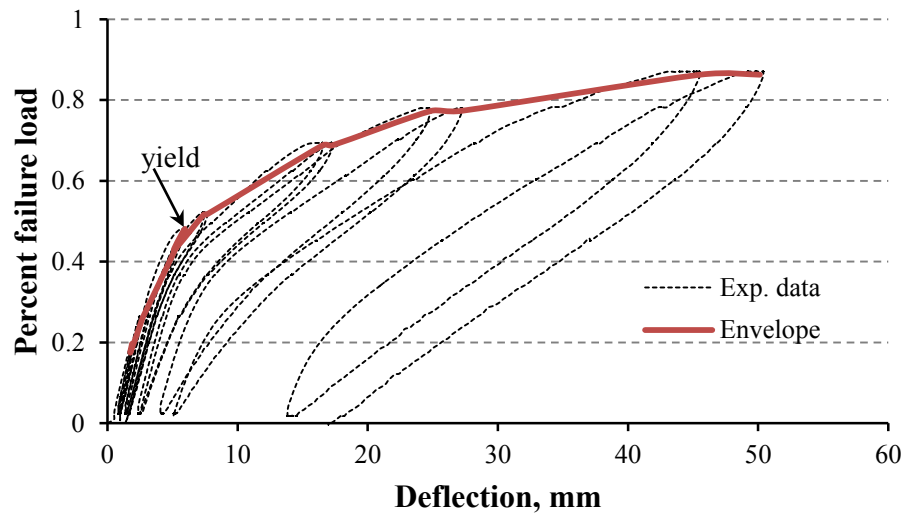
Figure 5.4: a) Load-deflection response for specimen U1, b) Load-deflection response for specimen C2-0.4
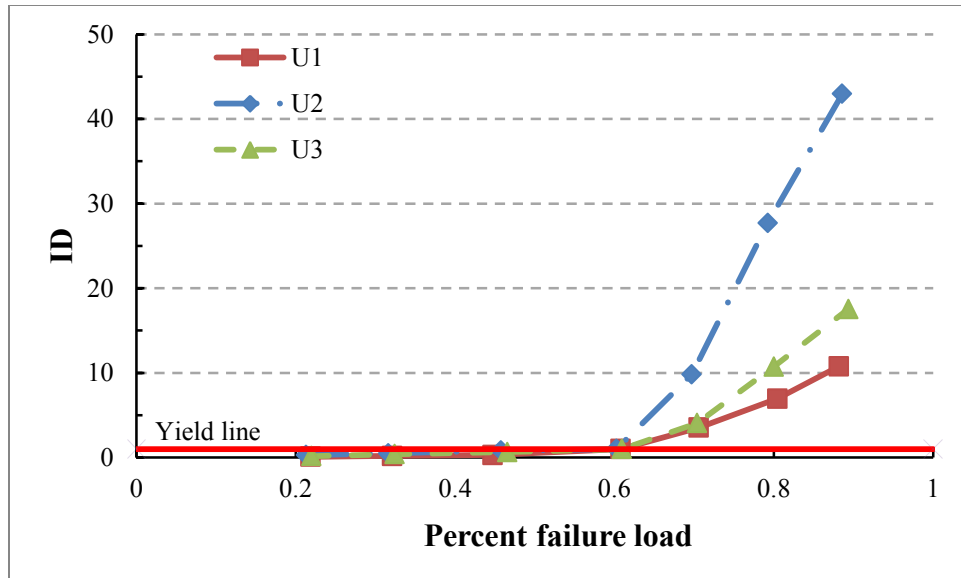
Figure 5.5: Index of damage versus load (normalized) for un-cracked specimens
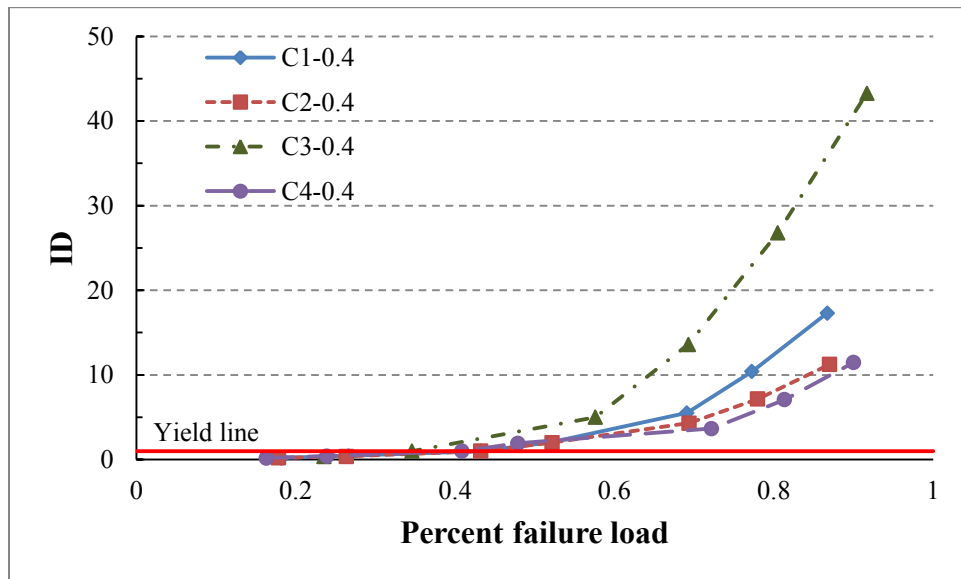
Figure 5.6: Index of damage versus load (normalized) for pre-cracked specimens

115
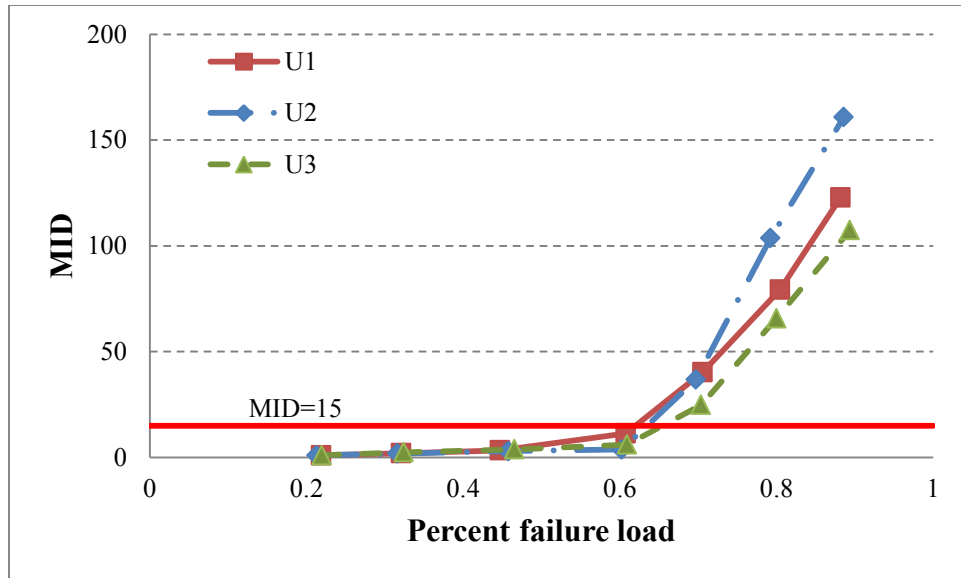
Figure 5.7: Modified index of damage for un-cracked specimens
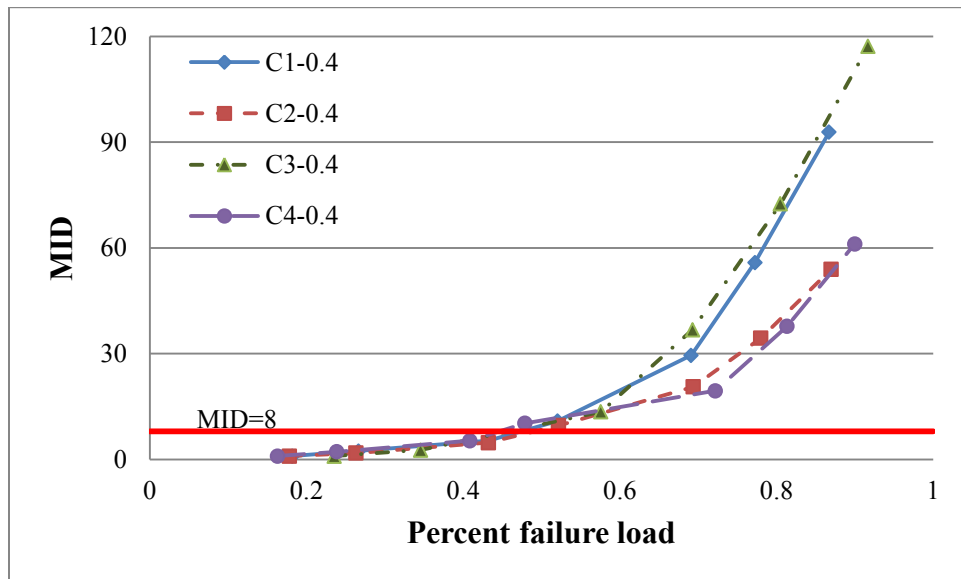
Figure 5.8: Modified index of damage for pre-cracked specimens
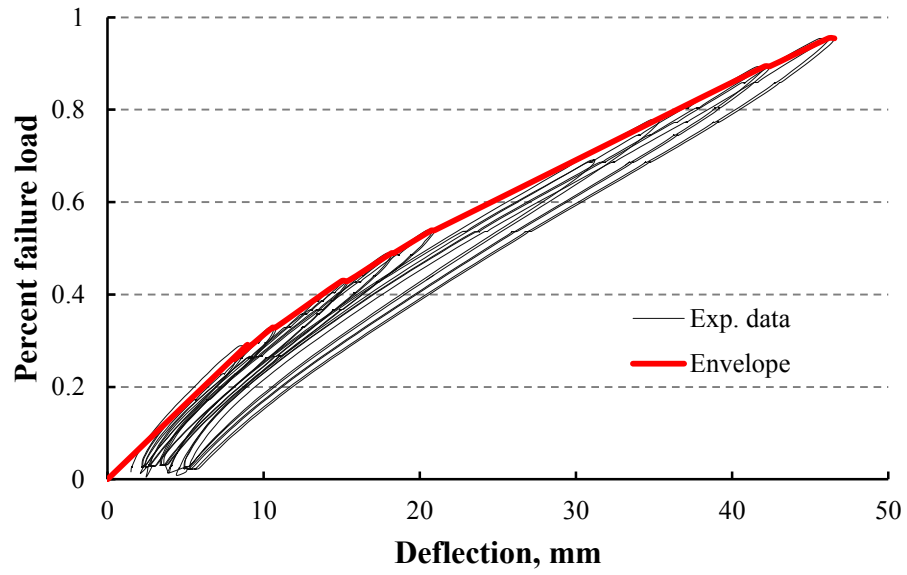
Figure 5.9: Load-deflection response for specimen C5-0.8
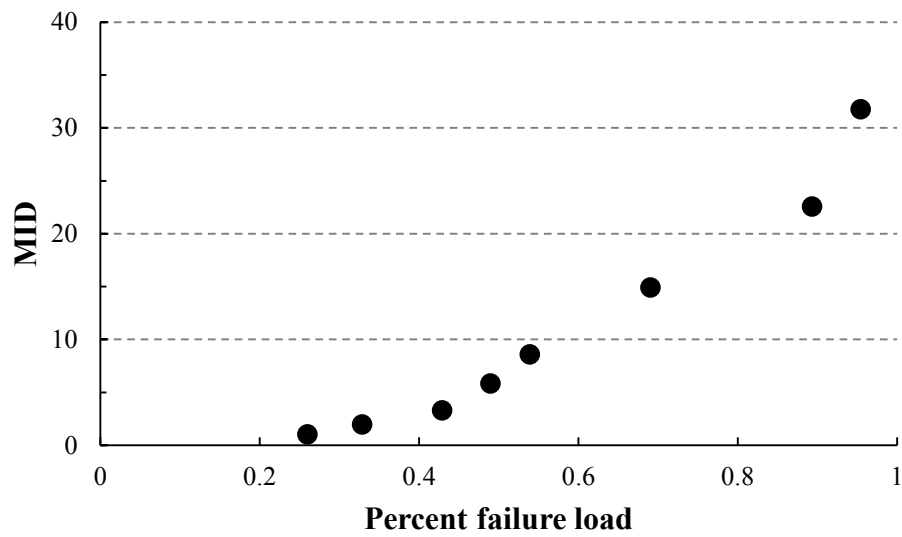
Figure 5.10: Modified index of damage for specimen C5-0.8

117

CHAPTER 6

SUMMARY AND CONCLUSIONS

6.1   SUMMARY

In this research, the ability of acoustic emission to detect different types of degradation mechanisms was assessed in three different studies. The first study explored the ability of AE to detect damage during load tests of different types of concrete structures. Factors such as specimen type, specimen size, sensor type, number of sensors, and type of loading were reported. The limits set for the evaluation criteria of each method were presented and discussed.

The second study provided a detailed review of corrosion detection methods in reinforced and prestressed concrete using AE. Recommendations regarding successful methods are presented. The main purpose of the first and second study was to provide useful recommendation to future researchers regarding successful AE based methods which have the promise of being applied in field investigations.

The last study used AE index of damage method to assess the condition of prestressed beams tested under cyclic load test (CLT) protocol. The specimens had different initial conditions to represent some of the existing problems in field structures. The method enabled proper assessment of the condition of the specimens; however, the applicability of the method in field is compromised. Therefore, a modification for the method was proposed to enable condition assessment of in-service structures. The

conclusions of each study are presented below along with general conclusions and recommendations for future research.

6.2 SUMMARY AND CONCLUSIONS OF EACH STUDY

6.2.1 AE in damage assessment during load tests

- Intensity analysis enabled successful damage identification in both laboratory and field tests. The results shows that the method may be independent on scale

- The calm ratio versus load ratio is not reliable as there are no consistent limits for damage classification.

- PCSS ratio was successfully used to assess damage for RC members in laboratory and field. The method failed to detect damage in PC members.

- No clear trend was seen when the relaxation ratio was used for RC and PC members.

- A b-value and Ib-value lower the unity are related to significant damage.

- Global performance index was developed from a field test; it uses data from AE and CLT protocol. A value exceeding unity is considered as an indication of significant damage.

6.2.2 AE in corrosion detection in concrete structures

- Acoustic emission can detect the onset of corrosion and nucleation of cracking before most electrochemical methods such as half-cell potential and galvanic current. Corrosion initiation and cracking can be identified by two periods of high AE activity. Conventional parameter such as counts, number of hits, cumulative event number and cumulative signal strength were successfully

119

used for this purpose. Condition assessment methods such as *b*-vale and *Ib*-value were also successful.

- Nucleation of tensile cracking due to corrosion was detected using the relationship between RA values and average frequencies. However, further research should investigate the feasibility of using this method to classify AE sources.

- AE can effectively locate the corrosion damage by using source location techniques which enables owners to perform repairs.

- SiGMA analysis can be used for mapping the location, type and orientation of cracks developed in the process of corrosion in RC specimens. However, the applicability of this method in field is questioned due to the large number of sensors required.

- Quantification of corrosion damage can be performed using intensity analysis chart. The chart is divided into different regions that correspond to different corrosion levels. Two sets of chart boundaries were proposed for the cases of un-cracked and cracked PC specimens. However, more investigation is needed to establish the proposed boundaries in field.

6.2.3 AE based damage assessment method for prestressed concrete structures

- The bond between the strand and the surrounded concrete was improved by the use of pre-corroded strands and consequently the slipping was prevented.

- AE damage assessment parameter, index of damage (ID), based on cumulative energy can be computed such that ID value less than one indicates that the

max allowable damage, which is defined here as global yielding, has not been reached by the specimen.

- ID showed promising results for un-cracked specimens and pre-cracked specimen, with initial crack width of 0.4 mm (0.016 in.). The results can be used to assess the amount of damage present in similar specimens. However, the method cannot be used in field or for specimens that had already exceeded the level of allowable damage; as the value of cumulative AE energy at maximum admissible damage would be unknown in these cases.

- The proposed modified index of damage (MID) enhances the feasibility of this method to be applied in field. MID results showed a clear correlation with the increasing damage and can easily identify the yielding point.

- Evaluation criterion based on MID results is proposed where: MID greater than 15 for un-cracked specimens and MID greater than 8 for pre-cracked specimens indicate that the specimen had yielded. Further investigation is needed to verify these limits and its applicability on both laboratory and field implementations.

- Both ID and MID could not quantify the amount of damage for the heavily cracked specimen (C5-0.8). However, it can be visually concluded that the specimen had exceeded the level of permissible damage.

6.3   GENERAL CONCLUSIONS

This study showed the ability of AE to detect damage during load tests as well as to detect corrosion of steel reinforcement embedded in concrete. Some AE techniques have the ability to classify the degree of damage. For example, AE intensity analysis

121

charts can be developed to evaluate damage occurring during load tests as well as corrosion damage. The study also showed that this method may be independent on specimen size which is an important advantage for field implementation.

A modification for AE index of damage method was proposed in this research. The modified method is able to assess the condition of specimen in terms of yielding point. The method may be applied during field tests for further assessment.

6.4 RECOMMENDATIONS AND FUTURE WORK

A series of benchmark tests is needed to compare between different AE condition assessment methods. AE damage assessment criteria should set limits for damage classification based on standardized laboratory load tests. A clear definition of damage should be given with the proposed limits. These limits should be dependent on type of concrete, RC and PC, and the results of similar specimens loaded under similar condition should be comparable. After establishing damage classification limits for different criteria field tests should be commenced on structures with known conditions to verify the applicability of these methods to full scale specimens in field environment. The repeatability of test results has to be ensured through standardizing loading protocol, sensors placement, sensor type, and limits for AE damage assessment criteria.

Further studies should also be conducted for verifying the behavior of AE parameters due to corrosion process in different types of concrete specimens and setting limits for corrosion quantification. Future researchers should put emphasis on classifying AE source by differentiating between AE signals due to corrosion and signals due to load related deteriorations. This classification would broaden the application of AE for monitoring in-service structures and provide sufficient justification for maintenance

decisions. Studying the characteristics of AE signals (waveforms) produced in the two

cases is a possible approach to achieve reliable source classification.

REFERENCES

Aggelis, D.G., Shiotani, T., Momoki, S., Terazawa, M. 2007. Acoustic emission of full scale concrete beams for evaluation of joint effect. In: Ono K, editor. Advances in acoustic emission. Proceedings of the 6th international conference on acoustic emission, Lake Tahoe, Nevada, USA, October 29th–November 2nd, p. 390–5.

Aggelis, D.G., Shiotani, T., Momoki, S., and Hirama, A. 2009. Acoustic emission and ultrasound for damage characterization of concrete elements", ACI Mater J, 106 (6), 509‑514.

American Concrete Institute (ACI) Committee 222. 2001. Protection of Metals in Concrete Against Corrosion, ACI 222R-01, American Concrete Institute, Farmington Hills, Michigan, 41 pp.

American Concrete Institute (ACI) Committee 318. 2011. Building code requirements for structural concrete – ACI 318–11. ACI, Farmington Hills, MI, 503.

American Concrete Institute (ACI) Committee 437. 2007. Test load magnitude, protocol and acceptance criteria – ACI 437.1R-07. ACI, Farmington Hills, MI, 38.

American Society of Civil Engineers (ASCE). 2013. Report Card for America's Infrastructure. Reston, Virginia.

Andrade, C., Alonso, M.C., Gonzalez, J.A. 1990. An initial effort to use corrosion rate measurements for estimating rebar durability corrosion rates of steel in concrete. ASTM STP 1065, N.S. Berke et al. editors, ASTM, Philadelphia, 29-37.

ASNT. 1996. Nondestructive testing handbook. 2nd ed. Columbus, OH: American Society for Nondestructive Testing (ASNT), 581.

Assouli, B., Simescu, F., Debicki, G., and Idrissi, H. 2005. Detection and identification of concrete cracking during corrosion of reinforced concrete by acoustic emission coupled to the electrochemical techniques. NDT & E International, 38(8), 682-689.

ASTM C876. 2009. Standard Test Method for Half-Cell Potentials of Uncoated Reinforcing Steel in Concrete. American Standard for Testing and Materials, 1-7.

ASTM E1067/E1067M-11. 2011. Standard Practice for Acoustic Emission Examination of Fiberglass Reinforced Plastic Resin (FRP) Tanks/Vessels. American Standard for Testing and Materials, 1-15.

ASTM E1316. 2006. Standard Terminology for Nondestructive Examinations. American Standard for Testing and Materials, 1-33.

ASTM E 2478-06. 2006. Standard practice for determining damage-based design stress for fiberglass reinforced plastic (FRP) materials using acoustic emission. West Conshohocken, Pennsylvania: ASTM International, 6.

ASTM G59. 1997-Reapproved 2009. Standard Test Method for Conducting Potentiodynamic Polarization Resistance Measurements. American Standard for Testing and Materials, 1-4.

Auyeung, Y., Balaguru, B., Chung, L. 2000. Bond Behavior of Corroded Reinforcement Bars. ACI Materials Journal, 97(2), 214-220.

Barrios, F., and Ziehl, P. 2012. Cyclic Load Testing for Integrity Evaluation of Prestressed Concrete Girders. ACI Structural Journal (scheduled for publication).

Basri, S.R., Bunnori, N.M., Abdul kudus, S., Shahidan S., Md Jamil, M.N., and Nor, N.M. 2012. Evaluation of Reinforced Concrete Damage Using Intensity Analysis in Acoustic Emission Technique. International Conference on System Engineering and Modeling, IPCSIT vol. 34, Singapore.

Benavent-Climent, A., Gallego, A., Vico, J.M. 2011. An Acoustic Emission Energy Index for Damage Evaluation of Reinforced Concrete Slabs Under Seismic Loads. Structural Health Monitoring, V.11, No. 1, pp. 69-81.

Bennett, J.E., and Mitchell, T.A. 1992. Reference Electrodes For Use With Reinforced Concrete Structures. Corrosion 92-Nace, Paper191.

Bray, D. E. and Stanley R. K. 1997. Nondestructive evaluation: a tool in design, manufacturing, and service. New York: CRC Press, 586.

Broomfield, J.P., Rodriguez, J., Ortega, L.M., and Garcia, A.M. 1993. Corrosion rate measurement and life prediction for reinforced concrete structures. In: Proceedings Of Structural Faults and Repairs-93, vol.2: pp.155 (Engineering Technical Press, University of Eidenbugh).

Broomfield, J.P., Rodriguez, J., Ortega, L.M. and Garcia, A.M. 1994. Corrosion rate measurements in reinforced concrete structures by a linear polarization device. In: R.E. Weyers (ed.) Symposium on Corrosion of Steel in Concrete, Special Publication: SP 151-9, pp.163.

Broomfield, J.P. 1997. Corrosion of Steel in Concrete, Understanding, Investigation and Repair. (Chapman and Hall).

Carpinteri A, Lacidogna G and Pugno N. 2007. Structural damage diagnosis and life-time assessment by acoustic emission monitoring. Eng Fract Mech; 74(1–2): 273–289.

Clear, K.C. 1989. Measuring the rate of corrosion of steel in field concrete structures. Transportation Research Record 1211, (Transportation Research Board, National Research Council, Washington, DC.

Colombo, S., Main, I.G., and Forde, M.C. 2003. Assessing damage of reinforced concrete beam using b-value analysis of acoustic emission signals. J. Mater. Civil Eng. 5-6, pp. 280–286.

Colombo, S., Forde, M., Main, I., and Shigeishi, M. 2005. Predicting the ultimate bending capacity of concrete beams from the 'relaxation ratio' analysis of AE signals. Construction and Building Materials, Vol. 19, 746–754.

Dunegan, H.L. 1963. Acoustic emission: a promising technique. UCID 4643. Lawrence Radiation Laboratory: Livermore, CA; 203–238.

ElBatanouny, M., Mangual, J., Ziehl, P., and Matta, F. 2011. Corrosion Intensity Classification in Prestressed Concrete using Acoustic Emission Technique. Proc. American Society for Nondestructive Testing (ASNT) Fall Conference and Quality Testing Show 2011, Palm Springs, CA. October 24-28, pp. 10.

ElBatanouny, M.K. 2012. Implementation of Acoustic Emission as a Non-Destructive Evaluation Method for Concrete Structures. Dissertation, Department of Civil and Environmental Engineering, University of South Carolina, Columbia, SC, 184.

ElBatanouny, M.K, Larosche, A., Mazzoleni, P., Ziehl, P.H, Matta, F., and Zappa, E. 2012. Identification of Cracking Mechanisms in Scaled FRP Reinforced Concrete Beams using Acoustic Emission. Experimental Mechanics, DOI 10.1007/s11340-012-9692-3, November (online).

ElBatanouny, M., Mangual, J., Barrios, F., Ziehl, P., and Matta, F. 2012. Acoustic Emission and Cyclic Load Test Criteria Development for Prestressed Girders. Structural Faults and Repair 2012, Edinburgh, Scotland, UK.

Farid Uddin, A. K. M., Numata, K., Shimasaki, J., Shigeishi, M., and Ohtsu, M. 2004. Mechanisms of crack propagation due to corrosion of reinforcement in concrete by AE-SiGMA and BEM. Construction and Building Materials, 18(3), 181-188.

Flis, J., Sehgal, A., Li, D., KHO, Y.T., Sabotl, S., Pickering, H., Osseo-Assare, K., and Cady, P.D. 1992. Condition Evaluation of Concrete Bridges Relative to Reinforcement Corrosion. vol.2, method for measuring the corrosion rate of reinforcing steel, Natural Research Council, Washington, DC, SHRP-S/FR-92-104.

Fowler, T. J., and Gray, E. 1979. Development of an Acoustic Emission Test for FRP Equipment. American Society of Civil Engineers Convention and Exposition, Preprint 3538, Boston, 1-22.

Fowler, T.J. 1986. Experience with acoustic emission monitoring of chemical process industry vessels. Progress in Acoustic Emission III, JSNDI, 150-162.

Fowler,T.J., Blessing, J., Conlisk, P., and Swanson, T.1989. The MONPAC Procedure. Journal of Acoustic Emission, 8(3), 1-8.

Fowler, T., Blessing, J., and Conlisk, P. 1989. New Directions in Testing. Proc. 3rd International Symposium on AE from Composite Materials, Paris, France.

Golaski, L., Gebski, P., and Ono, K. 2002. Diagnostics of Reinforced Concrete by Acoustic Emission. Journal of Acoustic Emission, Vol. 20, 83-98.

Golaski, L., Swit, G., Kalicka, M., Ono, K. 2006. Acoustic emission behavior of prestressed concrete girder during proof loading. J Acoust Emission 2006;24:187–96.

Green A.T., Lockman C.S., and Haines H.K. 1963. Acoustical Analysis of Filament-Wound Polaris Chambers. Report 0672-01F. Aerojet-General Corporation: Sacramento, CA.

Green A.T., Lockman C.S., Brown S.J., and Steel R.K. 1964. Feasibility Study of Acoustic Depressurization System. Final Report, NASA CR-55472. Aerojet-General Corporation: Sacramento, CA.

Hearn, S.W., and shield, and C.K. 1997. Acoustic Emission Monitoring as a Nondestructive Testing Technique in Reinforced Concrete. ACI Materials Journal, V. 94, No. 6, 510-519.

Heidersbach, R. 1986. Corrosion Performance of Weathering Steel Structures. California Polytechnic State University, San Luis Obispo. Metallurgical Engineering Dept.

Idrissi, H., and Limam, A. 2003. Study and characterization by acoustic emission and electrochemical measurements of concrete deterioration caused by reinforcement steel corrosion. NDT & E International, 36(8), 563-569.

Isecke, B. 1982. Collapse of the Berlin Congress Hall Prestressed Concrete Roof. Materials Performance, PP. 36-39.

Janney, J.R. 1954. Nature of Bond in Pretensioned Prestressed Concrete. ACI Journal, 50(9), 717–736.

JSCE Concrete Committee. 2001. Standard Specifications for Concrete Structures—Maintenance. Guidelines for Concrete, No. 4, Japan Society of Civil Engineers, 170 pp.

Kaiser, J. 1953. Erkenntnisse und Folgerungen aus der Messung von Ger¨auschen bei Zugbeanspruchung von metallischen Werkstoffen. Archiv f˙ur das Eisenh¨uttenwesen 24(1–2),43–45.

Kawasaki, Y., Tomoda, Y., and Ohtsu, M. 2010. AE monitoring of corrosion process in cyclic wet–dry test. Construction and Building Materials, 24(12), 2353-2357.

Knill, I.L., Franklin, I.A., and Malone, A.W. 1968. A study of acoustic emission from stressed rock. International Journal of Rock Mechanics and Mining Sciences 5,87–121.

Koch, G. H., Brongers, M. P. H., Thompson, N. G.,Virmani, Y. P., and Payer, J. H. 2001. Corrosion costs and preventive strategies in the United States. FHWA-RD-01-156. Federal Highway Administration, Washington, D.C., 2001.

Larosche, A.K. 2012. Behavior of Prestressed Pile to Bent Cap Connections and Damage Evaluation with Acoustic Emission. Dissertation, Department of Civil and Environmental Engineering, University of South Carolina, Columbia, SC, 207.

Lean, J.B., and Plateau, J. 1959a. Observation des ondes sonores prenant naissance au cours de la d´eformation plastique des m´etaux. en relation avec le probl`eme de la rupture fragile de l'acier doux. M´emoires Scientifiques de la Revue de M´etallurgie, 56(1),91–99.

Lean, J.B., Plateau, J., and Crussard, C. 1959b. Contribution `a l´´etude du m´ecanisme de la rupture fragile de l'acier doux. M´emoires Scientifiques de la Revue de M´etallurgie, 56(4), 427–452.

Li, Z., Zdunek, A., Landis, E., and Shah, S. 1998. Application of Acoustic emission Technique to Detection of Reinforcing Steel Corrosion in Concrete. ACI Materials Journal, 95(1), 68-76.

Liu, Z., and Ziehl, P. 2009. Evaluation of RC Beam Specimens with AE and CLT Criteria. ACI Structural Journal, Vol. 106, No. 3, pp. 1-12.

Lovejoy, S. 2008. Acoustic Emission Testing of Beams to Simulate SHM of Vintage Reinforced Concrete Deck Girder Highway Bridges. Structural Health Monitoring, Vol. 7, 327-346.

Mangual, J., ElBatanouny, M., Ziehl, P., and Matta, F. 2012. Corrosion Damage Quantification of Prestressing Strands Using Acoustic Emission. ASCE Journal of Materials in Civil Engineering, in press.

Mangual, J., ElBatanouny, M. K., Ziehl, P., and Matta, F. 2013. Acoustic-Emission-Based Characterization of Corrosion Damage in Cracked Concrete with Prestressing Strand. ACI Materials Journal, 110(1), 89.

Melchers, R. E., and Li, C. Q. 2006. Phenomenological Modeling of Reinforcement Corrosion in Marine Environments. ACI Materials Journal, V. 103, No. 1, Jan.-Feb., pp. 25-32.

Nair, A. 2006. Acoustic emission monitoring and quantitative evaluation of damage in reinforced concrete members and bridges. Master's thesis, Department of Civil and Environmental Engineering, Louisiana State University and Agricultural and Mechanical College.

Nair, A. and Cai, C.S. 2010. Acoustic emission monitoring of bridges: Review and case studies. Engineering structure, 32 (6), 1704-1714.

NCHRP. 1998. Durability of precast segmental bridges. NCHRP Web Document No. 15, Project 20-7/Task 92 (Editors: Poston, R.W. & Wouters, J.P.), National Cooperative Highway Research Program, Transportation Research Board, National Research Council, Washington, D.C., USA.

NDIS 2421. 2000. Recommended practice for in situ monitoring of concrete structures by acoustic emission. Japanese Society for Non- Destructive Inspection.

Novokshchenov, V. 1989. Salt-Penetration and corrosion in Prestressed concrete Members. FHWA-RD-88-269.

Novokshchenov, V. 1997. Corrosion, 53(6): pp.489.

Ohtsu, M., Uchida, M., Okamoto, T., and Yuyama, S. 2002. Damage assessment of reinforced concrete beams qualified by acoustic emission. ACI Structural Journal 99 (4), 411–417.

Ohtsu, M., and Tomoda, Y. 2008. Phenomenological Model of Corrosion Process in Reinforced Concrete Identified by Acoustic Emission. ACI Materials Journal, 105(2), 194-199.

Olaszek, P., Swit, G., and Casas, J.R. 2010. Proof load testing supported by acoustic emission: an example of application. A: International IABMAS Conference on Bridge Maintenance, Safety and Management. "V International IABMAS Conference on Bridge Maintenance, Safety and Management". Philadelphia: CRC Press, 472-479.

Ono, K. 2010. Application of Acoustic Emission for Structure Diagnosis. Konferencja Naukowa, 317-341.

Park, Y. and Ang, A. 1985. Mechanistic Seismic Damage Model for Reinforced Concrete. J. Struct. Eng., 111(4), 722–739.

Perrin, M., Gaillet, L., Tessier, C., and Idrissi, H. 2010. Hydrogen embrittlement of prestressing cables. Corrosion Science, 52, 1915–1926.

Pollock, A.A. 1986. Classical Wave Theory in Practical AE Testing. Progress in AE III, Proceedings of the 8th International AE Symposium, Japanese Society for Nondestructive Testing, 708-721.

Pollock, A. A. 1995. Inspecting bridges with acoustic emission—inspection details about in-service steel bridges and monitoring weld operations: application guidelines.

Prateepasen, A., and Jirarungsatian, C. 2011. Implementation of Acoustic Emission Source Recognition for Corrosion Severity Prediction. Corrosion, Vol. 67, No. 5, pp. 11.

Proverbio, E. 2011. Evaluation of deterioration in reinforced concrete structures by AE technique. Materials and corrosion, 62,161-169.

Ramadan, S., Gaillet, L., Tessier, C., and Idrissi, H. 2008. Detection of stress corrosion cracking of high-strength steel used in prestressed concrete structures by acoustic emission technique. Applied surface science, 254(8), 2255-2261.

Ridge, A., and Ziehl, P. 2006. Evaluation of Strengthened Reinforced Concrete Beams: Cyclic Load Test and Acoustic Emission Methods. ACI Structural Journal, Technical paper 103-S84, 832-841.

Robson, A., and Brooman, H. 1997. A3/A31 Flyover - Case History of an Externally Posttensioned Bridge. Proceeding of the Seventh International Conference on Structural Faults and Repair, Vol. 1, July 1997, pp. 307-315.

Sammonds, P.R., Meredith, P.G., Murrel, S.A.F., and Main, I.G. 1994. Modelling the damage evolution in rock containing pore fluid by acoustic emission. Eurock '94, Balkerna, Rotterdam, The Netherlands.

Schofield, B.H, Barreiss, B., and Kyrala, A. 1958. Acoustic Emission under Applied Stress WADS. Technical Report 58-194. Lessells and Associates: Boston, MA.

Schumacher, T. 2008. AE techniques applied to conventionally reinforced concrete bridge girders. Oregon DOT Report SPR633, 199.

Shahidan, S., Bunnori, N.M., Nor, N.M.,and Basri, S.R. 2011. Damage severity evaluation on reinforced concrete beam by means of acoustic emission signal and intensity analysis. Industrial Electronics and Applications (ISIEA), 2011 IEEE Symposium, 337-341.

Shahidan, S., Bunnori, N.M., Bhardwaj, N., Nor, N.M., Basri, S.R., and Abdul Kudus S. 2012. Intensity Analysis Method for Measurement the Damage Severity of Concrete Structure by Utilizing the Acoustic Emission Technique. International Journal of Applied Physics and Mathematics, Vol. 2, No. 1.

Shamina, O.G. 1956. Elastic pulses in the fracture of specimens of rocks. Izvestiia Akademii Nauk SSSR, Seriia Geofizicheskaya 5(5), 513–518.

Shearer, P. M. 1999. Introduction to seismology. Cambridge University Press, Cambridge, England, 1–189.

Shiotani, T., Fujii, K., Aoki, T., and Amou, K. 1994. 'Evaluation of progressive failure using AE sources and improved b-value on slope model tests. Prog. Acoust. Emiss VII, 7, 529–534.

Shiotani, T., Yuyama, S., Li, Z. W., and Othsu, M. 2000. 'Quantitative evaluation of fracture process in concrete by the use of improved b-value.' 5th Int. Symposium Non-Destructive Testing in Civil Engineering, T. Uohoto, ed., Elsevier Science, Amsterdam, 293–302.

Shiotani, T., Ohtsu, M., Ikeda, K. 2001. Detection and evaluation of AE waves due to rock deformation. Construction and Building Materials, 15(5-6), 235-246.

Shiotani T, Aggelis DG. 2007. Evaluation of repair effect for deteriorated concrete piers of intake dam using AE activity. J Acoust Emission, 25:69–79.

Shiotani T, Aggelis DG, Makishima O. 2007. Global monitoring of concrete bridge using acoustic emission. J Acoust Emission ,25:308–15.

Song, G., and Shayan, A. 1998. Corrosion of steel in concrete : causes, detection and prediction : a state-of-the-art review. Vermont South, Vic. : ARRB Transport Research.

Tinkey, B.V., Fowler, T.J., and Klingner, R.E. 2002. Nondestructive Testing of Prestressed Bridge Girders with Distributed Damage. Research Report 1857-2, pp. 106.

Trejo, D., Pillai, R.G., Hueste, M.B., and Reinschmidt, K.F. 2009. Parameters Influencing Corrosion and Tension Capacity of Post-Tensioning Strands. ACI Materials Journal, 106(2), 144-153.

Videm, K. 1997. Instrumentation and Condition Assessment Performed on Gimsoystraumen Bridge. In: Aage Blankvoll (ed.), Proceedings of International Conference-Repair Of Concrete Structures, From Theory To Practice In A MarineEnviroment, pp.375 (Norway).

Vidya Sagar, R., and Raghu Prasad, B. K. 2012. A review of recent developments in parametric based acoustic emission techniques applied to concrete structures. Nondestructive Testing and Evaluation, Vol. 27, Iss. 1, 2012.

Vinogradov ,S.D. 1964. Acoustic Observations of the Processes of Fracture of Rocks. [in Russian]. Nauka: Moscow.

Weng, M.S., Dunn, S.E., Hartt, W.H. Brown, R.P. 1982. Application of acoustic emission to detection of reinforcing steel corrosion in concrete. Corrosion, 38 (1), pp. 9‑14.

Wevers, M. and Lambrighs, K. 2009. Applications of Acoustic Emission for SHM: A Review. Encyclopedia of Structural Health Monitoring.

Whiting, D., Stejskal, B., and Nagi, M. 1993. Condition of Prestressed Concrete Bridge Components – Technology Review and Field Surveys. Publication No. FHWA-RD-93-037, Federal Highway Administration, McLean, VA.

Woodward, R.J. , and Williams F.W. 1988. Collapse of Ynes-y-Gwas bridge, west Glamorgan. In: Proceedings Of The Institution Of Civil Engineers Part I, 84, PP.635-69.

Xu, J. 2008. Nondestructive evaluation of prestressed concrete structures by means of acoustic emission monitoring. Dissertation, Dept. of Civil Engineering, Univ. of Auburn, Auburn, Alabama, 308.

Xu, J., Barnes, R. W., and Ziehl, P. H. 2013. Evaluation of Prestressed Concrete Beams based on Acoustic Emission Parameters. Materials evaluation, 71(2), 176-185.

Yunovich, M., and Thompson, N. 2003. Corrosion of Highway Bridges: Economic Impact and Control Methodologies. ACI International, American Concrete Institute, Vol. 25, No.1, Detroit, USA, pp. 52-57.

Yuyama, S., Okamoto, T., and Nagataki, S. 1994. Acoustic Emission Evaluation of Structural Integrity in Repaired Reinforced Concrete Beams. Materials Evaluation, 86-90.

Yuyoma, S., Okamoto, T., Shigeishi, T.,Ohtsu, M., and Kishi, T. 1998. A Proposed Standard for Evaluating Structural Integrity of Reinforced Concrete Beams by AE. Acoustic Emission: Standards and Technology update, ASTM, STP 1353, 25-40.

Zdunek, A., and Prine, D. 1995. Early Detection of Steel rebar Corrosion by Acoustic Emission Monitoring. Corrosion, Paper no. 547, ITI technical report no. 16, 1-9.

Ziehl, P., Engelhardt, M., Fowler, T., Ulloa, F., Medlock, R., and Schell, E. 2009. Design and Live Load Evaluation of a Hybrid FRP/RC Bridge Superstructure System. ASCE Journal of Bridge Engineering, Vol. 14, No. 5, pp. 309-318.

Ziehl, P., and Fowler, T. 2003. Fiber Reinforced Polymer Vessel Design with a Damage Approach. Journal of Composite Structures, V. 61, No. 4, 395-411.

Ziehl, P. 2008. Applications of Acoustic Emission Evaluation for Civil Infrastructure. SPIE Proc. SPIE Smart Structures NDE, San Diego, CA, 9.

Ziehl, P. H., Galati, N., Nanni, A., and Tumialan, J. G. 2008. In situ evaluation of two concrete slab systems. II: Evaluation criteria and outcomes. J. Perform. Constr. Facil., 22(4), 217–227.

Ziehl, P., and Pollock, A. 2012. Acoustic Emission, Chapter 1: Acoustic Emission for Civil Infrastructure, Intech (ISBN 979-953-307-372-8).